THE EFFECTS OF INITIAL STATIC SHEAR STRESS ON THE LIQUEFACTION RESISTANCE OF ÇİNE SAND

A THESIS SUBMITTED TO
THE GRADUATE SCHOOL OF NATURAL AND APPLIED SCIENCES
OF
MIDDLE EAST TECHNICAL UNIVERSITY

BY

BERKAN SÖYLEMEZ

IN PARTIAL FULFILLMENT OF THE REQUIREMENTS
FOR
THE DEGREE OF DOCTOR OF PHILOSOPHY
IN
CIVIL ENGINEERING

JULY 2024

Approval of the thesis:

THE EFFECTS OF INITIAL STATIC SHEAR STRESS ON THE LIQUEFACTION RESISTANCE OF ÇİNE SAND

submitted by **BERKAN SÖYLEMEZ** in partial fulfillment of the requirements for the degree of **Doctor of Philosophy** i**n Civil Engineering, Middle East Technical University** by,

Prof. Dr. Naci Emre Altun
Dean, **Graduate School of Natural and Applied Sciences** _____

Prof. Dr. Erdem Canbay
Head of the Department, **Civil Engineering** _____

Prof. Dr. Kemal Önder Çetin
Supervisor, **Civil Engineering, METU** _____

Examining Committee Members:

Prof. Dr. Berna Unutmaz
Civil Engineering, Hacettepe University _____

Prof. Dr. Kemal Önder Çetin
Civil Engineering, METU _____

Prof. Dr. Nihat Sinan Işık
Civil Engineering, Gazi University _____

Assoc. Prof. Dr. Nabi Kartal Toker
Civil Engineering, METU _____

Assoc. Prof. Dr. Nejan Huvaj Sarıhan
Civil Engineering, METU _____

Date: 26.07.2024

I hereby declare that all information in this document has been obtained and presented in accordance with academic rules and ethical conduct. I also declare that, as required by these rules and conduct, I have fully cited and referenced all material and results that are not original to this work.

Name Surname: Berkan Söylemez

Signature:

ABSTRACT

THE EFFECTS OF INITIAL STATIC SHEAR STRESS ON THE LIQUEFACTION RESISTANCE OF ÇİNE SAND

Söylemez, Berkan
Doctor of Philosophy, Civil Engineering
Supervisor: Prof. Dr. Kemal Önder Çetin

July 2024, 119 pages

The effects of initial static shear stress on the liquefaction behavior of saturated Çine sand were evaluated through hollow cylinder cyclic torsional tests. The relative density and the initial static and cyclic shear stresses were considered as the variables of the cyclic testing program. The variation of excess pore water pressure and shear strain were monitored throughout the applied shear cycles, allowing for a comprehensive understanding of the impact of these variables on liquefaction resistance. Soil liquefaction triggering was identified with the onset of 10 % double amplitude cyclic shear strains level. The cyclic resistance ratio (CRR) vs. equivalent number of shear stress cycles (N) curves were developed for the samples tested under zero and nonzero initial shear stresses. The effects of initial static shear stresses were assessed by simply taking the ratio of CRR values from these two sets of tests. This ratio is defined as slope correction factor, K_α. It is concluded that the presence of initial static shear stresses increases CRR values for dense soil specimens whereas decreases it for the loose ones, consistent with the recommendations of NCEER (1997).

Keywords: Çine sand, liquefaction, cyclic torsion, slope correction factor

ÖZ

BAŞLANGIÇ STATİK KAYMA GERİLMESİNİN ÇİNE KUMUNUN SIVILAŞMA DİRENCİNE ETKİLERİ

Söylemez, Berkan
Doktora, İnşaat Mühendisliği
Tez Yöneticisi: Prof. Dr. Kemal Önder Çetin

Temmuz 2024, 119 sayfa

Başlangıç statik kayma gerilmesinin doygun Çine kumunun sıvılaşma davranışı üzerindeki etkileri, içi boş silindir döngüsel burulma testleri ile değerlendirilmiştir. Döngüsel yüklemeli testlerde değişkenler olarak rölatif yoğunluk ile başlangıç statik ve döngüsel kayma gerilmeleri seçilmiştir. Aşırı boşluk suyu basıncı ile kalıcı ve toplam şekil değişimleri, uygulanan kayma döngüleri boyunca izlenerek belirtilen değişkenlerin sıvılaşma direnci üzerindeki etkileri kapsamlı bir şekilde çalışılmıştır. Zemin sıvılaşmasının tetiklenmesi, %10 çift genlikli döngüsel kayma birim deformasyon seviyelerine ulaşılan ilk an olarak tanımlanmıştır. Başlangıç kayma gerilmelerinin olduğu ve olmadığı durumlarda test edilen numuneler için döngüsel direnç oranı (CRR) ve eşdeğer kayma gerilmesi döngü sayısı (N) eğrileri geliştirilmiştir. Başlangıç statik kayma gerilmelerinin etkileri, başlangıç kayma gerilmelerinin olduğu ve olmadığı durumlar için geliştirilen CRR-N eğrileri oranlanarak elde edilebilir. Bu oran, eğim düzeltme faktörü, K_α olarak tanımlanır. Başlangıç statik kayma gerilmelerinin varlığı, NCEER (1997) önerileriyle tutarlı olarak, sıkı zemin numuneleri için CRR değerlerini artırırken, gevşek numuneler için bu direnci azaltmaktadır.

Anahtar Kelimeler: Çine kumu, sıvılaşma, döngüsel burulma, eğim düzeltme faktörü

To my beloved family

ACKNOWLEDGMENTS

I want to gratefully thank Dr. Kemal Önder Çetin, without whom I would not be able to complete my thesis. I wish to express my appreciation for his continuous and unconditional guidance and support at each step of this study. His unlimited assistance, patience, and tolerance made my research come to this stage and should never be forgotten. My appreciation is not only his being a mentor in academic and professional life, but also making me feel as comfortable as a friend or a brother in the last six years.

Thanks are also due to the members of my dissertation committee, Dr. Kartal Toker and Dr. Nihat Sinan Işık, for their constructive suggestions and subjective comments throughout this research period. I also want to thank Dr. Berna Unutmaz and Dr. Nejan Huvaj for participating to my defense committee and improving the quality of this study with their comments.

If you are reading this thesis, you should know that none of this would be possible without the help of our wonderful technical staff. Making tests with a new test setup creates/reveals new problems very often and lucky for me, these people were always there to help me. Ahmet Sağlam, Kamber Bilgen, Necdet Aydoğan, Emre Kavak, Hüseyin Gündoğdu, Cuma Yıldırım, Osman and Hüseyin from Structure Lab, Mustafa abi from Mechanical Engineering. Thank you all. Special thanks to Ümit Önkol, the legendary deus ex machina who solved all the most difficult problems with his mechanical engineering knowledge. Thank you all and also thanks to Ostim people (where amazing happens)

I also want to thank my colleagues for their enormous support, friendship and helps during the last seven years. Thank you all for always being kind, positive, and helpful during this long period. Elife, Hayri, Umut, Sefa, Maham, Yiğit, Yakup, Ahmet, Soner, Fikret, Emir, Ekin, Berkay, Emre, Sarıçiçek, and many more I can't write due to space constraints. I am sure that it would be even more difficult to complete this dissertation without his considerable aid and support during both the research and writing steps.

I want to thank my research mates, Moutasem and Ahmed Al-Suhaily, especially. These two genius friends gave life to the equipment and helped me progress far better in a robust manner. I hope these two will be writing their thesis as soon as possible too. Shukran !

I also would like to acknowledge the financial support by Scientific Research Projects Coordination Unit of Middle East Technical University via project numbered TEZ-D-303-2022-10880: Cyclic Torsional Shear Testing of Çine Sands and The Assessment of K_α Effects on Cyclic Response completed in October 2023. It is greatly appreciated.

It is generally said that family comes first, but in many of the thesis, people thank their family at the end. I believe it is because whatever you do (good or bad), they are always there for you, support you and love you unconditionally. My mom Songül, my dad Cafer and my handsome brother, Serkan… thank you for all your supports. I can say family is similar to soil type, if you have a strong one, you can bear all the difficulties/loads coming to you (the foundation) safely.

Last but not least and from now on always the first priority. I thank my beloved wife Katya and our little rabbit, little daughter of us, Sofia. Having you both in my life enlightened my dark and desperate periods of the last part of the doctorate. Canım Koty, thank you for the all patience. I think now that is really over (hopefully) Let's start our new chapters; you, me and Sofidichky

Thanks to all.

TABLE OF CONTENTS

LIST OF TABLES

TABLES

LIST OF FIGURES

LIST OF ABBREVIATIONS

CSR: Cyclic stress ratio

CRR: Cyclic resistance ratio

SPT: Standard Penetration Test

CPT: Cone Penetration Test

SPT-N: Standard Penetration Test blow count

OCR: Over consolidation ratio

CW: Clockwise

CCW: Counterclockwise

FHWA: Federal Highway Administration

USCS: Unified Soil Classification System

FC: Fineness Content

SP: Poorly graded sand

ASTM: American Society for Testing and Materials

LVDT: Linear Variable Differential Transformer

NCEER: National Center for Earthquake Engineering Research

LIST OF SYMBOLS

K_α : Correction for sloping sites

τ_{max} : Maximum shear stress

σ'_o : Initial effective stress (Effective overburden stress)

A_{max}: Maximum acceleration at the ground surface

g : Gravitational acceleration

γ : Unit weight of the soil

τ : Shear stress

F : Force

m : Mass

a : Acceleration

z : Depth

τ_{rigid} : Shear stresses at the base of the rigid soil block

σ_v : Total vertical stress

σ'_v : Effective vertical stress

γ': Effective unit weight of the soil

$\tau_{deformable}$: Shear stresses at the base of the deformable soil block

r_d : Stress reduction coefficient, mass participation ratio

$\tau_{average}$: Average shear stress

q_c : Cone tip resistance

Vs_{30} : Shear wave velocity for the top 30m of the soil layer

MSF : Magnitude scaling factor

K_σ : Correction for overburden pressure

$CRR_{\sigma'_v,\alpha,M_w}$: Cyclic resistance ratio for atm, and Mw

$CRR_{\sigma'_v=1\ atm,\alpha=0,M_w=7.5}$: Cyclic resistance ratio for 1 atm, level ground, Mw=7.5

FS : Factor of safety

σ_1 : Major principal stress

σ_3 : Minor principal stress

σ'_o : Effective overburden stress

P_a : Atmospheric pressure

M: Magnitude

M_w : Moment magnitude

$(N_1)_{60}$: Corrected blow count for 60% energy efficieny

$(N_1)_{78}$: Corrected blow count for 78% energy efficieny

r_u : Excess pore water pressure ratio

K_{Mw} : Correction for earthquake magnitude

α : Normalized static stress ratio

D_r : Relative density

D_{50} : Relative density

e_{max} : Maximum void ratio

e_{min} : Minimum void ratio

C_u : Coefficient of uniformity

C_c : Coefficient of curvature

R_i : Inner radius

R_o : Outer radius

$(R_i)_0$: Initial inner radius

$(R_o)_0$: Initial outer radius

ε_v : Volumetric strain

ε_a : Axial strain

P_m : Vertical load carried by membranes

A_m : Total membrane cross-section area

E_m : Elastic modulus of membrane material

σ_m : Vertical stress on the membranes

ε_z : Axial strain of the membranes

R_m : Mean radius of the outer membrane

r_m : Mean radius of the inner membrane

t_o : Thickness of the outer membrane

t_i : Thickness of the inner membrane

ϕ' : Internal friction angle

ϕ_{cs} : Critical state angle of shearing resistance

B : Skempton coefficient

f : Frequency

CHAPTER 1

INTRODUCTION

1.1 Overview

Despite numerous studies since the recognition of soil liquefaction phenomena, current understanding of soil liquefaction still remains incomplete. Since the 1964 Niigata earthquake in Japan, many research studies have been conducted, both in the laboratory and in the field, to better understand the mechanisms of liquefaction and soil resistance.

Many site elements contribute to the engineering analysis of liquefaction triggering. One significant issue currently lacking transparently presented laboratory test data is the effect of initial static shear stress on the triggering of liquefaction and behavior under cyclic loading. These initial static shear stresses are often present in slopes and embankments. Some experimental data is available (Seed and Harder, 1990; Boulanger, 2003; Cetin and Bilge, 2015), but a consensus on the effects of static shear stress has not yet been reached. As a result, current state of practice in liquefaction evaluations either ignores its effects or uses controversial correction sets. These choices result in biased liquefaction engineering evaluations and may lead to unsafe engineering design solutions.

On the basis of this background, the aim of this thesis is defined as to conduct hollow cylinder cyclic torsional shear tests on Çine sand specimens and study the effects of initial static shear stresses on liquefaction resistance.

The following chapters are organized to present the discussions included within the scope of this thesis:

Chapter 2 presents a comprehensive discussion on cyclic stress ratio (CSR) and cyclic resistance ratio (CRR) terminologies. After introducing these terms, the relevant corrections applied on either CSR or CRR are discussed, benefitting from the literature.

Chapter 3 introduces the hollow cylinder test set up, its role in advanced testing and components of the test system. Some of previous tests with hollow cylinder apparatus are

introduced. The constraints for achieving a satisfactory geometry to conduct these tests are explained, and the suitability of the test set up used in our studies, is discussed. Additionally, this chapter discusses the necessary equipment corrections, which need to be applied on the test results.

Chapter 4 presents the test samples prepared from Çine sand, and its features. The steps to prepare the samples are explained in detail. Test results and representative four-way plots of showing the test results are presented in this chapter.

Chapter 5 summarizes the overall findings of the study and compares resulting K_α correction factors with the values recommended in the literature. Potential topics for future studies are listed as in the concluding remarks.

.

CHAPTER 2

LITERATURE REVIEW

2.1 Introduction

Liquefaction occurs when the soil loses its shear strength and stiffness because of undrained cyclic or monotonic loading. This can cause significant damage during earthquakes, as observed in past events worlwide. Following major earthquakes in Niigata, Japan, and Alaska, USA, in 1964, researchers have gained substantial insights into the triggering mechanisms of liquefaction, particularly the effects of cyclic loading on saturated sands, its impacts on structures, and methods to mitigate its consequences. The damage caused by liquefaction during major earthquakes has made it a significant topic to be further evaluated in earthquake engineering (Bhattacharya et al, 2019).

This chapter briefly explains the terms, including cyclic stress ratio (CSR) and cyclic resistance ratio (CRR), which are essential for evaluating the triggering of liquefaction. Moreover, the chapter emphasizes the conditions of sloping ground (or the effect of initial static shear stresses), and additionally related correction factors applied on either CSR or CRR, are explained.

2.2 Induced CSR

It is important to evaluate the stresses that will be applied on the soil body during an earthquake. For this purpose, generally two methods are used:

a) Dynamic Response Analysis

For horizontally layered sites, the wave propagation theory is employed. In this approach, earthquake time histories are applied at the base and a dynamic response analysis is carried

out. The calculated maximum shear stress (τ_{max}) is divided by the corresponding initial vertical effective stress (σ'_v) at the depth of interest to estimate, CSR, as defined in Eq. 2.1.

$$CSR = {}^{0.65\,\tau_{max}}/_{\sigma'_v} \tag{2.1}$$

Various software, including SHAKE (Schnabel et al. 1972), NERA (Bardet and Tobita, 2001), STRATA (Kottke and Rathje, 2008), and DeepSoil (Hashash and Park, 2001), can be used to perform these site response analyses (Bhattacharya et al., 2019).

b) Simplified Method

Seed and Idris (1971) suggested the use of simplified method to estimate induced CSR levels during earthquakes. It is stated that during an earthquake, maximum acceleration at the ground surface, A_{max} (generally given in terms of g, gravitational acceleration), will cause a force of inertia at the soil body mass with respect to the Newtonian equation of motion. (Figure 1).

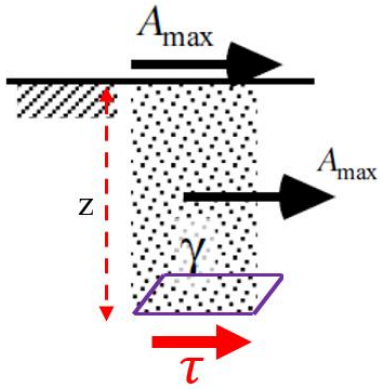

Figure 1. Rigid body block analysis on soil block

Considering the soil body as rigid (ideal case), no shear strains will be developed within the rigid block, and acceleration will be constant over the soil column. Under these conditions, the soil body with a unit weight of γ will be subjected to a maximum shear force at the base of the soil column, which is expressed in Equation 2.2 as:

$$F = m \cdot A_{max} = \int_0^z \frac{\gamma}{g} * (Base\ Area) * dz * A_{max} \tag{2.2}$$

It should be noted that assuming a level ground condition results in the cancellation of the left and right side of the lateral earth pressures acting on the soil block. Dividing both sides with the base area of the soil column (purple rectangle in Figure 1), the equation becomes:

$$\tau_{rigid} = \sigma_v * \frac{A_{max}}{g} \tag{2.2}$$

Furthermore, the effective vertical stress of the soil column can be calculated as follows:

$$\sigma_v = \int_0^z \gamma dz \tag{2.3}$$

As stated before, CSR is calculated as the ratio of shear stress to the initial vertical effective stress. However, the soil body is assumed to be rigid in shear stress calculations. Since the soil column is deformable, shear strains on the horizontal plane will be induced, and this will usually yield smaller maximum acceleration values than the A_{max} at the ground surface. A factor should be applied to convert τ_{rigid} to $\tau_{deformable}$ as follows:

$$\tau_{deformable} = \tau_{rigid} * r_d \tag{2.4}$$

In Eq. 2.4, r_d is defined as the mass participation ratio. The mass participation ratio is first proposed by Seed and Idriss (1971) (Figure 2). The parameter is broadly studied by various research groups (e.g. Imai et al. (1981), Golesorkhi (1989), Idriss (1999), Cetin and Seed (2004), Lasley et al (2016), etc.) based on 1-D site response analysis.

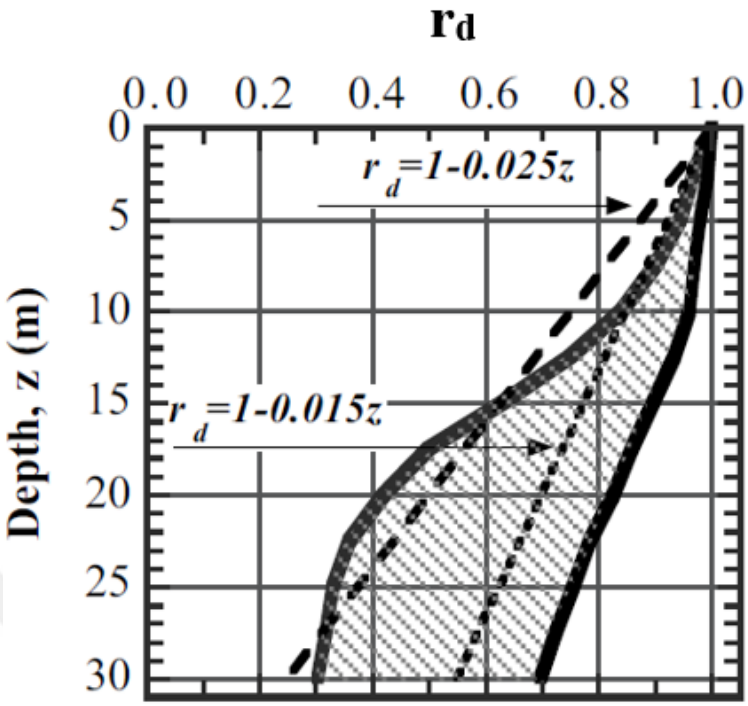

Figure 2. Correction for rigid idealization (after Seed and Idriss, 1971)

Seed and Idriss (1971) suggested that $\tau_{average}$ can be represented well by considering the 65% of the maximum shear stresses (τ_{max}). Hence, CSR can be calculated as:

$$CSR = \frac{\tau_{average}}{\sigma'_v} = 0.65 * (\frac{A_{max}}{g}) * (\frac{\sigma_v}{\sigma'_v}) * r_d \quad (2.5)$$

At this point, one should realize that CSR does not take into consideration the:

1. duration of cyclic loading (number of shear stress cycles)
2. transient nature of arthquake motion.

These and other corrections that affect the resistance of the soil will be explained briefly in the following sections.

2.3 CRR

CRR is the CSR value of a soil mass that triggers liquefaction. In practice, mostly two approaches are followed to estimate the cyclic resistance ratio of the in-situ soil deposits. These are a) field-case-history-based and b) laboratory-based approaches. (Figure 3).

In the field-case history-based approach, an in-situ index value, usually SPT-N from the Standard Penetration Test, tip resistance from the Cone Penetration Test (CPT), or V_{S30} from shear wave velocity tests is selected to represent the resistance or initial relative density of the soil mass. Then, the resistance parameter CRR is compared with the CSR value based on field case-history performance information, and data pairs are drawn in a graphical form. The boundary differentiating these liquefied and non-liquefied case history data pairs defines the CRR.

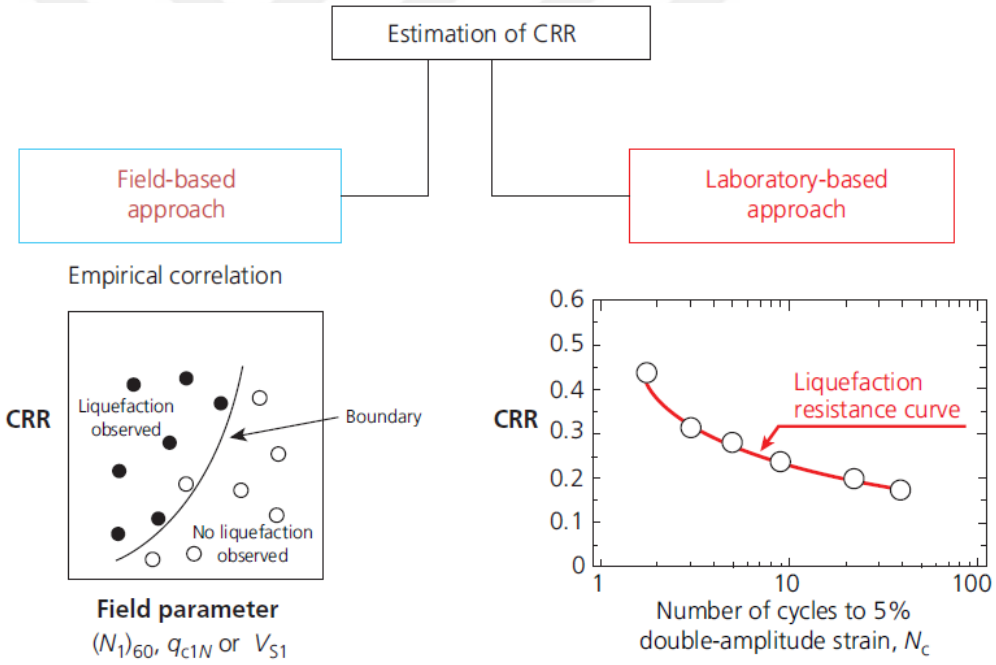

Figure 3. Approaches to estimate the CRR curve

Many researchers proposed chart solutions expressing CRR curves based on case history data. For example, as shown in Figure 4, the CRR is estimated as a function of SPT N value (Seed and Idriss, 1971; Seed et al., 1985; Cetin et al., 2004). Figure 5 illustrates the cone penetration test tip resistance CPT-q_c based CRR curves (Moss et al., 2006; Robertson and

Wride, 1998; Suzuki et al., 1995). Finally, Figure 6 shows the shear wave velocity Vs-based CRR curves (Andrus and Stokoe, 1997, 2000).

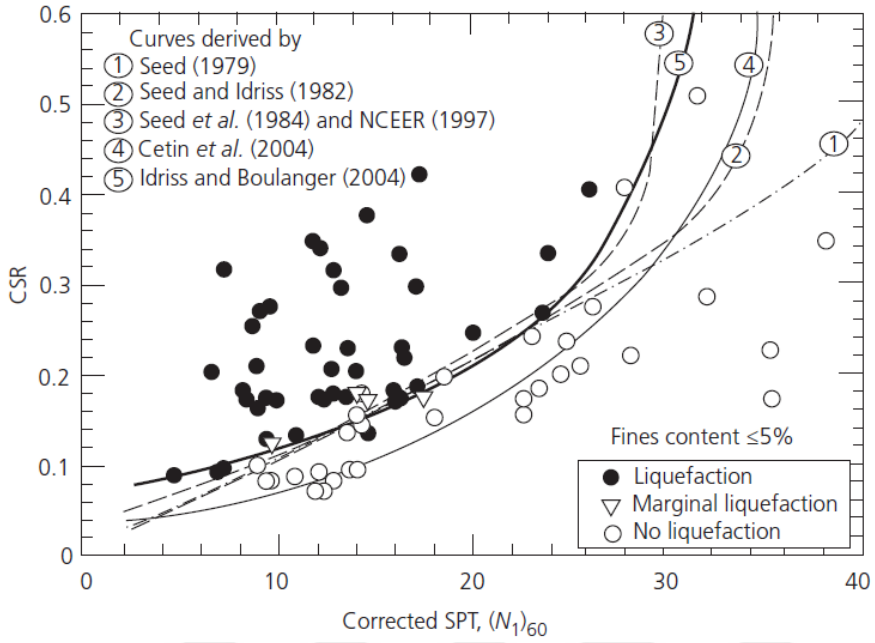

Figure 4. CRR estimated by SPT test results (Bhattacharya et al, 2019)

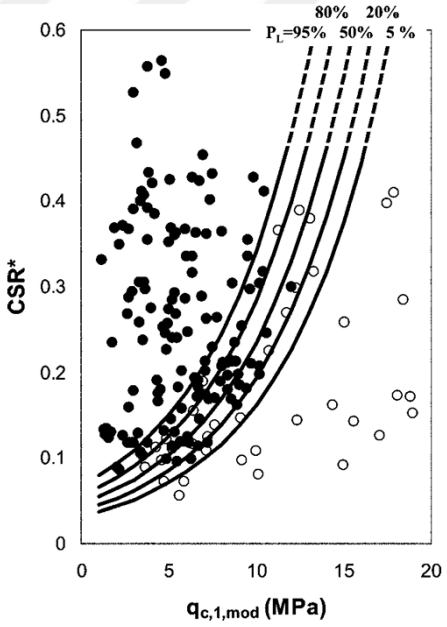

Figure 5. CRR estimated by CPT test results (Moss et al., 2006)

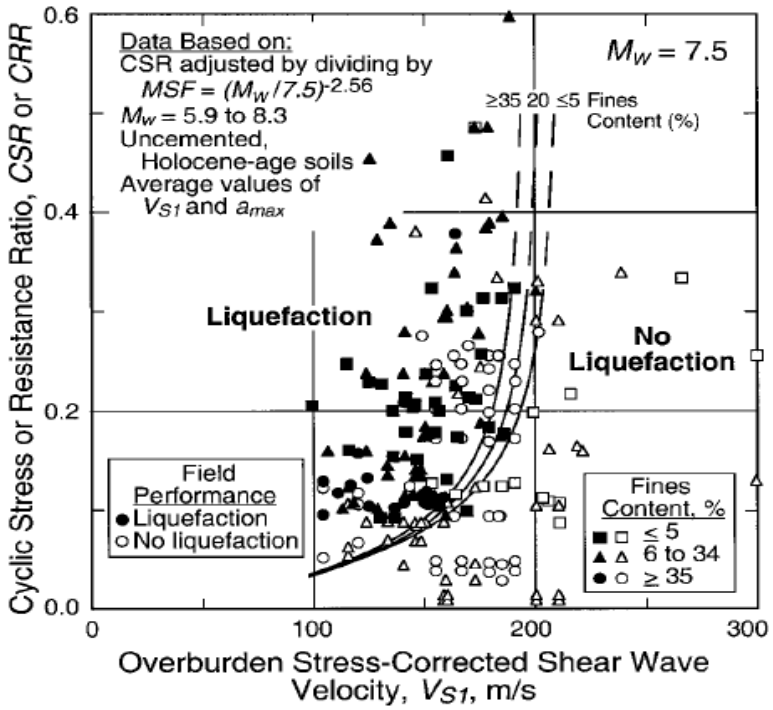

Figure 6. CR estimated by shear wave velocity test results (Andrus and Stokoe, 2000)

The liquefaction resistance of saturated cohesionless soils can be evaluated after applying some cyclic tests in which specimen volume is kept constant (i.e., undrained tests). For that purpose, uniform cycles of loadings are applied on the test specimen after consolidation is achieved. These cycles are continued until the specimen exhibits a substantial deformation or a threshold pore pressure value is reached (Figure 7). In lab practice, liquefaction can be defined by either

a) A target excess pore water pressure: generally, 0.95 of the consolidation pressures.
b) A critical shear strain level: For triaxial tests, 5% DA and, similarly, for simple shear tests, 7.5% DA shear strain for simple shear tests (Bhattacharya et al., 2019).

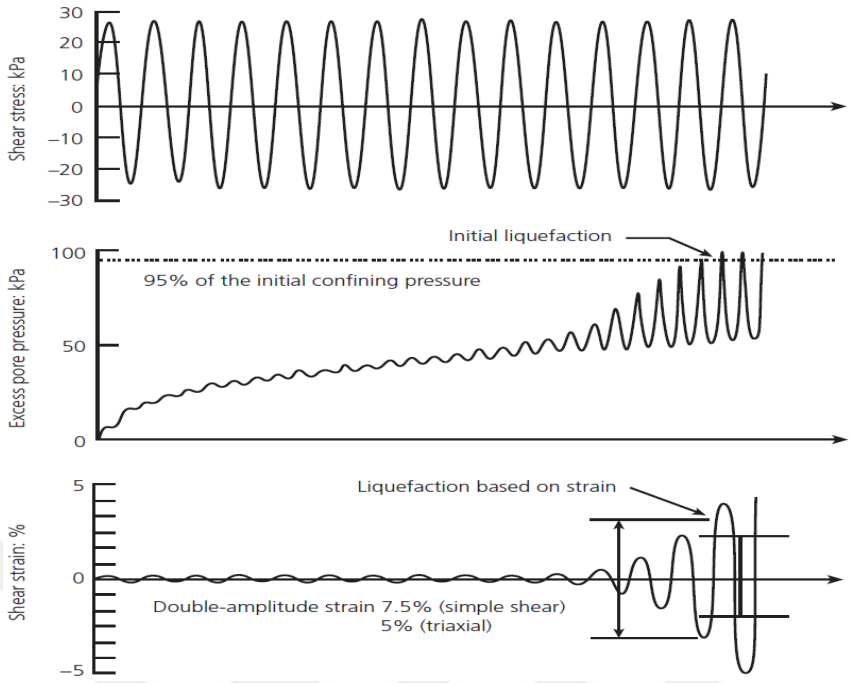

Figure 7. The onset of liquefaction during cyclic loading (Bhattacharya et al., 2019)

Liquefaction resistance is determined by analyzing the number of cycles needed to initiate liquefaction under various stress levels. Different magnitudes of cyclic stress are applied in three to five different tests, and the corresponding number of cycles leading to liquefaction is recorded in each of these tests (Figure 8).

The applied cyclic shear stress is compared to the consolidation stress to determine a normalized shear ratio (CRR). These CRR values are then plotted against the number of cycles. Generally, in terms of an earthquake event, in the field, soil is considered to be subjected to 15-20 cycles during earthquakes. That is why the cyclic strength of soil against liquefaction is the corresponding CSR that leads to threshold deformations in nearly 20 cycles (Ishihara, 1993).

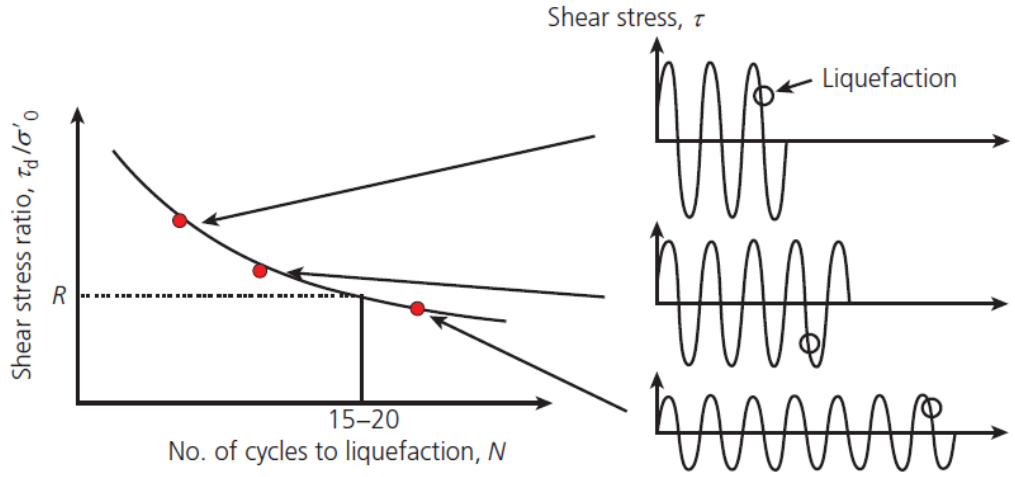

Figure 8. Illustrative determination of CRR by laboratory tests (Bhattacharya et al, 2019)

However, many researchers believe that the soil layers in the field will not show the same behavior as the ones in the laboratory due to differences in the state of stresses and earthquake loading (Towhata, 2008). Correction factors should be applied to CRR values obtained by laboratory tests depending on the test equipment, sample loading conditions (sinusoidal vs triangular), sample disturbance, sample densification during handling, etc.

Empirical suggestions, such as the ones given in Figures 4, 5, and 6 are used to estimate the field CRR values. Then, high quality soil samples are retrieved from the field and cyclic shear tests are performed in the laboratory. However, one should note that these empirical charts are provided for a free field level site shaken by a reference earthquake magnitude of M_w=7.5 and a soil layer under vertical effective stress of 1 atm. Therefore, site and event specific adjustments are made via magnitude scaling factors (MSFs), overburden correction factors (K_σ) and sloping ground correction factor (K_α) to account for the earthquake magnitude under consideration, the overburden stresses at the depth of interest and existence of initial static shear stresses. Overall, the site specific CRR ($CRR_{\sigma'_v,\alpha,M_w}$) is calculated as

$$CRR_{\sigma'_v,\alpha,M_w} = CRR_{\sigma'_v=1\ atm,\alpha=0,M_w=7.5} * K_\sigma * K_\alpha * MFS \quad (2.6)$$

In Figure 9, the flowchart illustrating the calculation steps of the factor of safety against liquefaction is shown. Upon determining CRR and CSR, the factor of safety against liquefaction is calculated as follows:

$$FS = \frac{CRR}{CSR} \tag{2.7}$$

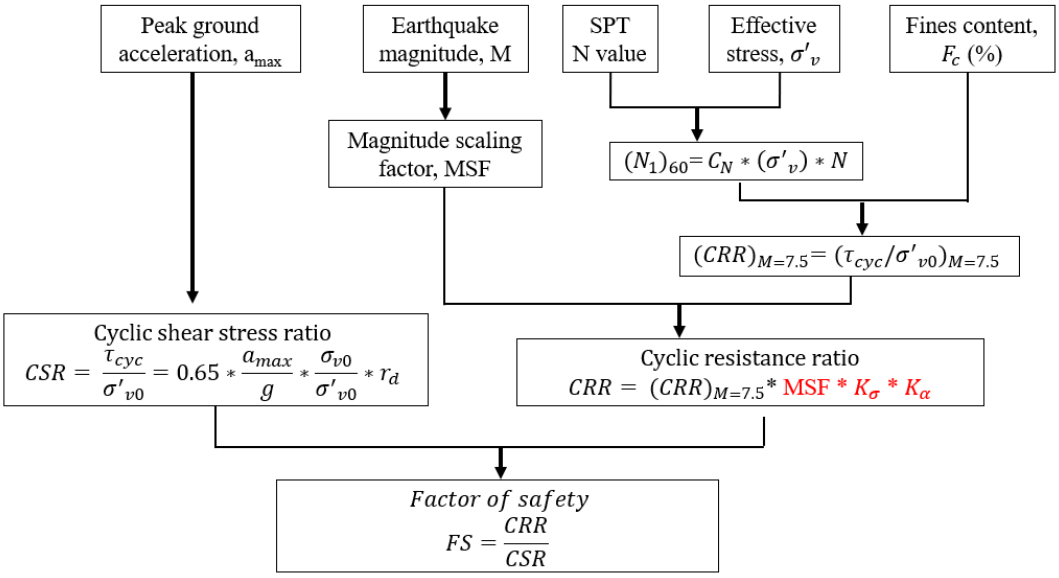

Figure 9. A flowchart showing the calculations steps of the factor of safety against liquefaction (Bhattacharya et al., 2019)

In the next sections, these correction factors will be explained briefly. Emphasis will be given to the discussion regarding the sloping ground condition correction, namely K_α.

2.3.1 Overburden stress correction, K_σ

Monotonic undrained shear strength of normally consolidated saturated soils increases with increasing consolidation (or confinement) stresses. The same response is also valid under cyclic loading. A typical example can be seen in Figure 10 that for any void ratio of the sand, the cyclic loading amplitude to initiate liquefaction increases with increasing confining

stress (Towhata, 2008). However, cyclic shear stress normalized with confining stress, referred to as cyclic stress ratio, tends to decrease as the slope of the failure envelope flattens out with increasing confining stresses (Cetin and Bilge, 2013).

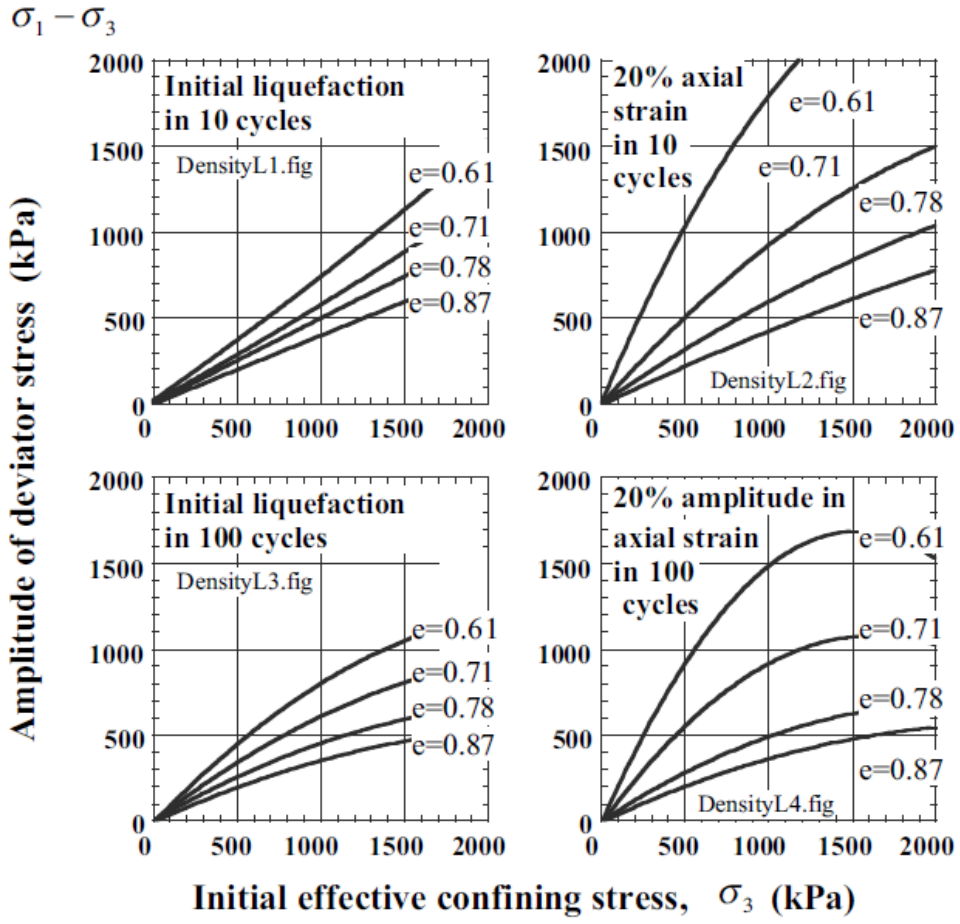

Figure 10. The variation of cyclic shear resistance with confining stress (Towhata, 2008).

Seed (1983) is the pioneering study that addresses the effects of overburden stresses at dam sites. He defined K_σ as follows:

$$K_\sigma = \frac{CRR_{\sigma'_{vc},\alpha=0}}{CRR_{\sigma'_{vc}=1\ atm\ ,\alpha=0}} \tag{2.8}$$

K_σ values by Seed (1983), which were determined from isotropically consolidated cyclic triaxial tests, are shown in Figure 11. K_σ values start to be less than 1 and decrease with

increasing confining stresses. Around 8 kg/cm^2confining stress, the corresponding CRR becomes 40- 60% of the CRR at 1 kg/cm^2.

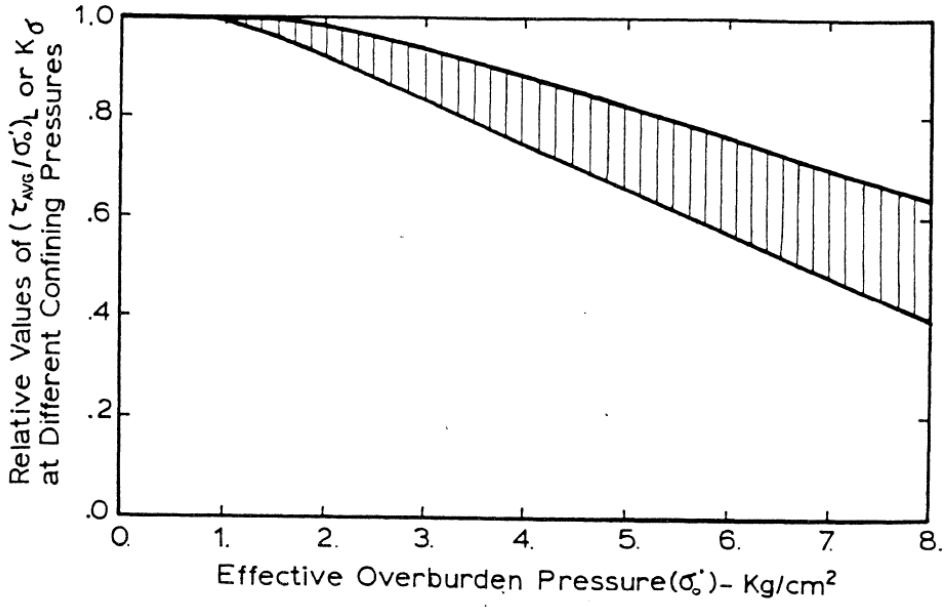

Figure 11. K_σ values by Seed (1983)

The overburden stress corrections were investigated mainly based on laboratory testing. Although there are also empirical and numerical studies in the literature, the significant contributions were made based on cyclic laboratory test results. Undrained cyclic laboratory tests, specifically simple shear or triaxial tests, were performed by Seed (1983), Olsen (1984), Harder (1988), Seed and Harder (1990), Pillai and Byrne (1994), Vaid and Thomas (1995), Vaid and Sivathayalan (1996), Harder and Boulanger (1997), Hynes and Olsen (1999), Youd et al. (2001), Vaid et al. (2001), Wu et al. (2003), Boulanger (2003a), Boulanger and Idriss (2004), Idriss and Boulanger (2006, 2008), Manmatharajan and Sivathayalan (2011), Montgomery et al. (2012, 2014), and Dobry and Abdoun (2015), etc. to understand the overburden stress effects on cyclic strength. These studies revealed that K_σ correction depends on relative density, overconsolidation ratio (OCR), fines content (FC), soil deposition method, aging, stress or strain history, cementation, and fabric.

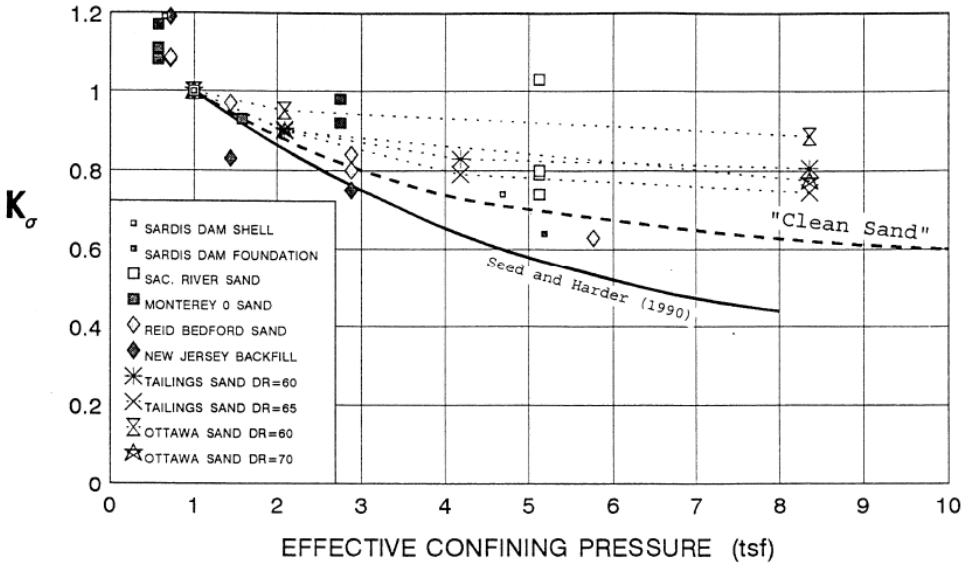

Figure 12. Comparison of Seed and Harder (1990) K_σ values for different specimens

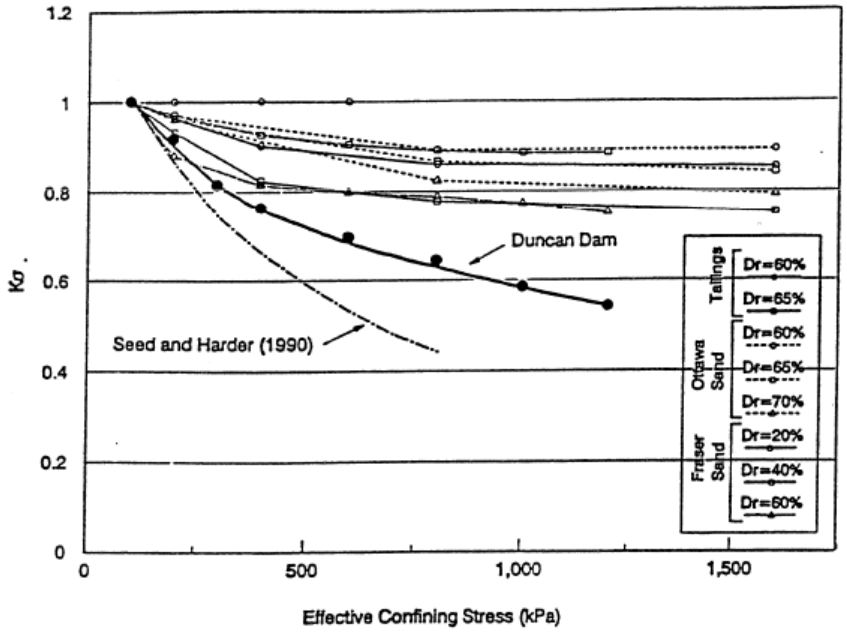

Figure 13. Comparison of Duncan Dam K_σ values with other available K_σ data

Based on the comparison of numerous relationships, it is seen that the scatter among these relationships is large at shallow depths. It should be noted that most of the liquefaction case history database consists of sites where the potentially liquefiable layer is located close to the surface, resulting in significant differences among the results of existing studies. K_σ corrections by Idriss and Boulanger (2010) and Cetin et al. (2004, 2018a) were plotted

comparatively in Figure 14, along with laboratory data of Montgomery et al. (2014) and Cetin and Bilge (2012).

It is also important to note that none of the liquefaction case histories include critical layers in which the vertical effective stress was greater than 2 atmospheres, corresponding to a depth below ground level of approximately 20 meters. Most cases correspond to vertical effective stresses of less than 1 atmosphere (National Academies of Sciences, Engineering, and Medicine, 2021). The differences in K_σ values suggested by different researchers generally agree over effective stresses ranging from 0.5 to 1.2 atmospheres due to normalization of the data at 1.0 atmosphere. Recommended values for K_σ begin to deviate beyond 1 atm. as can be seen in Figure 14.

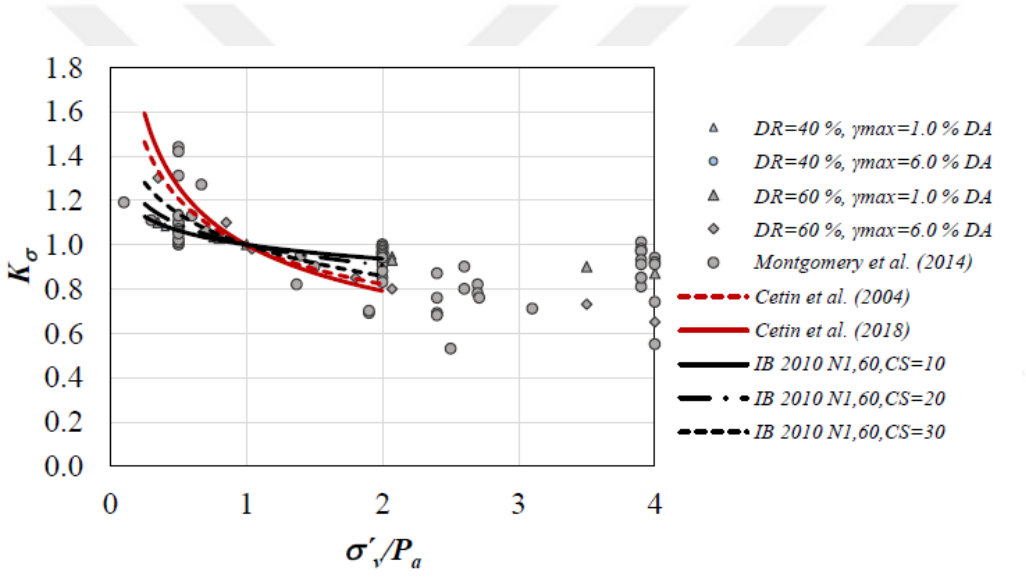

Figure 14. Comparison of K_σ corrections by Idriss and Boulanger (2010), Cetin et al. (2004, 2018a), Montgomery et al. (2014) and Cetin and Bilge (2012).

2.3.2 Magnitude (Duration) Scaling Factor, *MSF*

Seed and Idriss (1982) liquefaction triggering relationship is based on the presence/lack of liquefaction manifestations on the ground surface during earthquakes with magnitudes of about 7.5 such as 1964 Niigata, Japan (M=7.5), 1974 Haicheng, China (M=7.3), 1976 Tangshan, China (M=7.6), 1976 Guatemala (M=7.6), 1977 Western Argentina (M=7.4) and 1978 Miyagiken-Oki, Japan (M=7.4) as shown in Figure 15. (NCEER, 1997). However, to

assign CRR values for earthquakes other than M=7.5, a scaling is needed to be applied on CRR, increasing the value up or down. This adjustment is performed by using Magnitude Scaling Factors (MSFs), which Seed and Idriss (1982) initially developed based on estimates of the typical number of loading cycles for different earthquake magnitudes and laboratory test results (Figure 16). Numerous studies have been conducted since this pioneering study; some examples are shown in Figures 17 and 18.

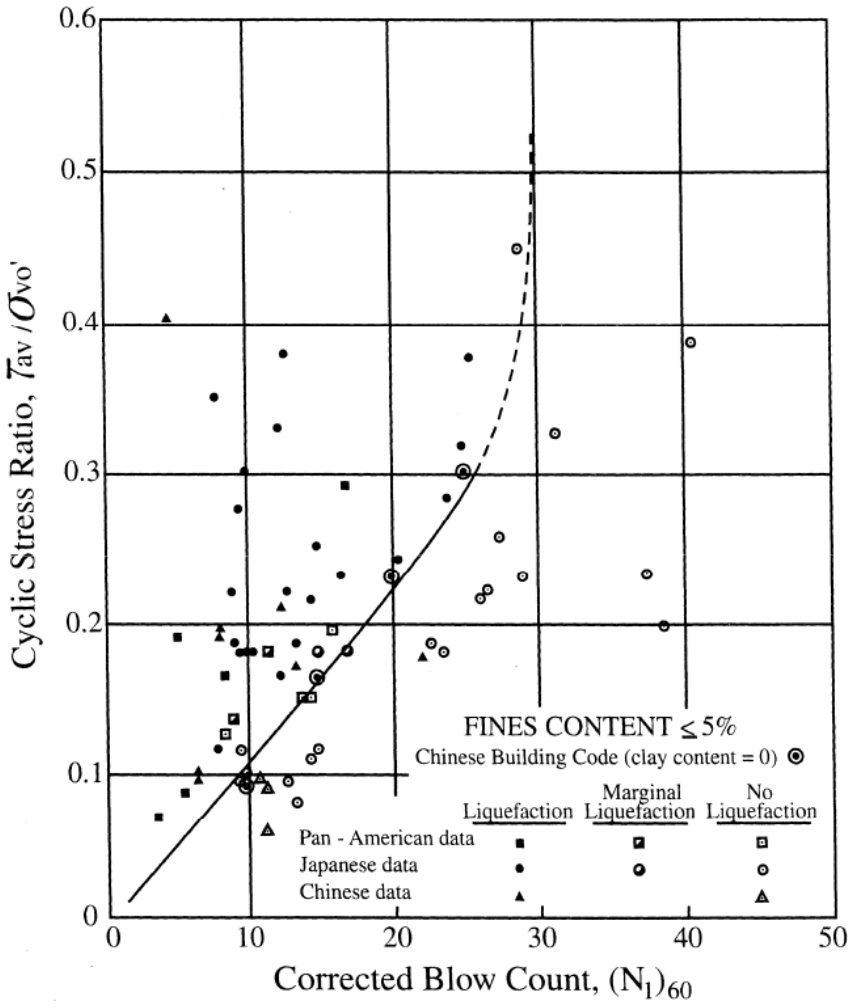

Figure 15. CSR vs $(N_1)_{60}$ values for M=7.5 earthquakes (after Seed 1984)

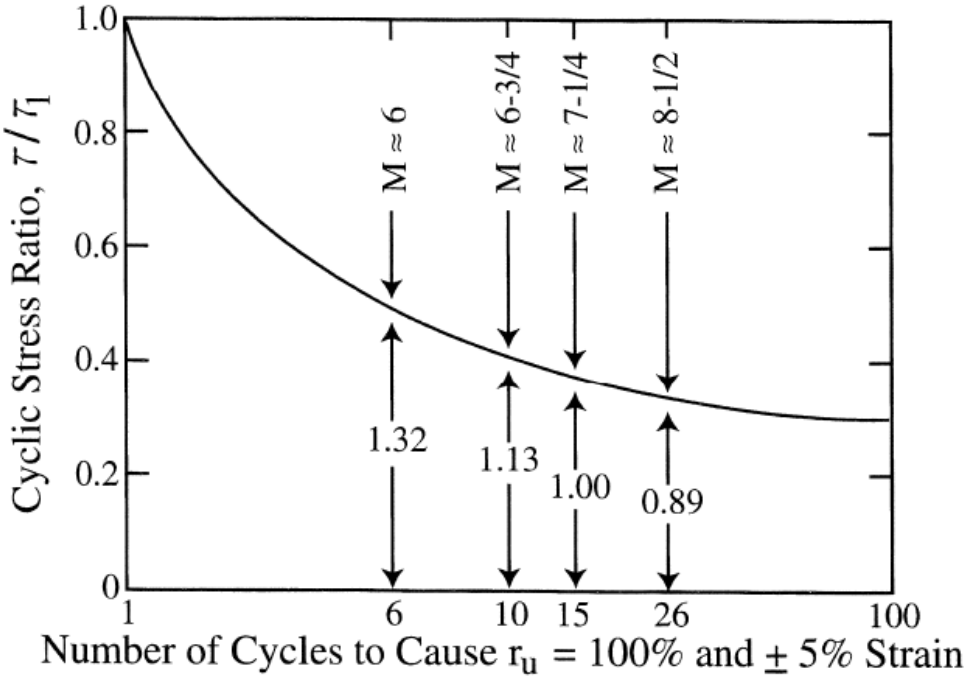

Figure 16. Number of cycles required to cause liquefaction for varying CSR values (After Seed and Idriss, 1982)

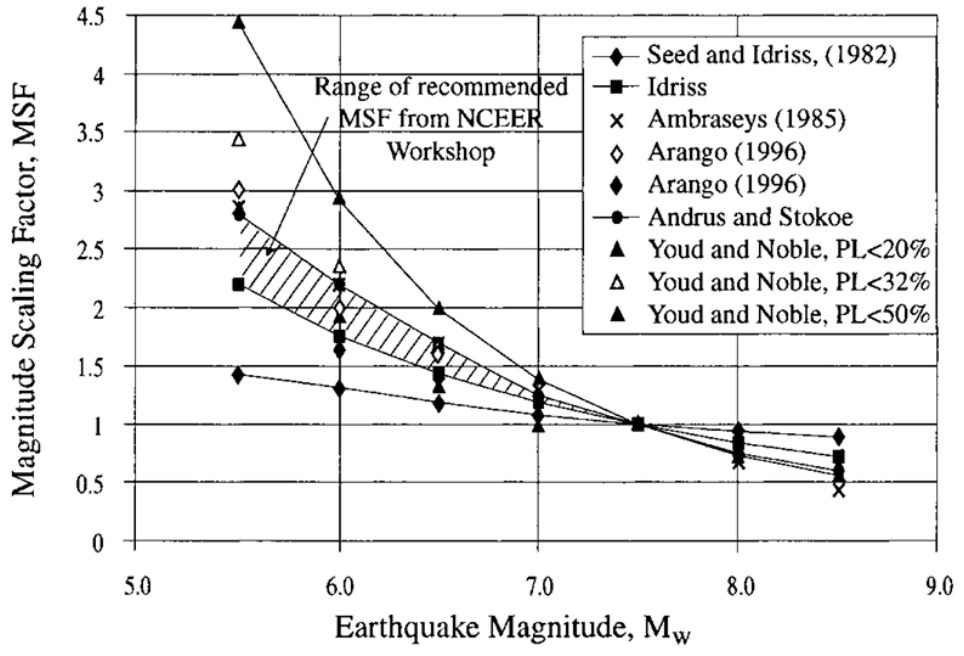

Figure 17. Magnitude Scaling Factors Derived by Various Investigators (Youd and Noble, 1997)

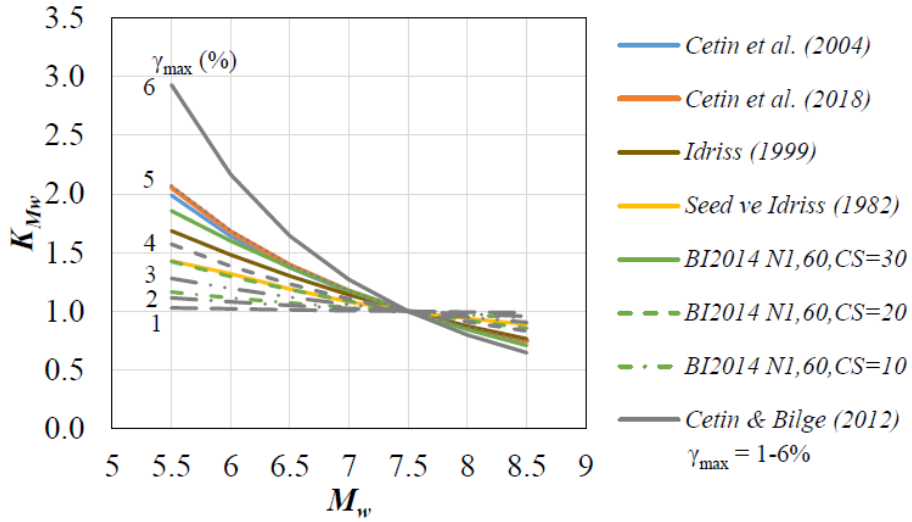

Figure 18. Comparison of MSF values suggested by different researchers

2.3.3 Sloping ground correction, K_α

The effect of initial static shear stresses (τ_{st}) on liquefaction resistance is one of the least studied topics of liquefaction engineering. Seed (1983) proposed a correction factor for static shear stresses, K_α: a factor that modifies the CRR to account for the effects of static shear stress on the horizontal plane (i.e., non-level ground conditions) on the liquefaction resistance of the soil. As the CRR relationships represent level or gently sloping ground (e.g., ground slope less than 6%) conditions, the CRR obtained from a CRR relationship for $\alpha = 0$ (i.e., level ground) conditions must be adjusted to consider site conditions with α to be greater than zero (e.g., slopes and soil layers in and under earth dams) (National Academies of Sciences, Engineering, and Medicine. 2021). A normalized static stress ratio term, α, is used for this purpose.

$$\alpha = \frac{\tau_{static}}{\sigma'_v} \tag{2.9}$$

Sloping ground induces static shear stresses on horizontal planes in a soil mass (Figure 19). Early studies suggested that the existence of initial shear always increases the CRR since higher cyclic stresses are needed to cause stress reversals. However, some of those initial

studies also showed that initial static shear stress can reduce liquefaction resistance for loose to medium-dense sands (Figures 20 to 22)

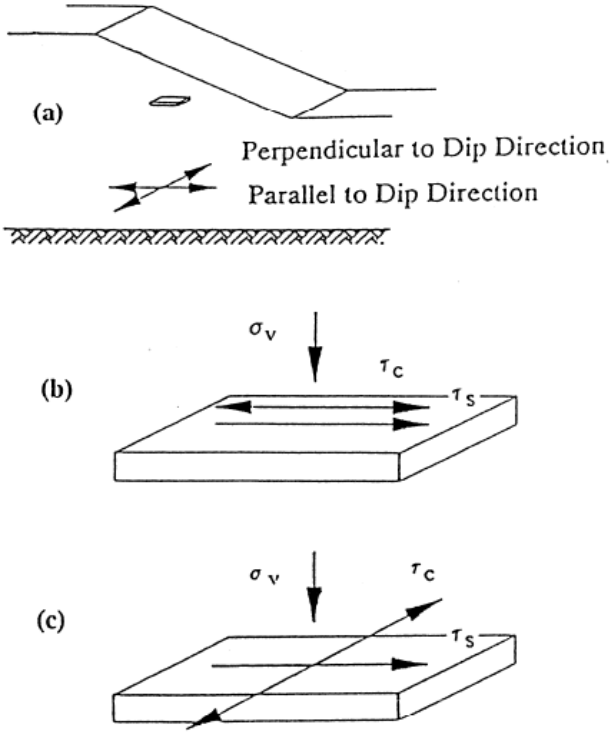

Figure 19. Static and cyclic stress conditions on horizontal planes beneath sloping ground (Boulanger and Seed, 1995)

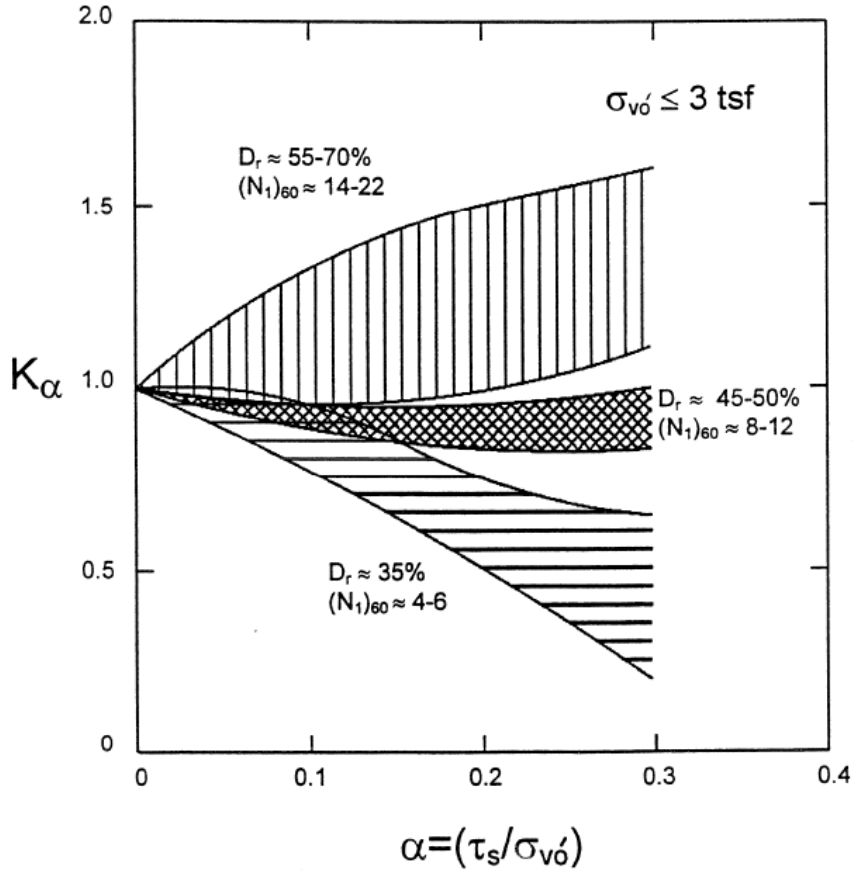

Figure 20. Suggested K_α values (NCEER, 1997)

Based on laboratory cyclic test data, various research teams studied the effect of initial static shear stresses on cyclic resistance and pore pressure generation responses of saturated cohesionless soils. (e.g. Vaid and Finn, 1979; Vaid and Chern,1983; Vaid et al., 1985; Seed and Harder, 1990; Boulanger et al., 1991; Youd et al.,2001, Harder and Boulanger, 1997, Vaid et al., 2001, Wu et al., 2003, Boulanger,2003b, Sivathayalan and Ha, 2011, Cetin and Bilge, 2013, Park et al., 2020, etc.). The available studies in the literature revealed that cyclic resistance depends on relative density, initial static shear stress, and cyclic shear strain level. There exists agreement on the need of applying K_α corrections in the literature. However, there is still no agreement on how initial static shear stresses influence the cyclic response of saturated cohesionless soils (Cetin and Bilge, 2013). A couple of examples from the literature are shown below to emphasize that relationships are inconsistent.

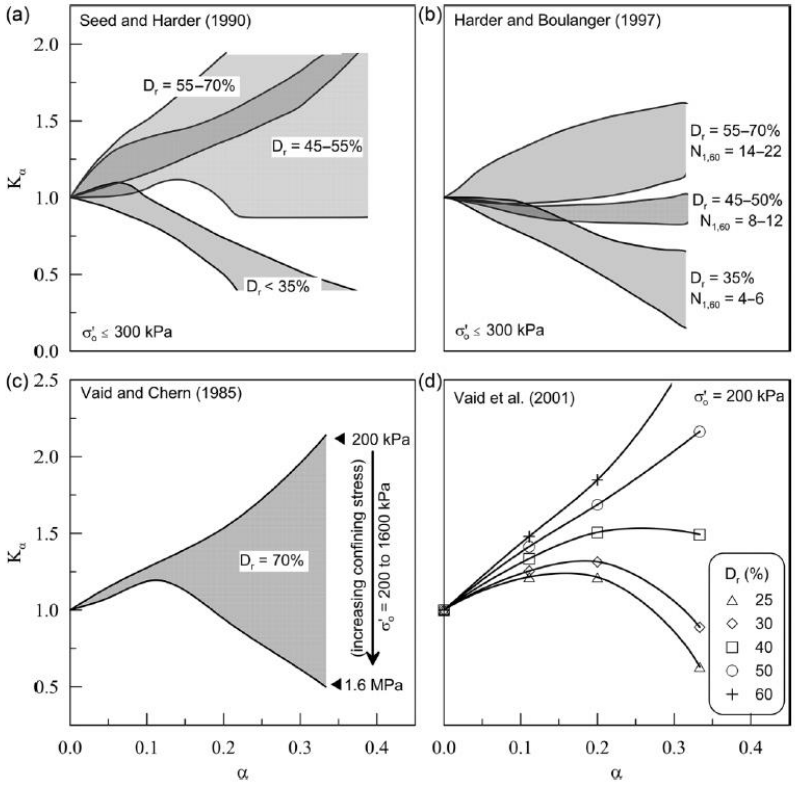

Figure 21. Range of K_α values reported in the literature (taken from Sivathayalan and Ha, 2011): a) Seed and Harder, (1990); b) Harder and Boulanger, (1997); c) Vaid and Chern, (1985); d) Vaid et al. (2001)

In their study, Sivathayalan and Ha (2011) compared two different soil types, silica sand and Frase River sand, with different test setups. Silica sand is very poorly graded with an average particle size D_{50} of about 0.42 mm, uniformity coefficient of $C_u = 1.6$, maximum and minimum void ratios e_{max} and e_{min} of 0.723 and 0.478, respectively, and the specific gravity of the sand is 2.66. Fraser River sand is a uniform sand with an average particle size D_{50} of about 0.30 mm, $C_u = 1.6$, e_{max} and e_{min} 0.806 and 0.509, respectively, and the specific gravity of the sand is 2.7. Their study shows that different test setups may yield dramatically different K_α values, as seen in Figure 23. Also, Fig 24 shows that applying initial static shear stresses on the same sand (silica sand) under similar conditions may suggest a negative effect when tested on the simple shear device (i.e.: $K_\alpha < 1$) whereas it shows a positive effect during a triaxial test (i.e.: $K_\alpha > 1$)

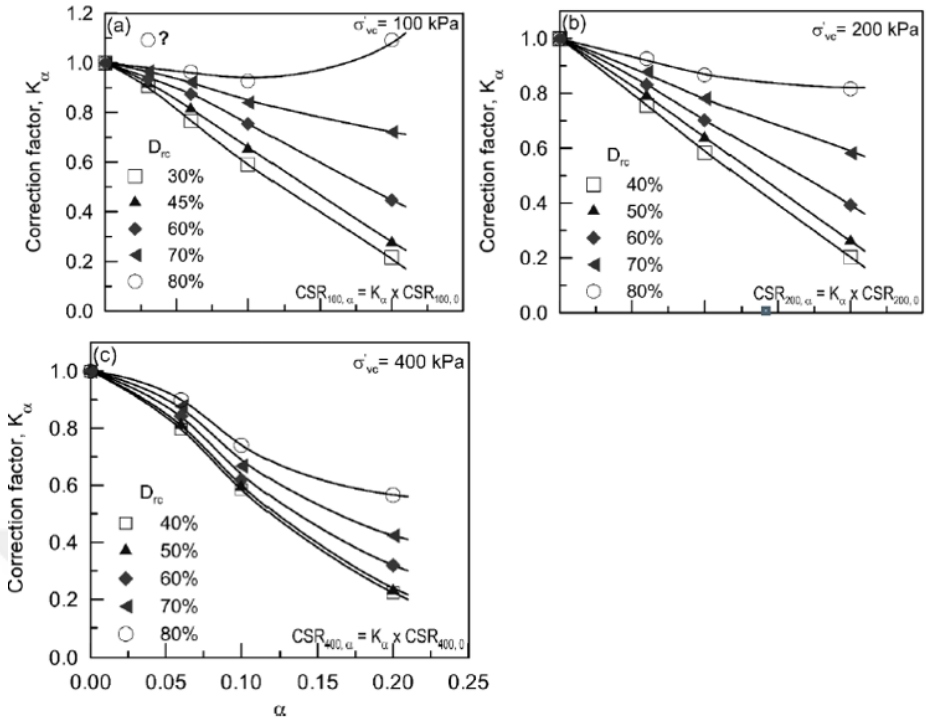

Figure 22. Variation of K_α with α for samples with different relative densities (Sivathayalan and Ha, 2011)

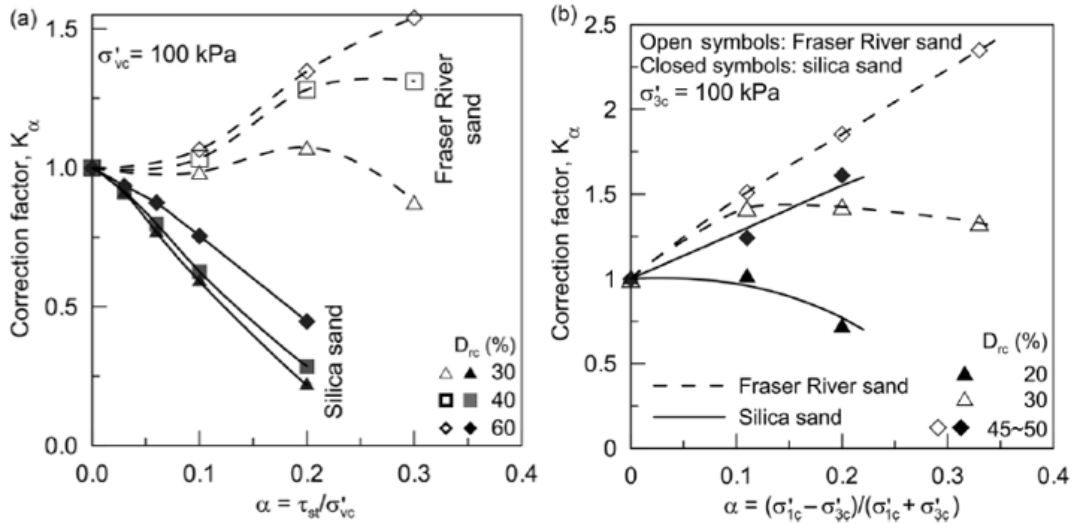

Figure 23. Variation of K_α with soil type and test set ups: a) simple shear loading test; b) triaxial loading (Sivathayalan and Ha, 2011)

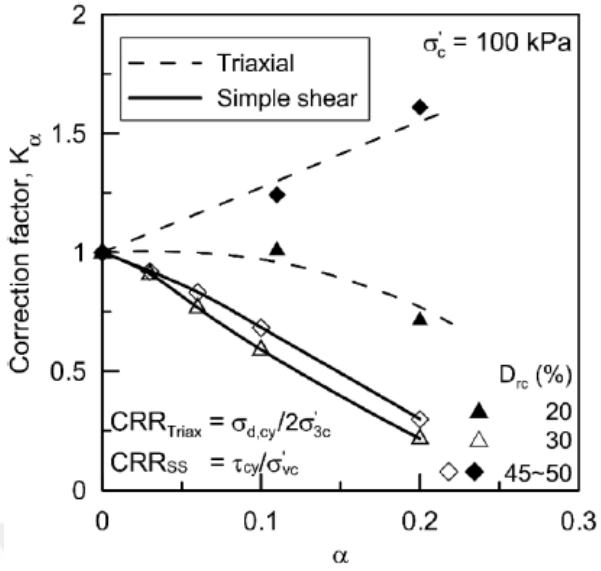

Figure 24. Dependence of K_α on loading mode in subrounded silica sand (Sivathayalan and Ha, 2011)

Umar et al. (2021) performed tests on Toyoura sand prepared by air pluviation by using a hollow cylinder cyclic test setup. They performed some tests with α value up to 0.3, and concluded that or loose and medium dense specimens, the effect of initial static shear is negative (Figure 25). On the contrary, for dense specimens, as initial static shear stress increased, dense specimens showed increased liquefaction resistance if $\alpha > 0.15$. They showed that for loose sand the K_α values are nearly strain independent for shear strain criteria of 3% and 7.5 %; however, for dense sand, K_α is increased as liquefaction criteria for shear strain increased from 3% to 7.5%.

Park et al. (2020) performed tests on the Nakdong River sands with the cyclic simple shear test setup. Their study consists of samples prepared with 40% and 80% relative density samples, and they applied initial static shear stress up to 20% of the consolidation stress, i.e. $\alpha = 0.2$. The measured K_α values showed a good agreement with the predicted K_α zones based on the Harder and Boulanger method (Figure 26).

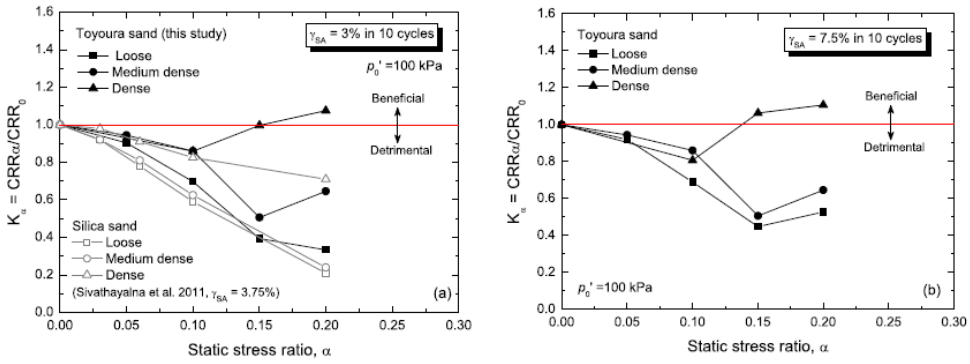

Figure 25. K_α dependence on different strain levels (Umar et al, 2021)

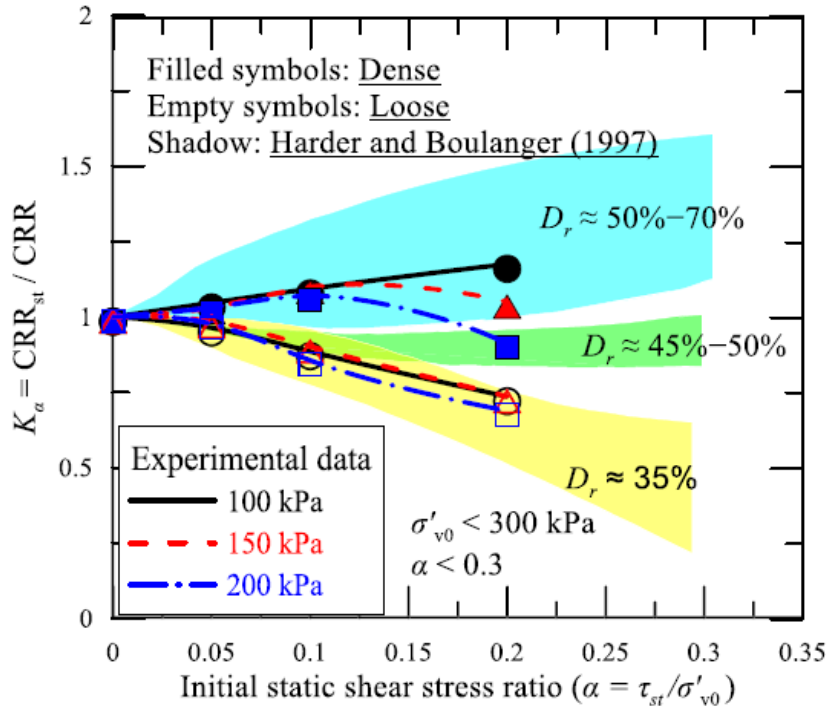

Figure 26. Comparisons of K_α curves with predictions by Harder and Boulanger method as a function of initial vertical effective stress (Park et. al. 2020)

CHAPTER 3

HOLLOW CYLINDER TORSIONAL SHEAR TESTS

3.1 Introduction

Numerous researchers performed laboratory tests to understand the soil liquefaction and the affecting parameters. For that purpose, varying dynamic tests were performed with different setups. This chapter presents a summary compiled from the literature for hollow cylinder cyclic torsional tests. Subsequently, the newly assembled test setup for this study will be introduced.

3.2 Hollow Cylinder Test in Literature

The hollow cylinder test specimen bears a resemblance to a triaxial test specimen, distinguished by its hollow configuration and the application of torsion. Torsion can be applied from either end of the specimen. When the internal cell pressure becomes different than the outer one, the sample is subjected to circumferential or tangential stresses. (Figure 27).

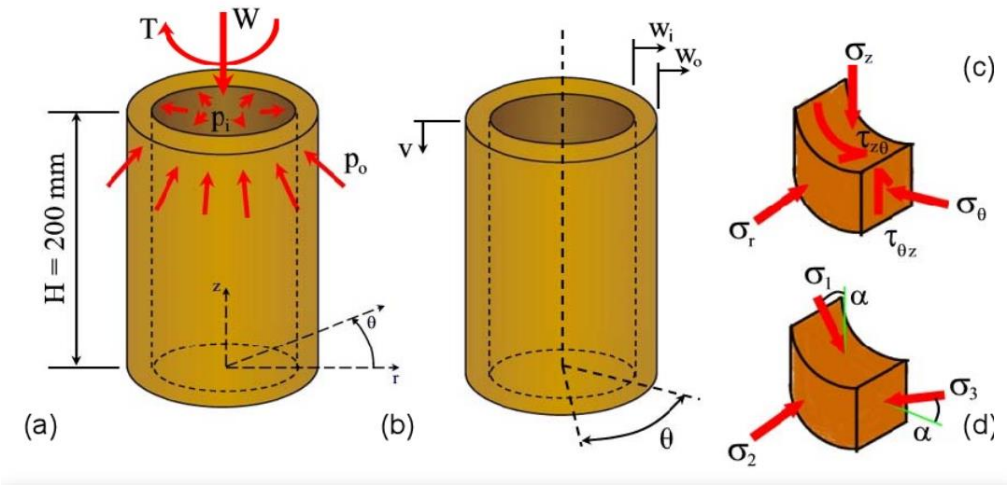

Figure 27. Stress and deformation states of the hollow cylinder sample

The combination of radial, axial, and tangential stresses, in tandem with torsional shear, confers the hollow cylinder test a remarkable degree of adaptability." (Jefferies and Been, 2016). The advantages of a hollow cylinder configuration were acknowledged in the early 1970s by researchers in soil dynamics. Hollow cylinders were used with resonant column devices by Drnevich (1970), Hardin (1972) in order to study damping ratios of sands, clays, and other materials. Researchers in Japan used hollow cylinders to study soil liquefaction. Ishibashi and Sherif (1974) studied the effect of initial coefficients of lateral stresses on liquefaction by using a torsional simple shear device.

Ishihara and Yasuda (1975) applied irregular excitations to sand samples and compared the results to those from dynamic triaxial compression tests. Iwasaki et al. (1978) combined the resonant column with a slower cyclic torsional device to investigate a broad range of shear deformation levels and study their effects on the moduli.

Saada et al. (1978) conducted extensive tests in the resonant column and determined and compared the moduli of isotropic and K_0 consolidated anisotropic kaolinite. In 1980, Ishihara et al. used hollow cylinders to study the effects of principal stress rotation and its influence on cyclic strength of sand.

In 1983, Hight et al. developed a large hollow cylinder device and used it to study anisotropy and the influence of the principal stress rotation on the behavior of saturated sands. They

used finite element simulations to determine the optimum dimensions to be given to the specimen. Various measuring devices were needed to ensure proper data acquisition and instrumentation, thus limiting the use of large hollow cylinder devices to laboratory-prepared specimens only. Saada and Macky (1984, 1985) and Saada (1988) studied the dynamic behavior of laboratory-prepared and natural clays.

Vaid et al. (1990) introduced a new hollow cylinder torsional apparatus suitable for investigating soil behavior under generalized stress paths, including principal stress rotations and characteristics of the earthquake and offshore wave loadings (Figure 28). Throughout the years, improved measurement systems have been used in torsional testing. A summary of the progress in hollow cylinder testing is presented in Table 1.

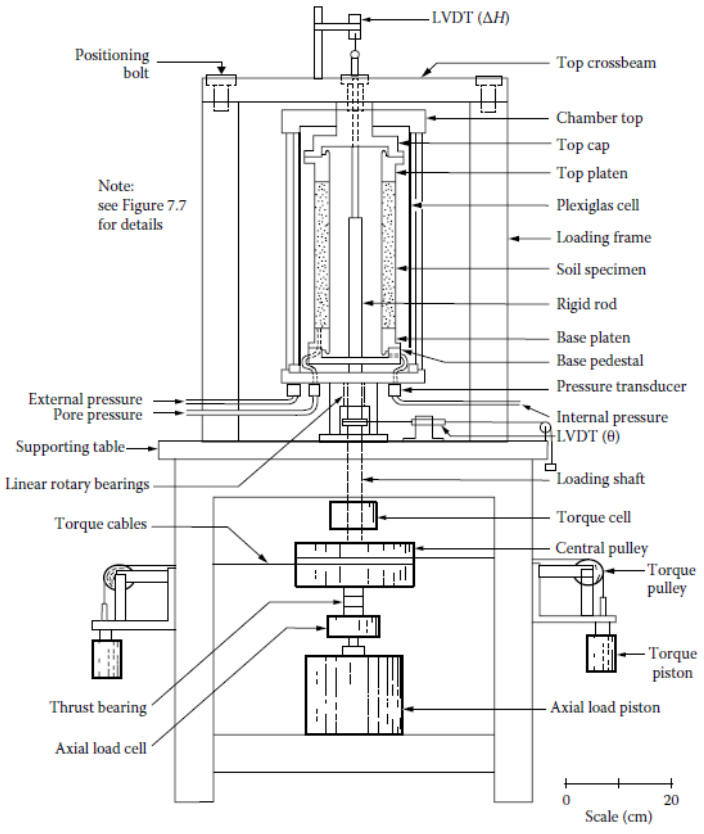

Figure 28. A schematic drawing of the test setup (Vaid et al., 1990)

Table 1. A summary of the hollow cylinder tests (Hight et al., 1983)

Reference	Sample dimensions(mm)			Loading capabilities			Subject of investigation
	D_i	D_o	H	p_o/p_i	W	M_T	
Kirkpatrick (1957)	63	102	152	+			Influence of σ_2 on failure of sand
Whitman & Luscher (1962)	25	38/51/76	76/127	+			Strength characteristics of hollow cylinders of sand
Broms & Ratnam (1963)	76	152	114	+	+		Effects on anisotropic consolidation on deformation and strength of clay
Wu et al. (1963)	76	102	152	+	+		Failure envelope in sand and clay
Broms & Jamal (1965)	76	152	305	+	+		Analysis of triaxial test on sand
Esrig & Bemben (1965)	76	102	203	+	+		Failure conditions in sand
Suklje & Drnovesk (1965)	40	64	80	+			Tensile deformation of clays
Broms & Casbarian (1965)	76	127	254	+	+	+	Effect of principal stress direction and magnitude of σ_2 on shear strength of clay
Saada & Baah (1967)	51	71	151	+	+	+	Anisotropy in the deformation and strength of clay
Lomise et al. (1969)	250	310	180	+	+	+	No data presented
Barden & Proctor (1971)	38	102	152	+	+		Drained strength of granular material
Jamal (1971)	25/51/76	102	203	$p_o=p_i$	+		Shear strength of sand in extension
Jamal (1972)	35	60	60	+	+		Analysis of triaxial test on clay
Ishibashi & Sherif (1974)	51	102	13-25	+	+	+	Effect of K_o on liquefaction of sand
İshihara & Yasuda (1975)	60	100	70	+	+	+	Liquefaction of sand under irregular cyclic loading
Lade (1975)	180	220	50	$p_o=p_i$	+	+	Influence of stress reorientation on stress-strain behaviour of sand
Ishihara et al. (1980)	60	100	106	+	+	+	Effect of principal stress rotation on liquefaction of sand
Dusseault (1981)	51	102	200/240	+	+		Tunneling and pressuremeter testing in sand
Muramatsu & Tatsuoka (1981)	60	100	100	$p_o=p_i$	+	+	Cyclic undrained stress-strain behavior

D_i = Inner diameter, **D_o** = Outer diameter, **H** = Height, **P_o** = Outer pressure, **P_i** = Inner pressure,

Po/Pi shows the ability of application of different outer and inner pressures,

W = Axial load, **M_T** = Torsional load

3.3 The hollow cylinder testing apparatus used in this study

The hollow cylinder torsional cyclic test setup, designed by Prof. Kemal Onder Cetin and Dr. H. Tolga Bilge and locally manufactured in Ankara, is used in this study. It is shown in Figure 29.

Figure 29. The hollow cylinder torsional shear apparatus used in this study

Test specimen has 15 cm and 10 cm outside and inside diameters, respectively. After numerous modifications to the setup, the final specimen height was limited to a maximum of 28 cm, considering the tendency of the dense specimens to dilate. As seen in Figure 30,

the pneumatic piston above the apparatus can apply the axial force on the specimen (if needed), and the torque is applied by a stepper motor placed under the base platform directly attached to the bottom pedestal of the test setup. To prevent the movement of the top pedestal during cyclic loading; it is attached to the sides of the frame by sliders. By doing so, the upper part is fixed against rotation; however, it is still free to move in the vertical direction, enabling axial deformations. Unlike the conventional triaxial specimens, the top pedestal has to be fixed to the top pedestal, which creates an uplift pressure and may cause an extension of the specimen. To prevent this, dead loads are applied via hangers attached to the top part of the specimen. While increasing back pressure on the specimen, the load cell and LVDT are checked carefully, and necessary dead loads are added to keep the initial height of the sample constant, as illustrated in Figure 31.

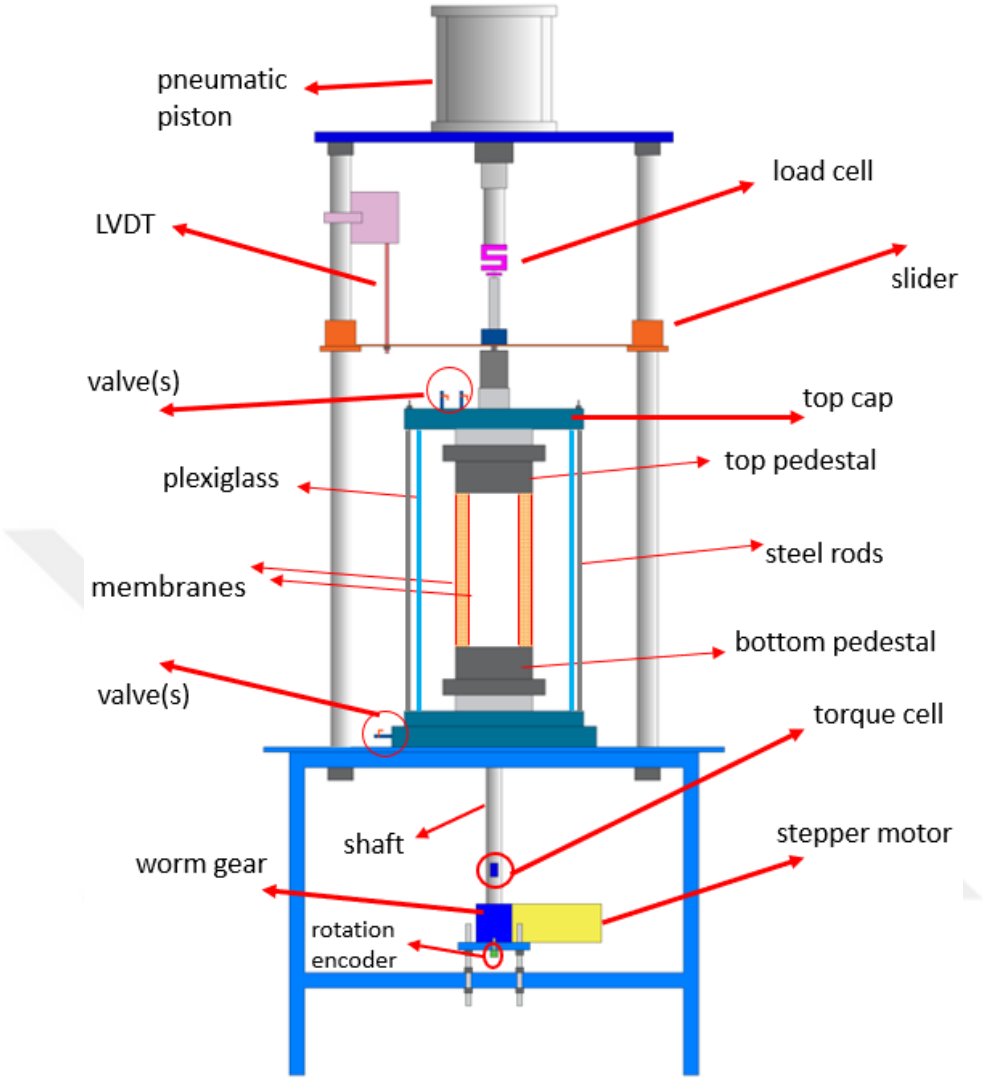

Figure 30. Schematic drawing of the test setup and its components

Figure 31. Dead load hangers were applied to prevent extension due to uplift

Axial load is monitored by the load cell attached between the piston and upper pedestal. A torque cell custom-designed and manufactured measures the torque applied to the specimen. As shown in Figure 31, pore pressure in the specimen was measured by a pore pressure transducer, which is attached to the same valve located at the bottom of the test setup. LVDT makes measurements of the axial displacements of the specimen. The rotation of the lower pedestal due to applied torque is measured by a rotational encoder attached to the shaft between the motor and the lower pedestal (Figure 30). This equipment will be further introduced during the discussions of the test preparation procedure.

A data logger is designed and manufactured to acquire custom-made torque cell and rotational encoder data. Inner and outer cell pressures (σ_2 and σ_3) were applied via the cell pressure unit. In this study, both inner and outer cell pressures were selected as identical. Therefore, only one single-cell pressure unit is used. The vacuum pump keeps the membrane stretched and maintains the sand specimen's shape and form during the test setup.

While developing the torsional shear test apparatus, several conditions were taken into consideration as suggested by Lade (1981):

- The apparatus should allow for significant normal and shear deformation without introducing uneven stress or strain distribution in cylindrical specimen.
- Specimen should have the least tendency to slip during loading. In our study, excluding the porous stone areas, a portion of the test specimen is glued to the cover of the top and bottom pedestals to prevent slippage between the pedestals and the test specimen. (Figure 32)
- The horizontal stresses on both surfaces of the test specimen (interior and exterior) should be identical to simplify the analyses. For that purpose, in our studies, the same water pressure is applied to both cells
- The volume of the specimen should be such that it behaves as a thin-walled tube, in which case the stress condition imposed on the specimen can be regarded as a plane stress condition. That leads to the satisfactory dimensions of the specimen, which will be discussed briefly while designing the test setup.

Specimen dimensions have significant effects on the test. Thus, the issues discussed below were considered while selecting sample sizes.

3.4 Geometry of the Samples

3.4.1 Thickness

Hight (1983) proposed the requirements for wall thickness to satisfy uniformity through the sample as follows:

• The wall thickness should be significantly greater than the largest grains so that the failure mechanisms are prevented from being restricted,

• The sample should have a volume ample enough to accommodate the possible disturbance caused by membrane penetration.

• The density should be consistent

In their study, the specimen has a width of one inch, almost identical to our device (Figure 32). Sayao and Vaid (1991) also proposed a specimen thickness between 20 - 26mm. In our tests, specimen thickness is around 25 mm.

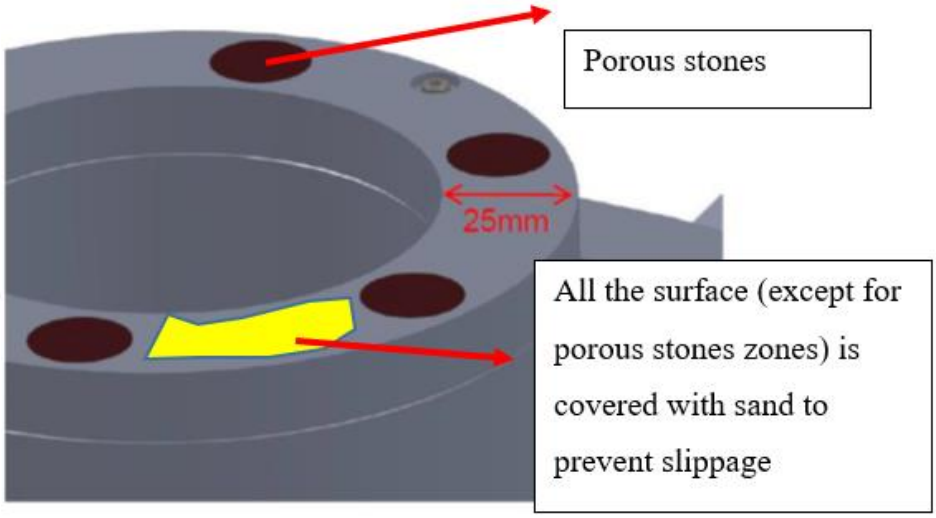

Figure 32. Thickness of the specimen

3.4.2 Radius

Moving away from the device's ends decreases the magnitude of the forces exerted on the specimen. The criteria proposed by Saada (1981) satisfy a reasonable central zone free from these boundary effects.

In addition to the thickness, the mean radius is of utmost importance for hollow cylinders. The radial frictional forces imposed upon the specimen by the platens cause various forces on the specimen, which quickly decrease away from the top and bottom.

Considering the specimen as a thin shell, Saada (1988) stated that satisfying the following criteria serves a reasonable central zone free from end effects and friction-induced stresses on the specimen

$$\frac{R_i}{R_o} \geq 0.65 \tag{3.1}$$

In Eq. 3.1, R_i is the inner, and R_o is the outer radii of the specimen. In our device, as seen in Figure 33, this ratio is 0.67 (5 / 7.5 = 0.67) and satisfies the criteria.

Sayao and Vaid (1991) also proposed an upper limit for this ratio, as given in Eq. 3.2, which is also satisfied in our test setup.

$$0.65 \leq \frac{R_i}{R_o} \leq 0.82 \tag{3.2}$$

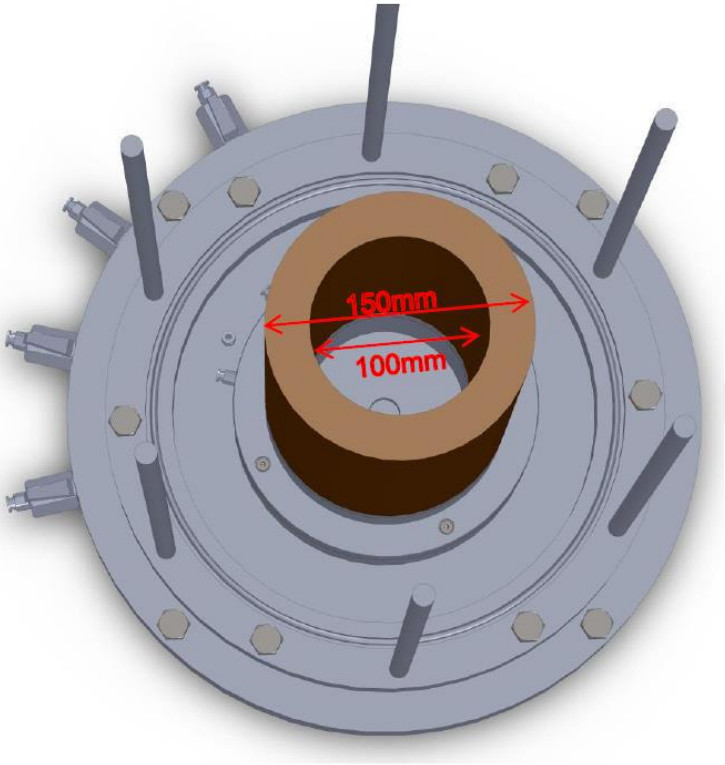

Figure 33. Inner and outer radius of the specimen

3.4.3 Height

To create a reasonable central zone free from end (boundary) affects, and enough height for proper stress, strain, and pore pressure measurements, Saada and Townsend (1981) proposed the criterion given in Eq. 3.3.

$$H \geq 5.44\sqrt{R_o - R_i} \tag{3.3}$$

In our device, as seen in Figure 34, the height satisfies this criterion, shown below.

$$H \geq 5.44\sqrt{7.5 - 5} = 8.6\ cm \tag{3.4}$$

Moreover, Lade (1981) proposed the following criterion as given in Eq. 3.5, where R_m is the mean radius of the specimen.

$$H > 1.5 * R_m \tag{3.5}$$

In our device, as seen in Figure 34, the height (H = 27 to 28cm ≥ 1,5 x (7.5 + 5) / 2 = 9.37 cm) satisfies this criterion.

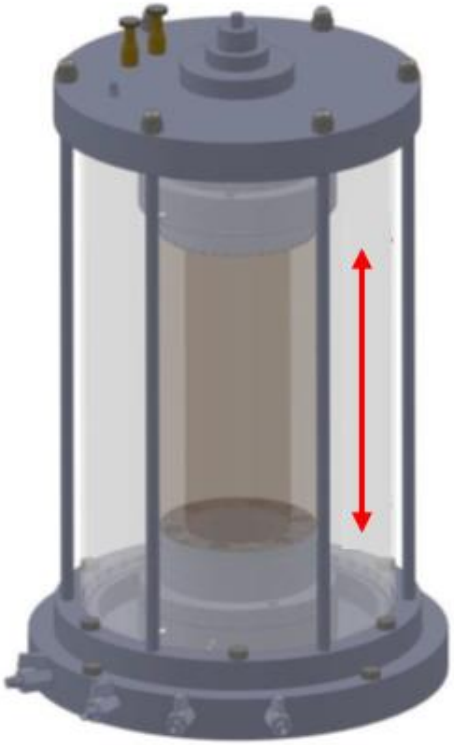

Figure 34. Height of the specimen with inner and outer membranes

3.5 Stress distribution during tests and necessary corrections

The hollow cylinder torsional test is one of the few equipment able to control all four parameters (3 principal stress values and their rotation). These are done by controlling the axial load, torsion, internal and external cell pressure.

During the tests, the quantities to be measured are listed as follows:

• Axial force

• Torque

• Pore water pressure (if undrained case)

• Pressures inside and outside Hollow Cylinder

• Axial deformation

• Changes in radius

• Volume change (if drained case)

• The relative rotation of two sections along the length of the sample

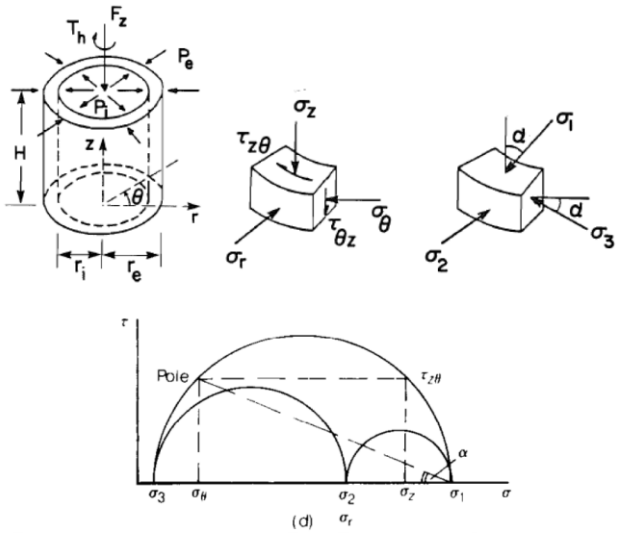

Figure 35. Stress distribution during the test on hollow cylinder specimen (Saada and Townsend, 1981)

Figure 35 shows the applied forces and stresses on the specimen and the resulting induced stresses during the tests. The combination of axial and torsional stresses leads to principal stresses, which are inclined on the axes of symmetry of the material.

The outcomes of these tests are analyzed by treating the whole specimen as a unified cylindrical element. Given the varying shear stresses across the cylinder's wall under different loading scenarios, it is essential to employ average stress and strain values.

Average stress and strain values have typically been calculated based on the principle of work equivalence, equating the work of applied forces and torques to the combined work of internal stresses and strains.

In hollow cylinder torsional shear tests, the radial stress (σr) generally represents the (σ2). When a torque is applied, the principal stresses rotate (α), as depicted in Figure 35. In order to determine average stress components, Mohr’s circle is utilized.

3.6 Post-processing of the test data

3.6.1 Corrections for Sample Geometry

Prior to the shearing phase, the specimen's geometry must be meticulously ascertained to determine induced stresses and strains. The height of the specimen and both radii of the specimen are obtained following the sample preparation. During consolidation, the specimen volume will change while allowing for drainage. Consequently, specimen dimensions should be adjusted to reflect any changes that happened in the consolidation stage. This necessitates the measurement of two features of the specimen: change in height and change in volume. If to assume uniform deformations occur during consolidation, corrections can be applied. As direct measurement of radial deformation is impractical, Tatsuoka et al. (1986) proposed a correlation between Ro and Ri based on volumetric and axial changes.

$$R_o = \sqrt{\frac{1-\varepsilon_v}{1-\varepsilon_z}}(R_o)_0 \tag{3.6}$$

$$R_i = \sqrt{\frac{1-\varepsilon_v}{1-\varepsilon_z}}(R_i)_0 \tag{3.7}$$

Equation 3.7 shows the initial outer diameter before consolidation as $(R_o)_0$ and inner radius $(R_i)_0$. ε_v and ε_z represent volumetric and axial strains. These equations posit that the proportional change in the outer radius relative to its initial value is equivalent to the proportional change in the inner radius relative to its initial value. In this study, inner and outer cell pressures are equal. Therefore, no significant change is expected during the shearing. Hence, the inner and outer diameter changes are not monitored in this study.

3.6.2 Corrections for System Compliance and Membrane

The cyclic loading is applied to the specimen via a stepper motor. Between the bottom pedestal and the motor, the friction between rotating parts of the setup becomes significant due to corrosion, and the actual torque applied on the specimen may be dramatically different than recorded during the tests. It is essential to apply corrections to the applied load, considering the abovementioned corrosion problem. Moreover, as deformation amounts increase, the membranes will stretch more and demand a portion of the applied load. To assign these losses, namely system compliance and membrane effect, some tests were made replacing soil specimen with water, and corresponding losses were obtained regarding the rotation amount under varying cell pressures. Applied tests and observed losses will be explained in the following sections.

3.6.2.1 Theoretical Background on Membrane Corrections

The test specimen is wrapped between 2 latex membranes (inner and outer membranes); therefore, the membranes will carry some of the loads applied to the specimen. The dimensions and thickness of the membranes affect the test results due to the following reasons:

- Torsional resistance of inner and outer membranes will reduce the stresses acting on the specimen,
- Especially in case of high pressures in the cell, penetration of the membrane inside the particles causes problems, the extent of which increases with increasing particle sizes. This is important in liquefaction tests on coarse-grained soils. During tests, pore pressure is generated, and effective stress is reduced, which causes the membrane to move outward. This movement mimics pore water drainage, leading to an overestimation of liquefaction resistance. (Towhata, 2009)

Due to geometry, the area exposed to loads is large, so applying corrections to data output becomes significant. Assuming both the membranes deform as cylinders, the vertical load

carried by the membranes, P_m, is often calculated by:

$$P_m = A_m * \sigma_m = A_m * E_m * \varepsilon_z \tag{3.8}$$

In Eq. 3.8, A_m is the total membrane cross-section area, σ_m is the vertical stress on the membranes, E_m is the elastic modulus of membrane material, and ε_z is the axial strain of the membrane, which is assumed to be the same as of the specimen, assuming no slippage occurs. In the tests, axial deformation of the specimen was negligible. Therefore, membrane correction due to axial strain was ignored.

The shear strain of membranes, γ_m, should be equal to the shear strain of the specimen during the test due to the continuum principle. The shear stress of the membranes is estimated as follows:

$$\tau_m = G * \gamma_m \tag{3.9}$$

The torque resisted by the outer and inner membranes will be:

$$T_m = \int R_m \tau_m dA + \int r_m \tau_m dA = \int_0^{2\pi} R_m^2 \tau_m t_0 d\theta + \int_0^{2\pi} r_m^2 \tau_m t_i d\theta = 2\pi\tau_m (R_m^2 t_0 + r_m^2 t_i) \tag{3.10}$$

In Eq. 3.10, R_m is the mean radius of the outer membrane, r_m is the mean radius of the inner membrane, t_o is the thickness of the outer membrane, and it is the thickness of the inner membrane.

As expressed by this equation, the torque resisted by membranes becomes significant once the soil is subjected to larger strains. In our study, sand specimens are liquified after double amplitude shear strain levels exceeding 8 to 12 %. Rather than dealing with the losses separately, i.e. loss due to system compliance and stretching of the membranes, resultant losses are directly measured against rotation under corresponding cell pressures. The conducted tests and results will be briefly explained in the next section.

3.6.2.2 Measuring System Compliance and Membrane Effects

Due to system compliance because of friction and membrane stretching under large deformations, a set of tests is done with 300 and 500 kPa confining stresses. Membranes were filled with water rather than soil, and large rotations were applied during the tests (Figure 36a). Upon applying the desired cell pressure, the test is started, and the system is rotated in clockwise and counterclockwise directions. During the tests, torque and deformation are obtained from the torque cell and rotational encoder, respectively. The results of the tests can be seen in Figures 37 and 38. At the beginning of the loading, when the average shear strain is zero for 300 kPa cell pressure, static shear stress is 5 kPa for clockwise (CW) direction movement and 8 kPa for counterclockwise (CCW) direction movement. These values become 11 kPa for the clockwise direction and 2 kPa for the counterclockwise direction when the test is conducted under 500 kPa. This means that regarding the cell pressure applied during the test, stress losses due to system compliance and membrane stretching vary, too. For that significant difference, a simplified model based on shear strain and cell pressure to assess system compliance and membrane stretching losses is established and considered both during cyclic loading and interpretation of test results steps.

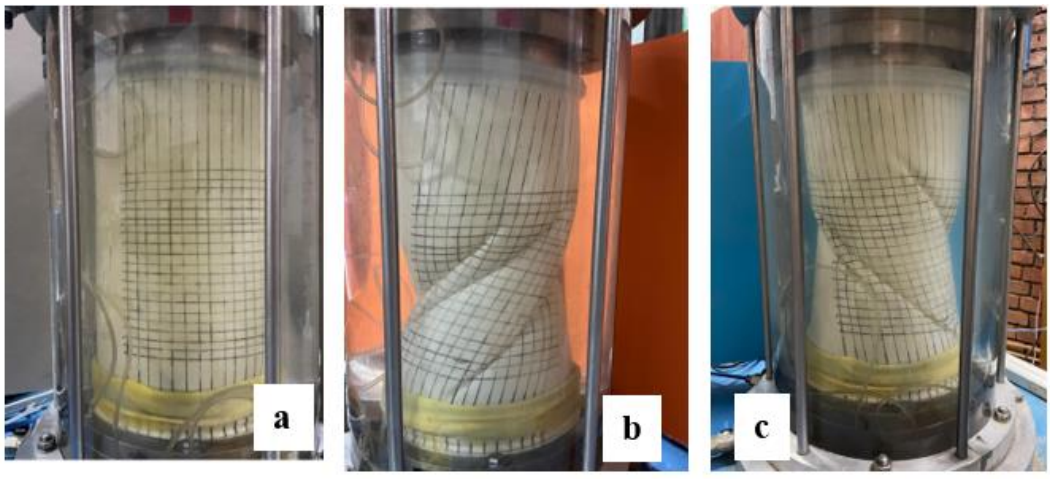

Figure 36. System compliance and membrane test a) initial situation; b) significant deformation in CW direction; c) significant deformation in CCW direction

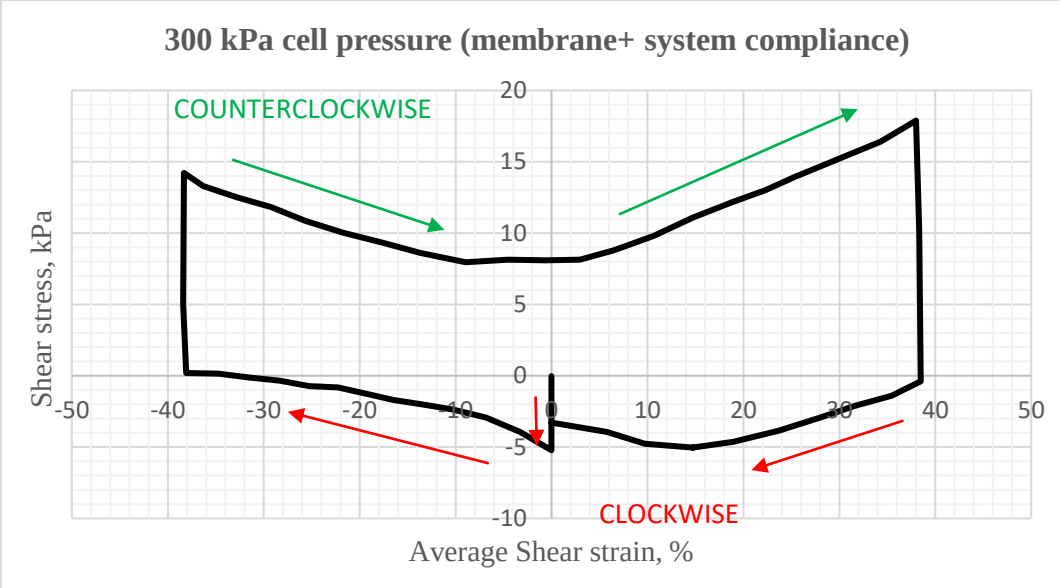

Figure 37. Resultant stress loss on specimen due to membranes and system compliance under 300 kPa cell pressure

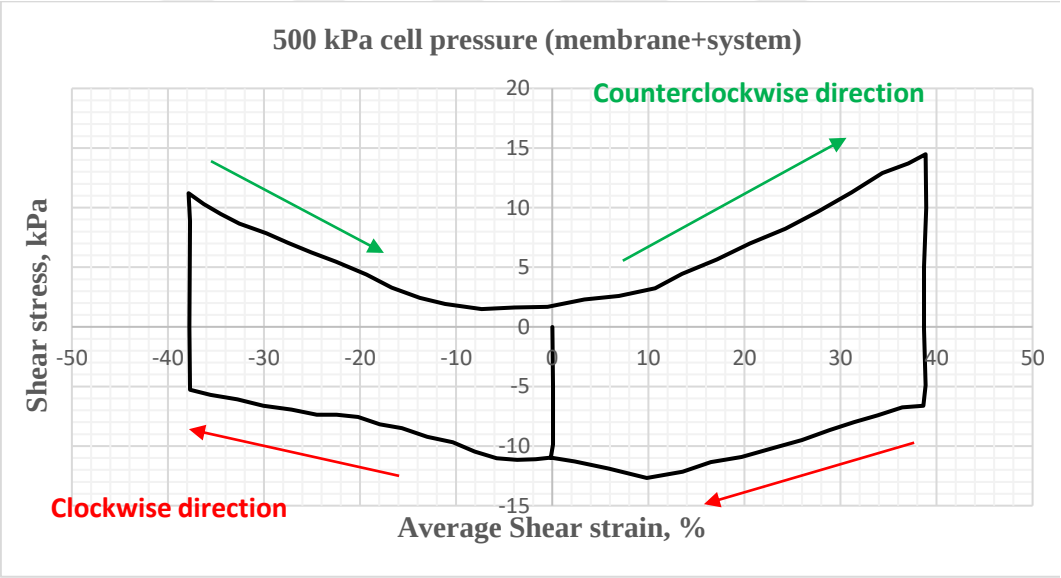

Figure 38. Resultant stress loss on specimen due to membranes and system compliance under 500 kPa cell pressure

3.6.2.3 A Simplified Shear Strain and Cell Pressure Dependent Model for Assessing System Compliance and Membrane Effects

Tests conducted to assess system compliance and membrane effects show that stress losses become significant if the system is subjected to large shear strains. Considering the start point of the test (i.e., zero shear strain), approximately 10% shear strain range in both directions has nearly a constant stress loss. However, passing beyond 10% shear strains in any direction significantly affects the stress loss, more particularly due to membrane stretching. That is why if the strains are not larger than 10% in any direction, a constant shear compliance can be presumed, and based on that value, shear stresses may be modified. However, for a larger degree of shear strains, a correction model is developed for both cases (300 kPa and 500 kPa), considering rotation directions, too. Figures 39 and 40 show the resulting fitted model for both directions under 500 kPa cell pressure.

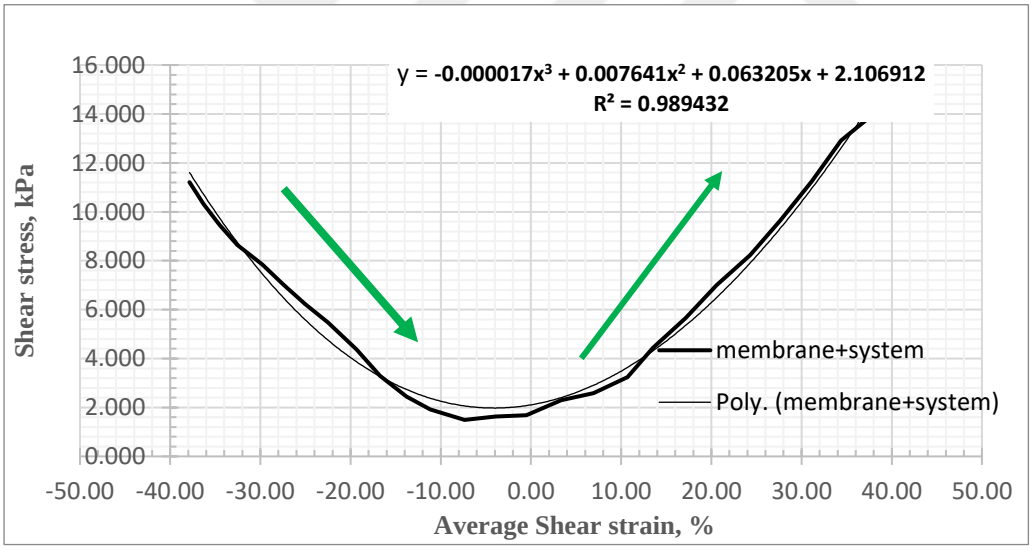

Figure 39. Model for counterclockwise direction (positive shear) under 500 kPa

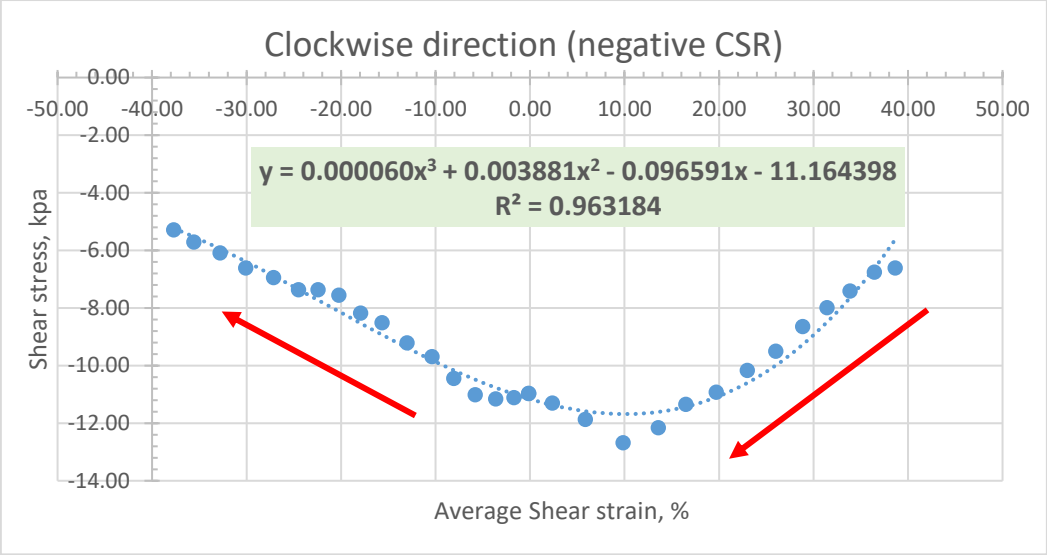

Figure 40. Model for clockwise direction (negative shear) under 500 kPa

The same model is also developed for the 300 kPa cell pressure case. In Table 2, the corresponding coefficients of the model are presented for 300 and 500 kPa cell pressures in both directions. Actual shear stress applied on the specimen at any strain level is calculated by taking the losses due to system compliance and membrane stretching into consideration during tests.

Table 2. Model coefficients for the system compliance + membranes

Cell pressure, kPa	Direction		Cell pressure, kPa	Direction	
500	CW	CCW	300	CW	CCW
Parameter	Coefficient		Parameter	Coefficient	
γ^3	0.000060	-0.000017	γ^3	0.000760	-0.000015
γ^2	0.003881	0.007641	γ^2	0.002800	0.005350
γ	-0.096591	0.063205	γ	-0.112168	0.072236
	-11.164398	2.106912		-3.980902	8.535960

CHAPTER 4

TESTING PROCEDURE AND RESULTS

4.1 Introduction

In this study, Çine sand samples are tested. They were prepared with three different relative densities. Preparation of these “loose,” “medium,” and “dense” specimens will be explained next followed by presentation and discussion of test results.

4.2 Çine Sand

Çine sand is a poorly graded sand composed of mainly Quartz minerals. A sample of sand is shown in Figure 41, along with its grain size distribution shown in Figure 42. The wet sieving technique is performed according to the ASTM D1140-17 specifications, and it is seen that the fines content of the Çine sand is less than 2%. Maximum and minimum void ratio of Çine sand is estimated according to ASTM D4253 and ASTM D4254. The index parameters of Çine sand can be seen in Table 3. Based on the test results, Çine sand is classified as poorly graded sand (SP) according to the Unified Soil Classification System (USCS). The angle of shearing resistance corresponding to different relative density levels obtained from the direct shear tests with a comparison with FHWA is provided in Table 4 and Figure 43 (Soylemez, 2017).

Figure 41. Çine sand

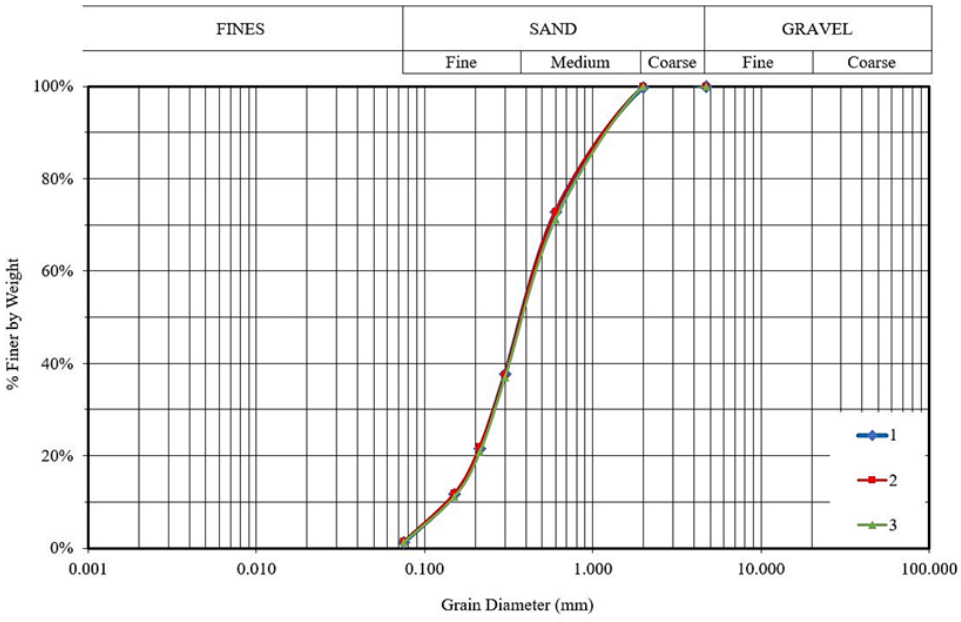

Figure 42. Grain size distribution of Çine sand

Table 3. Index properties of the Çine sand

D_{10} (mm)	0.135
D_{30} (mm)	0.255
D_{60} (mm)	0.47
C_c (coefficient of curvature)	1.02
C_u (coefficient of uniformity)	3.76
Fines content % (% finer than #200 sieve size)	1.35
Maximum Void Ratio (e_{max})	0.825
Minimum Void Ratio (e_{min})	0.505
Specific Gravity	2.66

Table 4. Direct shear test results (Soylemez, 2017)

Relative density, %	Internal friction angle, ϕ'
34	32.6
50	34.5
70	37.9

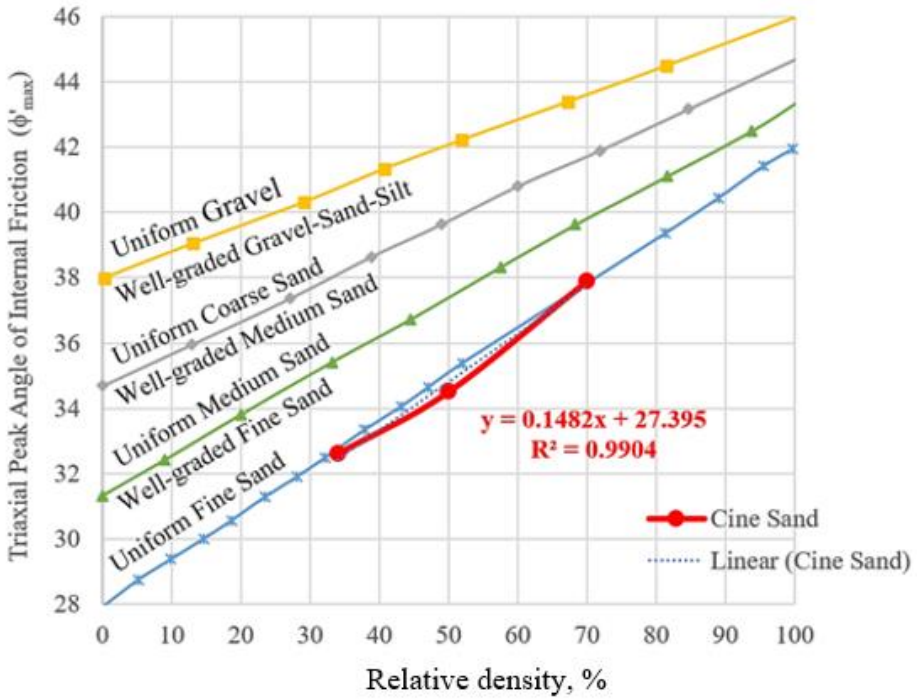

Figure 43. Direct shear test results as compared with FHWA

Moreover, as shown in Figure 44, the roundness (R) and sphericity (S) of the Çine sand grains are estimated as 0.28 and 0.58 based on the Zheng and Hryciw (2016) method (Aksoy, 2024). In the same study, the critical state angle of shearing resistance is also estimated using the simplified method suggested by Santamarina and Cho (2001). As seen in Figure 45, the critical state angle of the shearing resistance of Çine sand is measured as 33◦

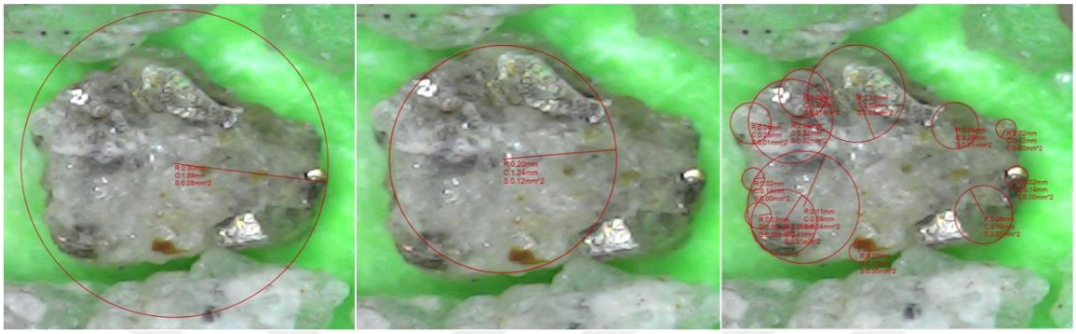

Figure 44. Circles are drawn to determine the roundness and sphericity of particles (Aksoy, 2024)

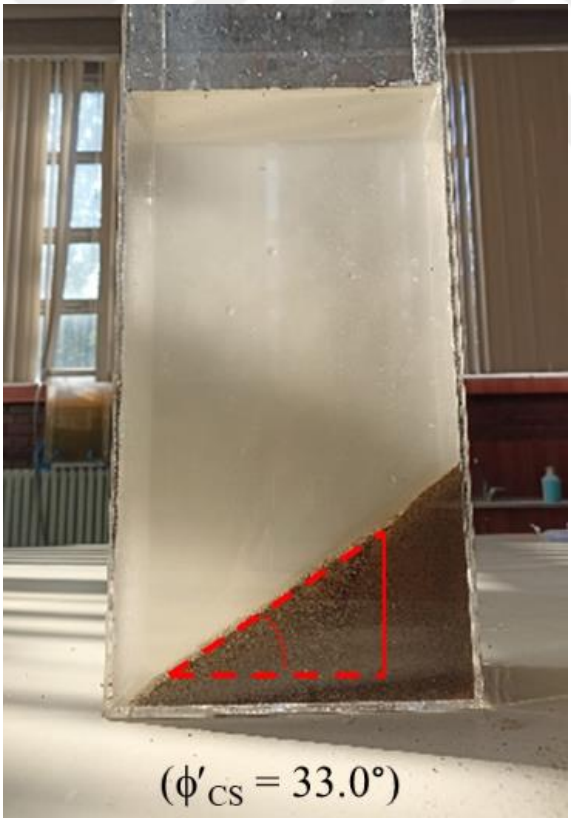

Figure 45. The critical state angle of shearing resistance of Çine sand (Aksoy, 2024)

4.3 Sample Preparation Steps

Test preparation steps are not very different from those of a triaxial test. However, the larger size of the hollow specimen and the presence of two membranes (inner and outer ones) demand more attention, and the sample procedure takes more time. A typical hollow cylinder triaxial test specimen preparation takes approximately 4-5 hours, depending on the relative density of the specimen. Test procedures and equipment are explained below.

Figure 46-a shows both inner and outer molds and membranes. A partially regulated vacuum pump was used to keep the membrane stretched and the sand specimen in its shape while filling the hollow volume. After it was filled with sand at the desired relative density, the vacuum was applied to the specimen (Figure 46b) while removing molds and placing the upper pedestal (Figure 47a). Specimens were prepared by the dry pluviation method, in which target relative density is obtained by pouring the dry sand from a determined height with a corresponding opening of a funnel tip. In this study, three target relative density values, namely 35-40% (loose specimen), 60-65 % (medium specimen) and 80-85% (dense specimen) were targeted to be tested. Loose specimens were prepared by pouring dry sand through a relatively large hose from 1 cm height (10 mm vs 4mm). On the contrary, medium and dense specimens were poured from smaller radius metal pipes (4 mm diameter) with 9 cm and 15 cm heights, respectively (Figure 48). While pouring the soil, a centralizer was used to keep the inner mold steady, and better-quality specimens were with homogenous thicknesses along the cross-section.

Figure 46. a) Inner and outer molds; b) both molds removed while the specimen is under vacuum

Figure 47. a) Upper pedestal is attached; b) top cap and plexiglass in placed

Figure 48. Air pluviation materials (centralizer, funnels, and metal pipes)

After the predetermined sand mass is poured, the top pedestal is placed on top of the sand, and membranes are wrapped around it and fixed by O-rings. Then, a vacuum is applied to the specimen, and the molds are removed carefully. Once vacuum is applied to the specimen (50-60 kPa), vacuum application is not stopped until the inner and outer cells are filled with water, and 50 kPa water pressure is applied to the cells to ensure the specimen keeps its shape without significant deformation. Having placed the upper pedestal, sample height is measured at 3 different locations, and their average is used as the sample height. Then, the plexiglass cell is placed and covered with the top cap to create a sealed environment to fill the cells with water (Figure 47b). After that, the vacuum is decreased gradually to zero while cell pressure is increased in small increments up to 50 kPa, intending to not load the specimen greater than the peak vacuum stress it was subjected to during sample preparation. That is why attention is given to keeping the applied stress on the specimen as constant as possible.

After both inner and outer cell pressures reach 50 kPa cell pressure, the vacuum valve is closed and pump stopped. Carbon dioxide gas is circulated through the specimen. This

procedure is performed to remove the oxygen that is trapped in the specimen. Carbon dioxide is more soluble in water and heavier than oxygen. Replacing oxygen with carbon dioxide is very important since it is desired to have a two-phase soil instead of a three-phase one, i.e., all voids should be filled with water. The carbon dioxide application rate is 2-3 bubbles per second (observed at the top outlet), and this procedure takes 45 to 60 minutes, depending on the relative density of the specimen. For denser specimens, the carbon dioxide application time was longer.

Following this step, de-aired distilled water is flushed through the specimen from the bottom (Figure 49a). At least 1.5 times the pore volume amount of water was flushed and collected at the top part of the specimen. After this, a 50 kPa difference of pressure difference between cell pressure (generally 250-450 kPa) and back pressure (generally 200-400 kPa) is applied to the system, and the specimen is left under these stresses one night (at least 12 hours) to ensure that carbon dioxide is solved in the water. As stated above, corresponding dead weights are placed on the arms while back pressure is increased progressively (Figure 49b).

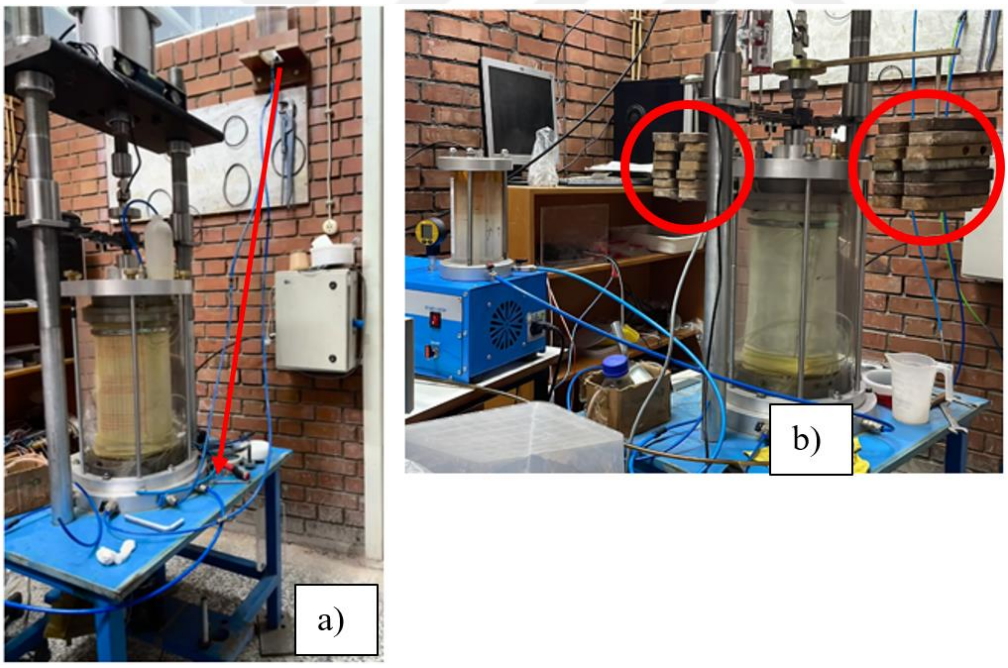

Figure 49. Cells are filled with water, and deaired water is flushed from the container on the wall; b) Dead weights are applied to prevent extension during back pressure

The next day, the degree of saturation is checked by progressively increasing the cell pressure while blocking the back pressure and observing the change of pore pressure of the specimen. If a B value (ratio of the increase in pore pressure to the applied isotropic stress increment) equal to or greater than 0.95 is achieved, then specimen is regarded as saturated. Following this stage, the planned test can be executed with or without an initial shear stress application. If in the test an initial static shear is to be applied, after the consolidation, specimen is sheared until the target torque is observed and then again, sometime is waited until the dissipation of generated excess pore pressure due to initial shearing is completed.

Cyclic loading is applied through the motor (Figure 50) that is attached to the base pedestal of the test set up. It is worthwhile to pronounce that in the tests with initial static shear stresses, initial shear is always applied in the same direction (clockwise direction) and following this, after dissipation of excess pore pressure, cyclic loading is started in the opposite direction (counter clockwise direction). The motor's torque is 12 Nm without considering the losses due to friction and this torque is low. To increase the torque of motor, worm gear is used for a mechanical advantage of 50 times (Figure 50). This modification has a trade off in the form of a reduction in the speed. Motor applies the torque, which induces shear stresses on the specimen, and it is measured by the torque cell that is directly attached in between the motor and the lower pedestal. The rotation of the bottom pedestal is measured by the rotational encoder (Figure 50). The frequency of the loading is 0.025 Hz, and it was kept the same for the all tests in this study. Determination of this frequency can be explained considering Figure 51. The 1st cycle is observed at t_1= 54 min, 21 seconds and 21st cycle is observed at t_2= 77 min, 28 seconds. During this 787 seconds, 20 homogenous cycles are created, by which loading frequency is calculated as

$$f\ (in\ Hz) = \frac{Number\ of\ cycles}{time\ duration\ (in\ second)} \tag{4.1}$$

By using equation (4.1), frequency is calculated as

$$f\ (in\ Hz) = \frac{Number\ of\ cycles}{time\ duration\ (in\ second)} = \frac{20}{787} = 0.025\ Hz$$

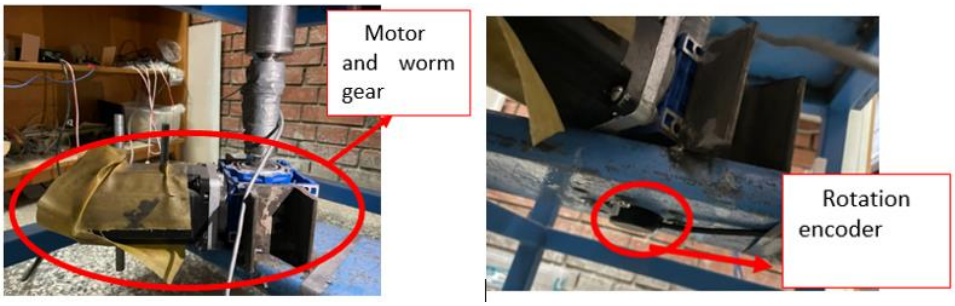

Figure 50. Motor, worm gear and rotation encoder

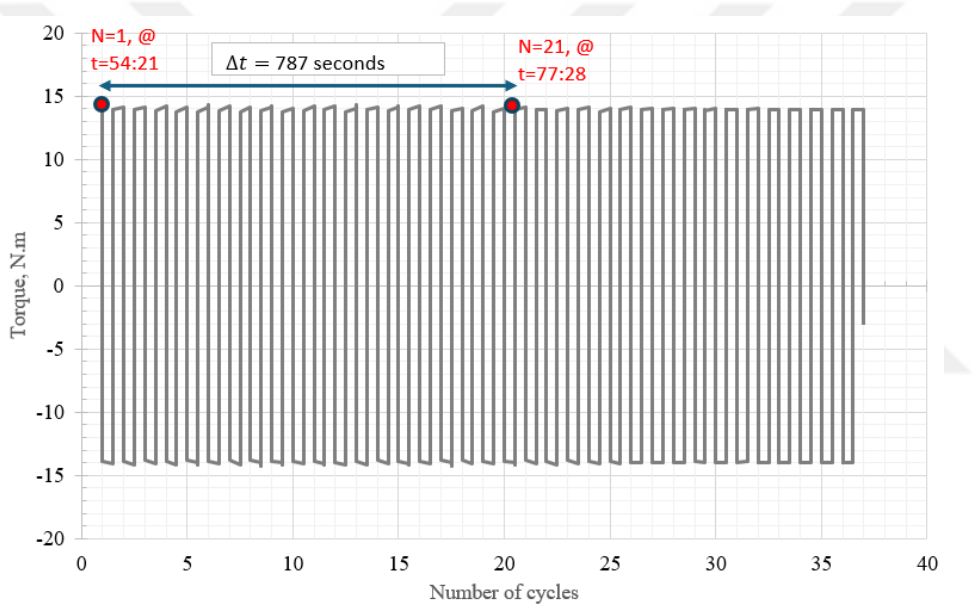

Figure 51. Determination of loading frequency, f=0.025 Hz

The axial load applied to the specimen is measured by an S-type load (capacity is 500 kgf), and the pore pressure generated in the specimen is measured by a pore pressure transducer (capacity is 10 bars). Axial deformation is measured by an LVDT attached to rotation blockers (capacity is 100 mm). Rotation blockers prevent the top cap from rotating but let it move in the axial direction, i.e., the upper part is free to move up and down, but it is fixed against rotation. Therefore, the lower part of the specimen rotates the most while the uppermost part of the specimen has nearly zero deformation (since it is fixed). Tests were

performed in a stress-controlled manner, or it would be better to say torque-controlled manner for undrained specimens, a fixed cyclic stress is applied, and corresponding deformation (axial and rotational) and generated pore pressure are measured. Loading rates, magnitudes, and motor directions are controlled by Arduino software. Tests are continued after liquefaction triggers, and a couple more cycles are applied (attention is paid to the membranes not deforming severely). As mentioned above, the preparation of the test takes 5-6 hours; then a longer duration is needed (generally overnight) to saturate the specimen, followed by a degree of saturation check and consolidation step (nearly 1-2 hours) and finally performing the test takes about 30-45 minutes. One successful test can be performed in two days if things run smoothly.

During the tests, axial deformation, specimen rotation, applied torque, axial load, and generated pore pressure due to loading are measured. A newly designed data logger is used to measure the torque and rotation of the specimen (Figure 52). A software written in Python language is used to obtain and record the data (Figure 53). The relationships summarized in Table 5, which have the test data, are used to develop 4-way plots of the test results, which will be presented in the following pages.

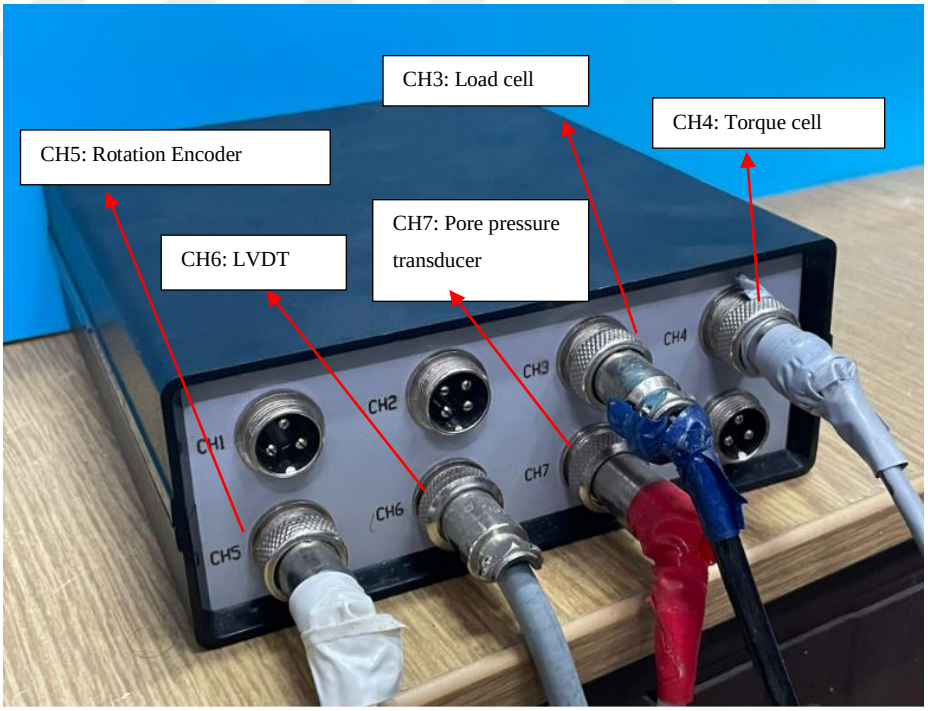

Figure 52. Newly manufactured data logger and used sensors during the tests

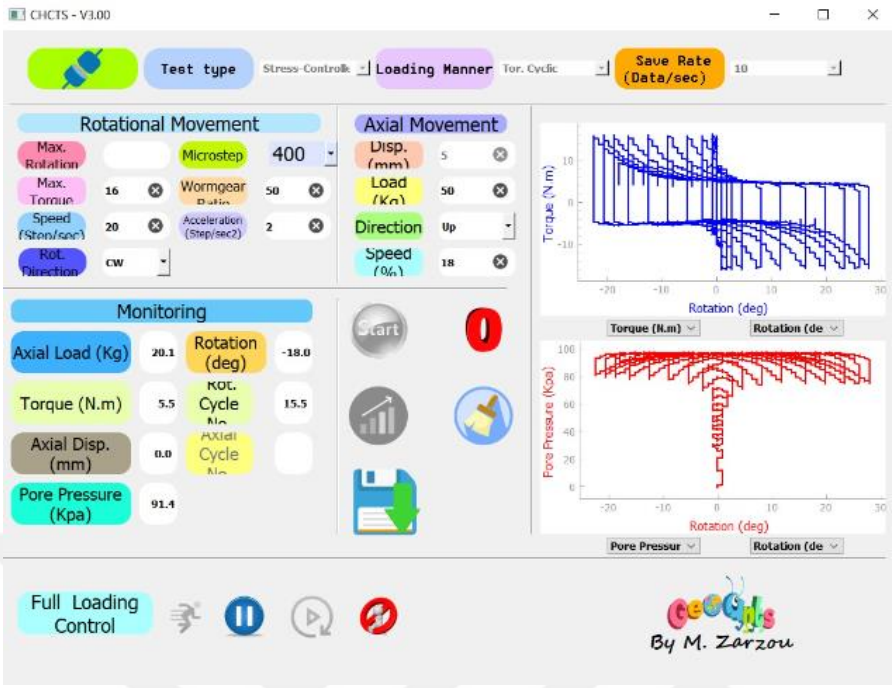

Figure 53. Recorded data and simultaneously drawn graphs

Table 5. Parameters for hollow cylinder testing and their definitions (adapted from Tastan and Carraro, 2022)

Parameter	Definition
Average vertical (or axial) stress	$\sigma_z = \frac{W}{\pi \cdot (r_o^2 - r_i^2)} + \frac{p_o r_o^2 - p_i r_i^2}{r_o^2 - r_i^2}$
Average radial stress	$\sigma_r = \frac{p_0 r_0 + p_i r_i}{r_0 + r_i}$
Average circumferential stress	$\sigma_\theta = \frac{p_0 r_0 - p_i r_i}{r_0 - r_i}$
Average shear stress	$\tau_{z\theta} = \frac{3 \cdot T}{2\pi \cdot (r_0^3 - r_i^3)}$
Average vertical (or axial) strain	$\varepsilon_z = \frac{\Delta H}{H}$
Average radial strain	$\varepsilon_r = -\frac{l_0 - l_i}{r_0 - r_i}$
Average circumferential strain	$\varepsilon_\theta = -\frac{l_0 + l_i}{r_0 + r_i}$
Average shear strain	$\gamma_{z\theta} = \frac{2\theta \cdot (r_0^3 - r_i^3)}{3H \cdot (r_0^2 - r_i^2)}$
Major principal stress	$\sigma_1 = \frac{\sigma_z + \sigma_\theta}{2} + \sqrt{\left(\frac{\sigma_z - \sigma_\theta}{2}\right)^2 + \tau_{z\theta}^2}$
Intermediate principal stress	$\sigma_2 = \sigma_r$
Minor principal stress	$\sigma_3 = \frac{\sigma_z + \sigma_\theta}{2} - \sqrt{\left(\frac{\sigma_z - \sigma_\theta}{2}\right)^2 + \tau_{z\theta}^2}$
Major principal strain	$\varepsilon_1 = \frac{\varepsilon_z + \varepsilon_\theta}{2} + \sqrt{\left(\frac{\varepsilon_z - \varepsilon_\theta}{2}\right)^2 + \gamma_{z\theta}^2}$
Intermediate principal strain	$\varepsilon_2 = \varepsilon_r$
Minor principal strain	$\varepsilon_3 = \frac{\varepsilon_z + \varepsilon_\theta}{2} - \sqrt{\left(\frac{\varepsilon_z - \varepsilon_\theta}{2}\right)^2 + \gamma_z^2}$
Major principal stress direction from vertical	$\alpha = \frac{1}{2}\tan^{-1}\left(\frac{2\tau_{z\theta}}{\sigma_z - \sigma_\theta}\right)$

σ_v	Vertical stress
σ_h	Horizontal stress
W	Vertical load
T	Torque about vertical access
p_i and p_o	Inner and outer cell pressures, respectively
r_i and r_o	Inner and outer hollow cylinder specimen radii, respectively
H	Specimen height
ΔH	Change in specimen height
l_i and l_o	Inner and outer surface displacements, respectively
θ	Rotation angle

4.4 Test results

As stated earlier, this study aims to assess the effects of initial static shear stresses on the liquefaction resistance of Çine sand. A custom-designed and manufactured hollow cylinder cyclic torsional test setup is used to perform these tests.

In the test program, three different relative density ranges (30-45%, 50-65%, and 70-85%) are studied under the same consolidation stress (nearly 100 kPa). A total of 25 tests were conducted, 14 of which had no initial static shear stress (i.e. α=0), whereas in the rest of the tests, varying α values were applied before the cyclic loading. During the tests, the number of cycles that cause %10 double amplitude shear strain levels are assigned as the required cycles to liquefy the specimen at that specific CSR value.

Figures 53, 54, and 55 present three sets of 4-way plots. Figure 53 shows a test result without initial static shear application, i.e. $\alpha = 0$. In this test, specimen is initially prepared with 71% relative density and CSR =0.26 is applied during the test. Four-way plots of this test show symmetrical shear strain accumulation with each cycle. Once the liquefaction initiates, CSR vs p'/p_0 starts to move along the failure envelope, which is actually the line making 33° with the horizontal axis and corresponds to the critical state angle of shear resistance of Çine sand. (Aksoy, 2024) Similarly, in other tests, specimens go over this line after liquefaction initiates.

Comparisons revealed that average shear strains become significant after r_u reaches a value of 0.8. Up to r_u=0.8, excess pore pressure generation progressed slowly and steadily, and specimens generally were not subjected to large average deformations. Some researchers refer to specific r_u values (r_u=0.8, 0.95, or 1.0) as the liquefaction initiation threshold, whereas others consider shear strain as the liquefaction threshold value. In this study, the average shear strain when it reaches 10% double amplitude is considered as the liquefaction initiation threshold value.

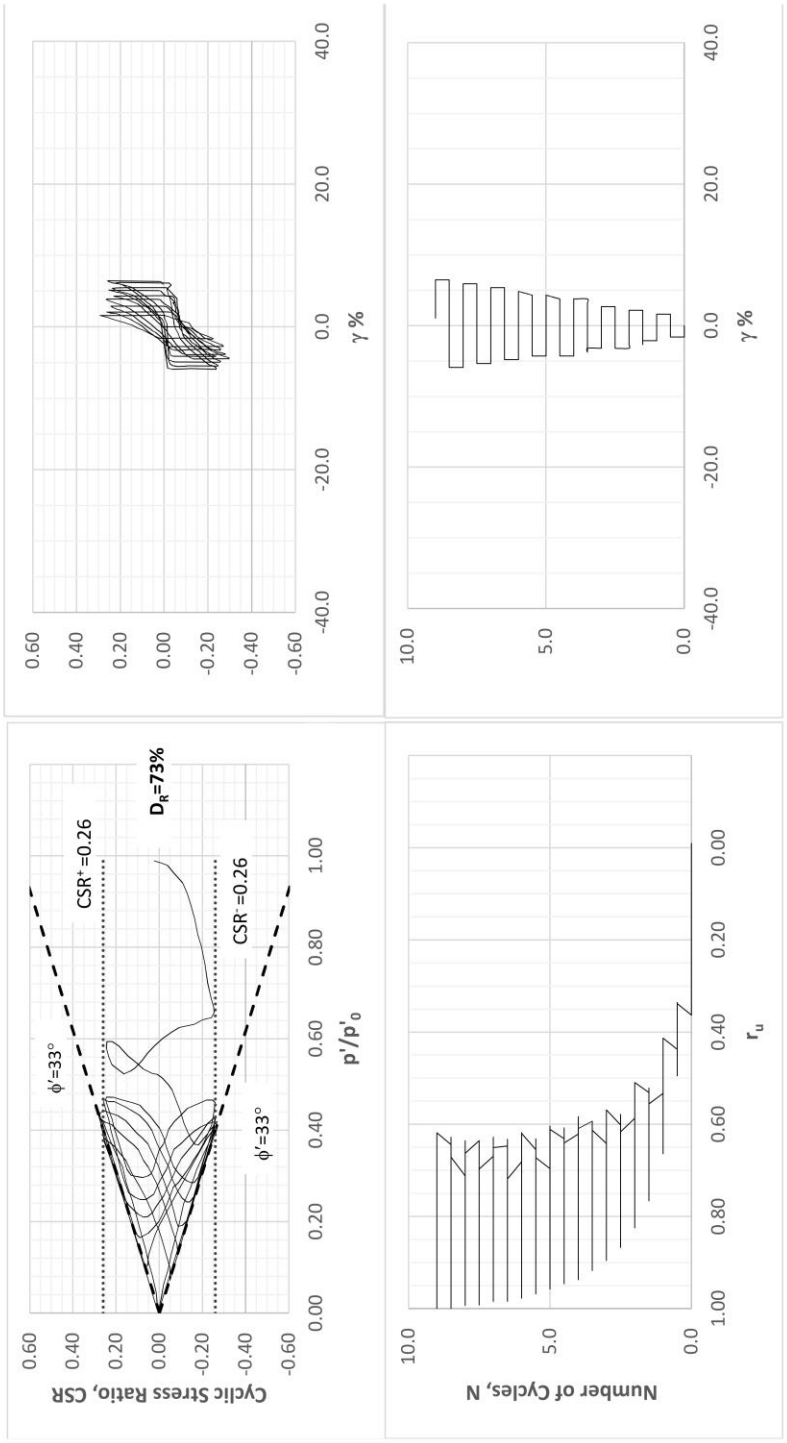

Figure 54. 4-way plots of specimen #15 with 73% relative density, consolidated isotopically 102.3 kPa with α=0.0, CSR=0.26

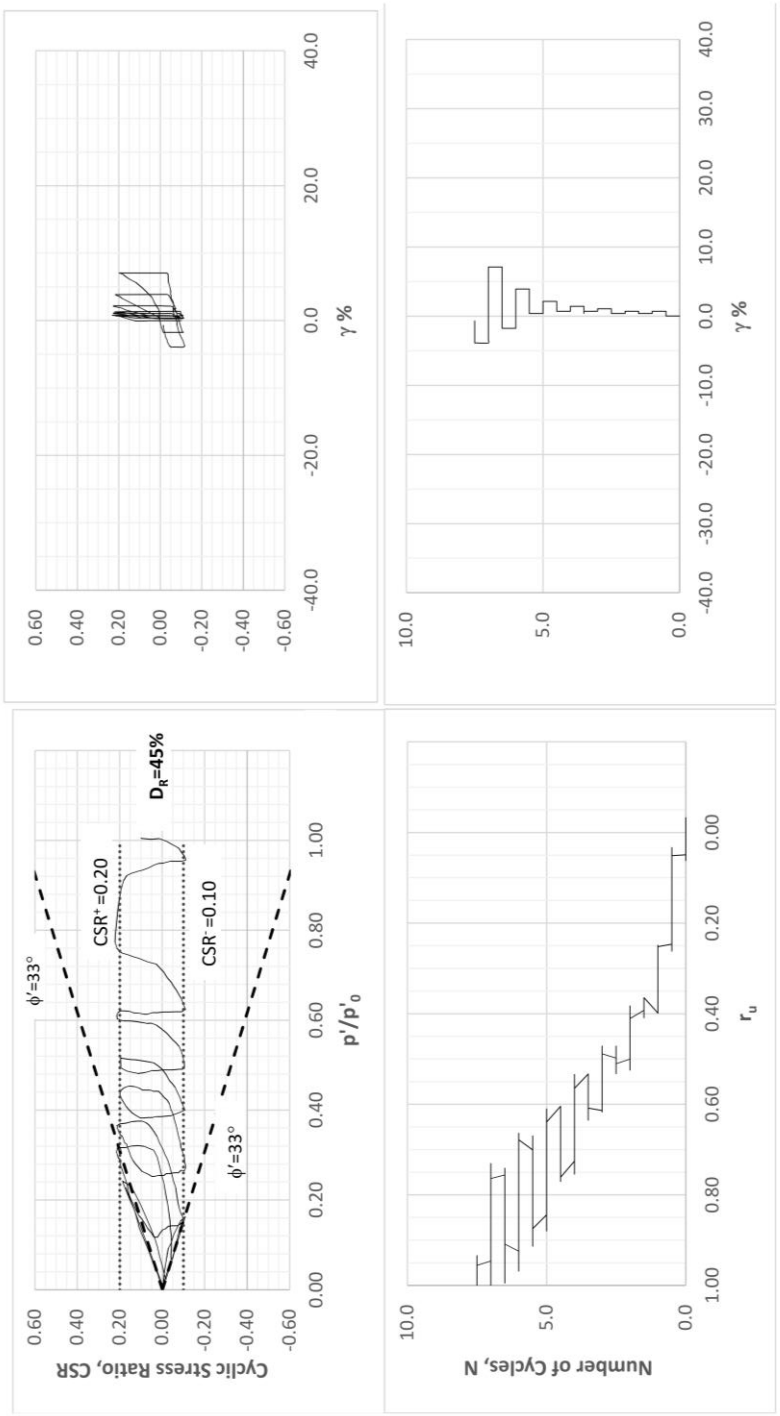

Figure 55. 4-way plots of specimen #22 with a relative density of 45%, consolidated isotopically 100.7 kPa with α=0.05, CSR=0.15

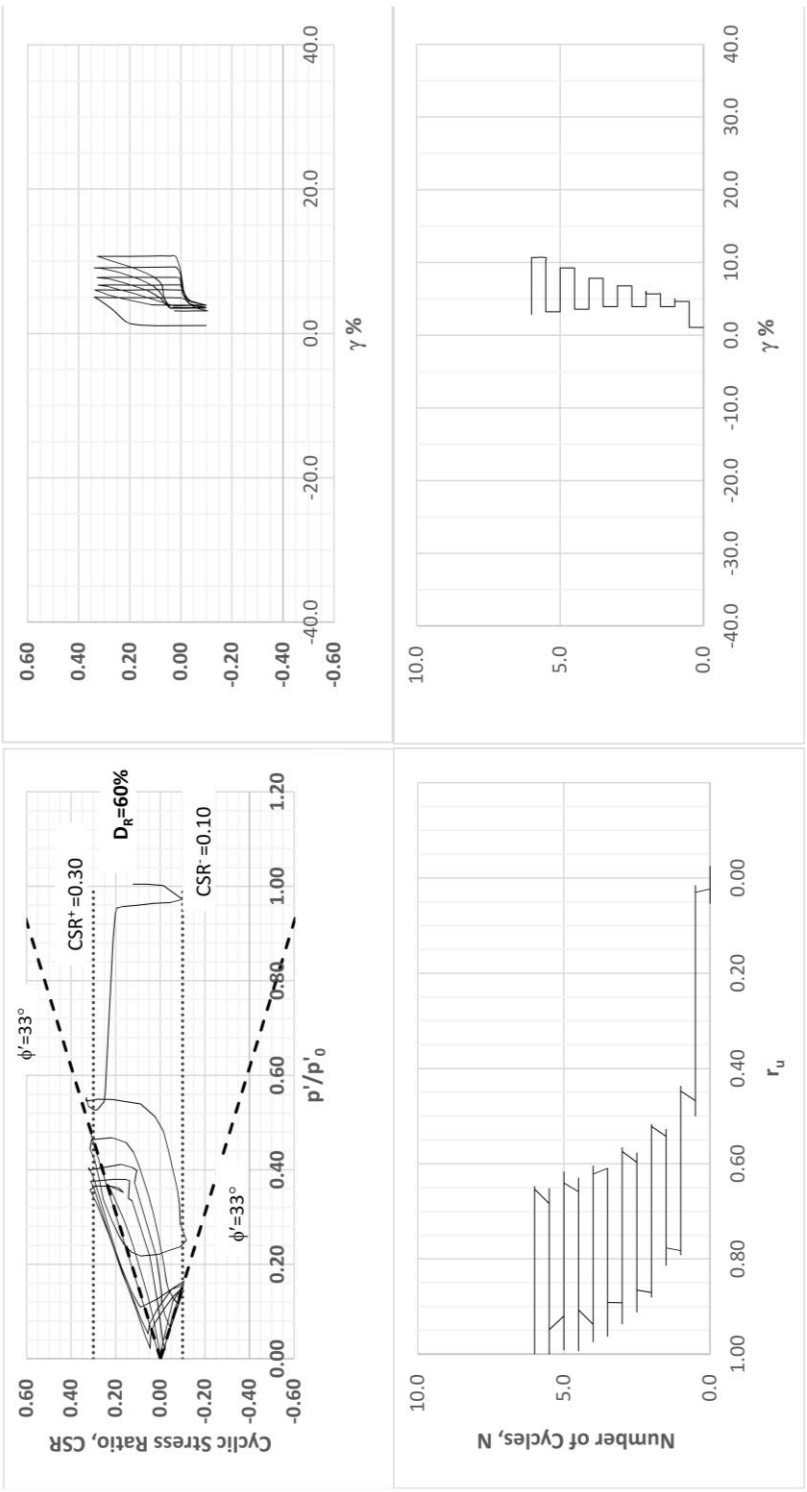

Figure 56. 4-way plots of the specimen #28 with 60% relative density, consolidated isotopically 102.8 kPa with α=0.13, CSR=0.20

Figure 55 shows the test results of sample #22. The specimen with an initial relative density of 45% is consolidated isotopically under 102.3 kPa. An $\alpha = 0.05$ is applied before cyclic loading; then cyclic loading is applied as a value of CSR =0.15. Compared to Figure 54 where test specimen #15 had $\alpha = 0.0$, specimen #22, with initial static shear stress, has asymmetrical strain accumulation. In Figure 56, strain accumulation asymmetry is more obvious due to the reason α =0.13; a higher initial static shear was applied to specimen #28. As the magnitude of initial static shear stresses increases, the asymmetry in average shear strains becomes more pronounced. This can be observed in many tested specimens' average shear strain vs. CSR graphs. In all of the tests, the corresponding number of cycles is obtained for 10% double amplitude shear strain and these values were used to assign the K_α for Çine sand.

In this study, all the specimens were subject to stress reversals because initial static shear values were intentionally applied smaller than would-be applied cyclic stress values. Under these stress conditions, banana curves, indicating soil liquefaction, were developed clearly. Illustrative test results from literature with and without shear stress reversals are shown in Figure 57.

During the tests, 10 or 20 data points per second were taken, and sometimes, the pore pressure transducer made some noise, leading to scattered data. Therefore, a smoothing algorithm was used to filter out the noise. Figure 58 shows the resultant 4-way plots with and without noise filtering. In the Appendix, all of the 4-way graphs are provided after applying the smoothing algorithm.

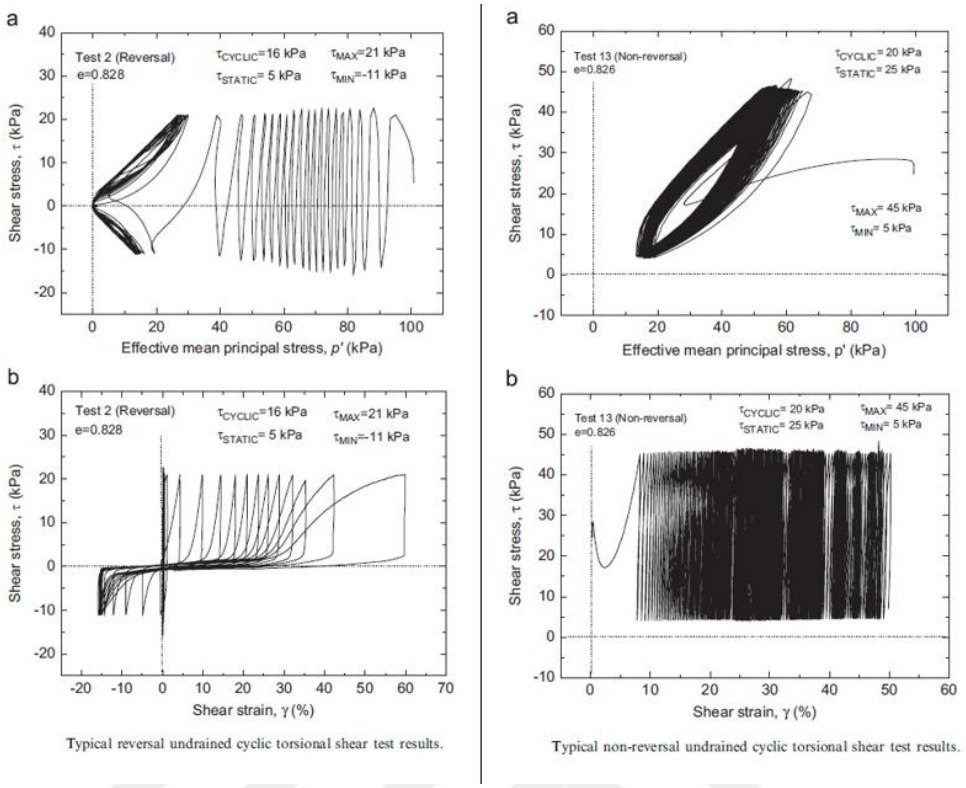

Figure 57. Typical reversal and non-reversal test results (Chiaro et al, 2012)

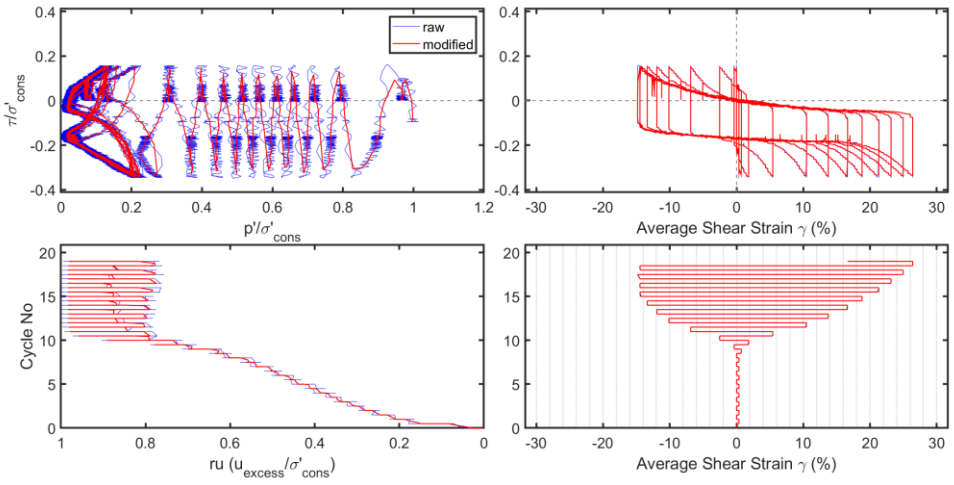

Figure 58. Raw data(blue) and modified data (red)

All test results are summarized in the CSR vs. N domain and can be seen in Table 6.

Table 6. Number of cycles to reach the target 10% double amplitude average shear strain level

TEST #	Dry Mass, g	Height, cm	Initial Void ratio, e_o	Initial relative density, D_{ro} %	Consolidation stress, σ_c	Void ratio after consolidation e_c	α	Void ratio after α, e_α	Relative density pre cyclic loading, Dr_{cyc} %	CSR	Number of cycles to reach %10 DA
1	4200	27.7	0.722	32	105.0	0.714	0.00	0.714	35	0.10	54.0
2	4200	27.7	0.722	32	102.7	0.714	0.00	0.714	35	0.12	30.0
3	4200	27.7	0.722	32	102.6	0.714	0.00	0.714	35	0.16	7.0
4	4200	27.8	0.729	30	102.0	0.718	0.00	0.718	33	0.22	1.0
5	4400	27.5	0.632	60	108.5	0.620	0.00	0.62	64	0.12	94.0
6	4400	27.7	0.644	57	106.3	0.638	0.00	0.638	58	0.15	29.0
7	4400	27.8	0.650	55	106.4	0.645	0.00	0.645	56	0.18	9.0
8	4400	27.6	0.638	58	101.0	0.632	0.00	0.632	60	0.30	1.0
10	4400	27.4	0.626	62	102.4	0.618	0.00	0.618	65	0.23	3.5
12	4550	27	0.550	86	102.9	0.547	0.00	0.547	87	0.15	59.0
13	4550	27.1	0.555	84	98.7	0.552	0.00	0.552	85	0.19	13.0
14	4500	27.1	0.555	84	101.0	0.550	0.00	0.55	86	0.30	2.5
15	4400	26.9	0.597	71	102.3	0.590	0.00	0.59	73	0.26	7.0
16	4200	27.7	0.722	32	101.6	0.714	0.13	0.714	35	0.16	5.0
18	4400	27.9	0.656	53	101.8	0.650	0.10	0.65	55	0.19	25.0
21	4200	27.9	0.735	28	103.1	0.728	0.05	0.728	30	0.15	6.5
22*	4200	27.9	0.728	30	100.7	0.673	0.05	0.672	45	0.15	6.5
23*	4200	27.9	0.672	48	102.7	0.636	0.20	0.635	64	0.25	10.0
24*	4200	27.9	0.635	59	102.4	0.612	0.15	0.611	73	0.31	10.0
25*	4200	27.9	0.611	67	102.2	0.590	0.18	0.59	80	0.32	20.0
26	4200	27.8	0.729	30	101.1	0.722	0.10	0.722	32	0.20	1.0
27*	4200	27.8	0.722	32	103.4	0.674	0.10	0.674	47	0.20	7.0
28*	4200	27.8	0.674	47	102.8	0.635	0.13	0.634	60	0.20	6.0
29*	4200	27.8	0.634	60	103.5	0.605	0.22	0.603	69	0.28	10.0
30*	4200	27.8	0.603	69	106.1	0.579	0.22	0.577	78	0.29	17.5

During this study, loose (28-45%), medium dense (47 – 65%), and dense specimens (70-87%) are tested, and the results of these tests will be explained in the following parts.

4.4.1 Loose samples

A total of 8 samples are grouped as loose specimens, half of which are tested without initial static shear stress, i.e. $\alpha = 0$. A summary of these tests can be seen in Table 7.

Table 7. Summary of loose specimen test results

Test ID	D_R %	p′(kPa)	α	CRR	N, # Cycles to 10% Double Amplitude Shear Strain	$CRR_{\alpha=0}$	K_α
#1	35	300.0	0.0	0.10	54.0	0.10	1.00
#2	35	300.0	0.0	0.12	30.0	0.12	1.00
#3	35	300.0	0.0	0.16	7.0	0.16	1.00
#4	33	500.0	0.0	0.22	1.0	0.22	1.00
#16	35	500.0	0.128	0.12	5.00	0.16	0.73
#21	28	500.0	0.05	0.15	6.5	0.16	0.96
#22	45	500.0	0.05	0.15	6.5	0.16	0.96
#26	30	500.0	0.1	0.20	1	0.23	0.89

Inspired by the Creep Theory (Mandokhail et al., 2017), CSR values are expressed in a power form, as shown in Eq. 4.1.

$$CSR = aN^b \tag{4.1}$$

In Equation 4.1, N represents the number of loading cycles. For the loose specimens, by best fitting a power function to available test results, the resulting expression is obtained as shown in Fig 58.

$$CRR_{Loose,\alpha=0} = 0.225 * N^{-0.195} \tag{4.2}$$

By comparing the $CRR_{\alpha=0}$ with CRR_α at the same N, K_α can be estimated as shown in equation (4.3)

$$K_\alpha = \frac{CRR_\alpha}{CRR_{\alpha=0}} \tag{4.3}$$

The calculation steps are explained illustratively next for Specimen # 16. During the test program, loose Specimen #16 at $\alpha = 0.128$ reached 10% double amplitude shear strain after 5 cycles at CSR =0.12. On the other hand, if there were no initial static shear, by

using Equation (4.2), the corresponding CSR to cause 10% DA shear strain would be estimated as

$$CRR = 0.225 * N^{-0.195} = 0.225 * 5^{-0.195} = 0.164$$

Therefore, K_α for the specimen with D_R=35% at $\alpha = 0.128$ will be calculated as 0.73 by using equation (4.3)

$$K_\alpha = \frac{CRR_\alpha}{CRR_{\alpha=0}} = \frac{0.12}{0.164} = 0.73$$

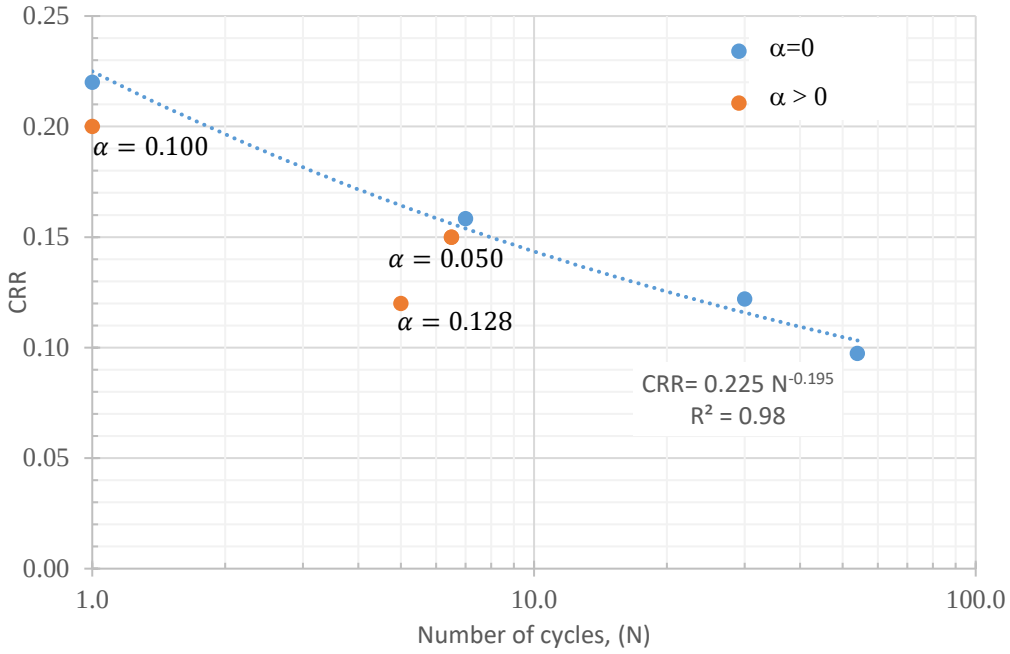

Figure 59. CRR vs. N response for the loose specimens

For the loose specimens with D_R=28-45%, the estimated K_α values varying with α are shown in Figure 60. Supported by test results, as α increases, K_α decreases.

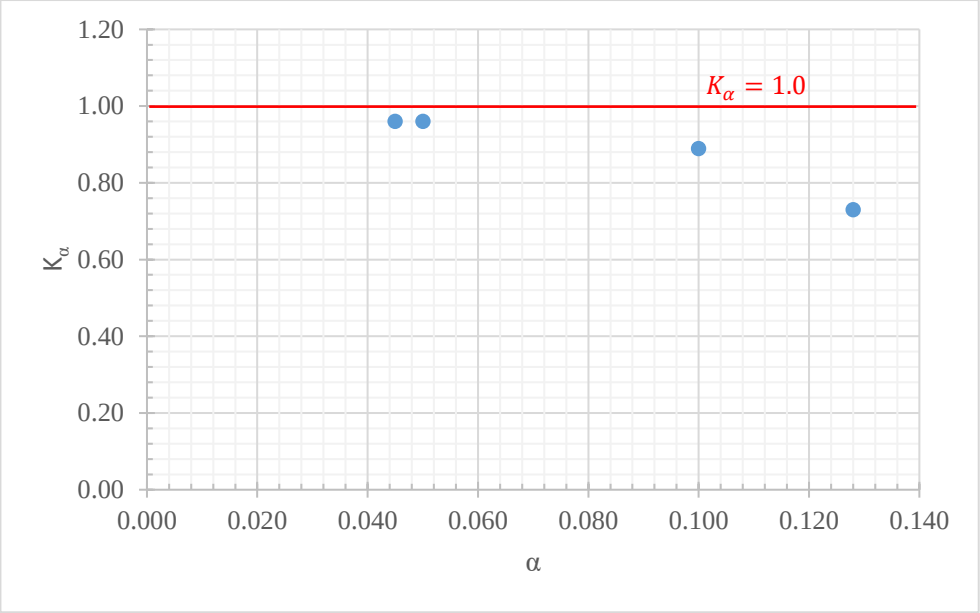

Figure 60. K_α with varying α values for loose specimens

4.4.2 Medium-dense samples

For the medium-dense samples (47 - 65 %), a total of 9 tests were conducted, and 4 of them were performed with initial static shear stress. The test results are presented in Table 8. Similarly, test results are also shown in the CSR vs. N domain in Figure 60.

CRR vs. N relationship is obtained for the medium-dense Çine sand specimens as

$$CRR_{M-Dense,\alpha=0} = 0.294 * N^{-0.204} \quad (4.4)$$

Table 8. A summary of medium-dense specimen test results

Test ID	D_R %	p′ (kPa)	α	CRR	N, # Cycles to 10% Double Amplitude Shear Strain	$CRR_{\alpha=0}$	K_α
#5	60	500	0.00	0.117	94	0.12	1.00
#6	58	500	0.00	0.151	29	0.15	1.00
#7	62	500	0.00	0.181	9	0.18	1.00
#8	60	500	0.00	0.3	1	0.30	1.00
#10	65	500	0.00	0.225	3.5	0.23	1.00
#18	55	500	0.10	0.19	25	0.15	1.25
#23	64	500	0.20	0.25	10	0.18	1.36
#27	47	500	0.1	0.20	7	0.20	1.01
#28	61	500	0.13	0.20	6	0.20	0.98

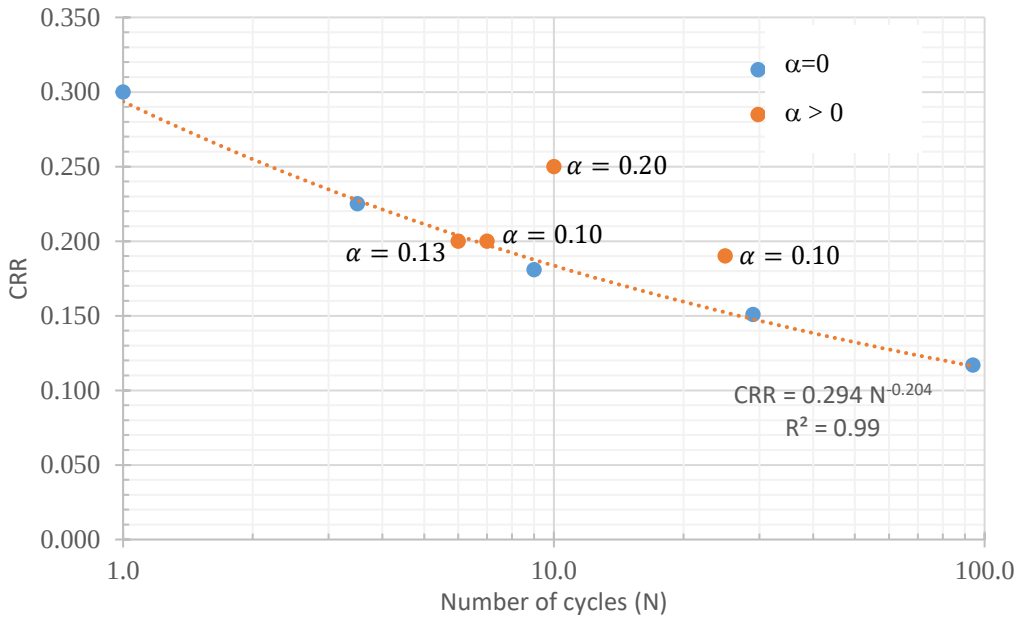

Figure 61. CRR vs. N response for the medium dense specimens

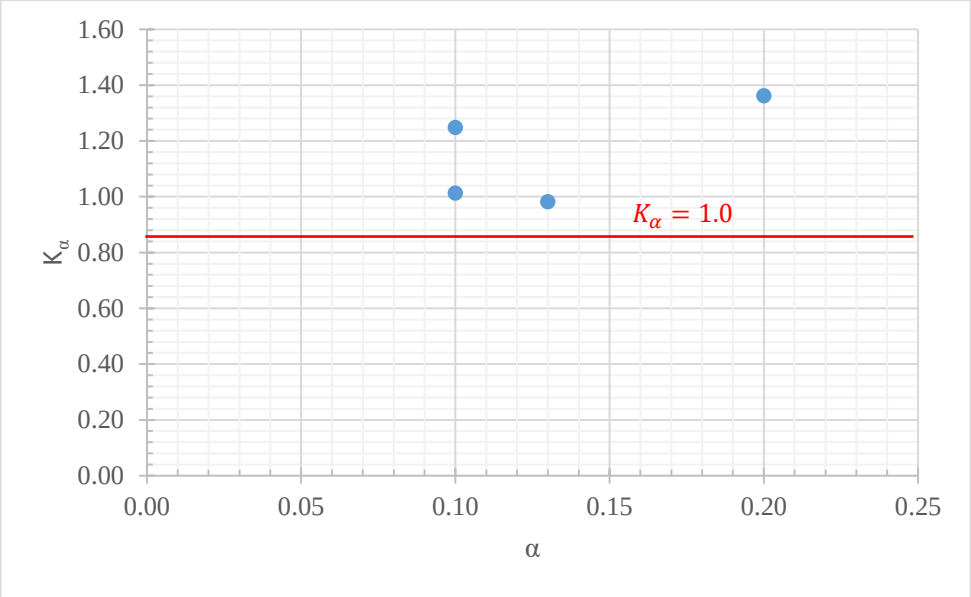

Figure 62. K_α with varying α values for medium-dense specimens

Figure 61 shows that, for the medium-dense specimens with initial static shear stresses, the liquefaction resistance of the Çine sand (test #23) slightly increases. In one sample this increase is as high as 40 %. On the contrary, in two tests (test #27 and #28), having an initial static shear did not affect the liquefaction resistance of Çine sand. For these tests, K_α is calculated as very close to unity. It may be deduced that as α increases, K_α also increases, but more tests should be done for wider ranges of α.

4.4.3 Dense samples

8 tests were conducted with dense samples whose relative densities vary in a range of 71-85%. Half of them were tested after applying an initial static shear stress. Summary of the tests can be seen in Table 9.

For the dense specimens of Çine sand, CRR vs. N relationship is assessed as shown on Fig 62.

$$CRR = 0.377 * N^{-0.235} \quad (4.5)$$

As can be seen in Figure 63, for the dense specimens, for a range of α =0.15 to 0.22, the liquefaction resistance increases in a range of 27% to 71%. The most significant increase against liquefaction resistance is observed for test #25, with a relative density of 80% and α = 0.18. Denser specimens showed greater resistance to liquefaction than loose and medium-dense ones under initial shear. Still, more tests should be conducted to understand better the significance of relative density and initial static shear stress on K_α

Table 9. Summary of the dense specimen test results

Test ID	D_R %	p′ (kPa)	α	CRR	N, # Cycles to 10% Double Amplitude Shear Strain	$CRR_{\alpha=0}$	K_α
#12	87	500	0.00	0.148	59	0.15	1.00
#13	85	500	0.00	0.189	13	0.19	1.00
#14	86	500	0.00	0.300	2.5	0.30	1.00
#15	73	500	0.00	0.260	7	0.26	1.00
#24	73	500	0.15	0.31	10	0.22	1.41
#25	80	500	0.18	0.32	20	0.19	1.71
#29	71	500	0.22	0.28	10	0.22	1.27
#30	79	500	0.22	0.29	17.5	0.19	1.51

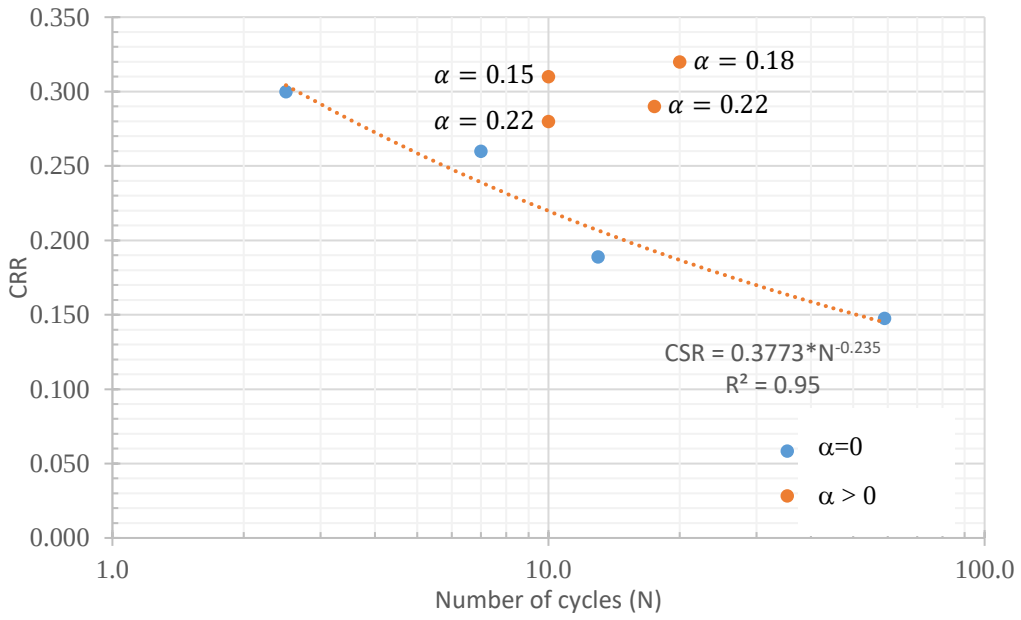

Figure 63. CRR vs. N response for the dense specimens

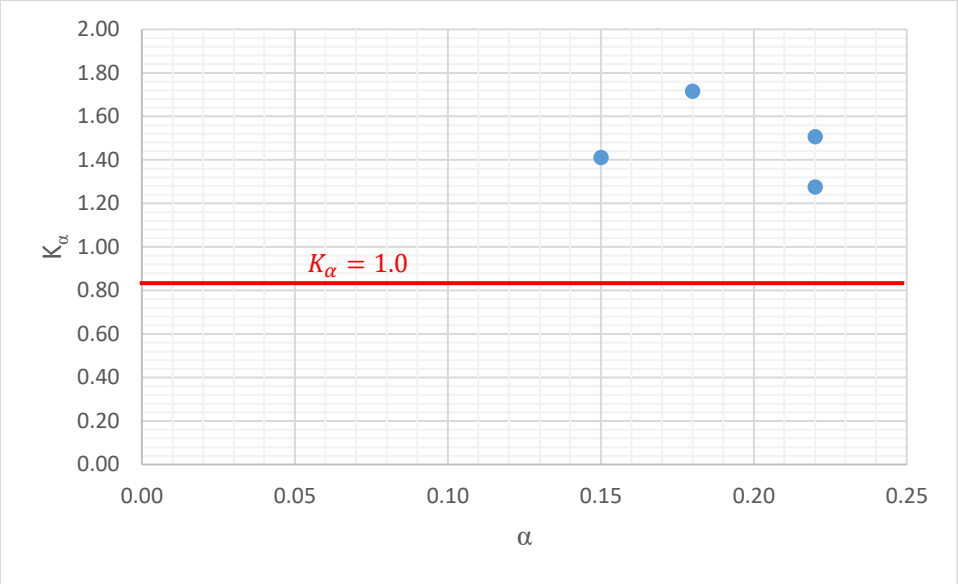

Figure 64. K_α with varying α values for the dense specimens

4.4.4 Comparison of b values with literature

In this study, 25 tests were performed to assess the effect of initial static shear stress on liquefaction resistance of Çine sand. Nearly half of these tests were conducted for level ground condition (α=0). As discussed earlier, CRR values are expressed in a power form as shown in Eq. 4.1.

The estimated b values are compared with the values reported in the literature. It is observed b value significantly depends on relative density and soil type, and it increases with increasing relative density. Our estimated b values are plotted as a function of relative density in Figure 65. An expected increasing trend with D_R is observed.

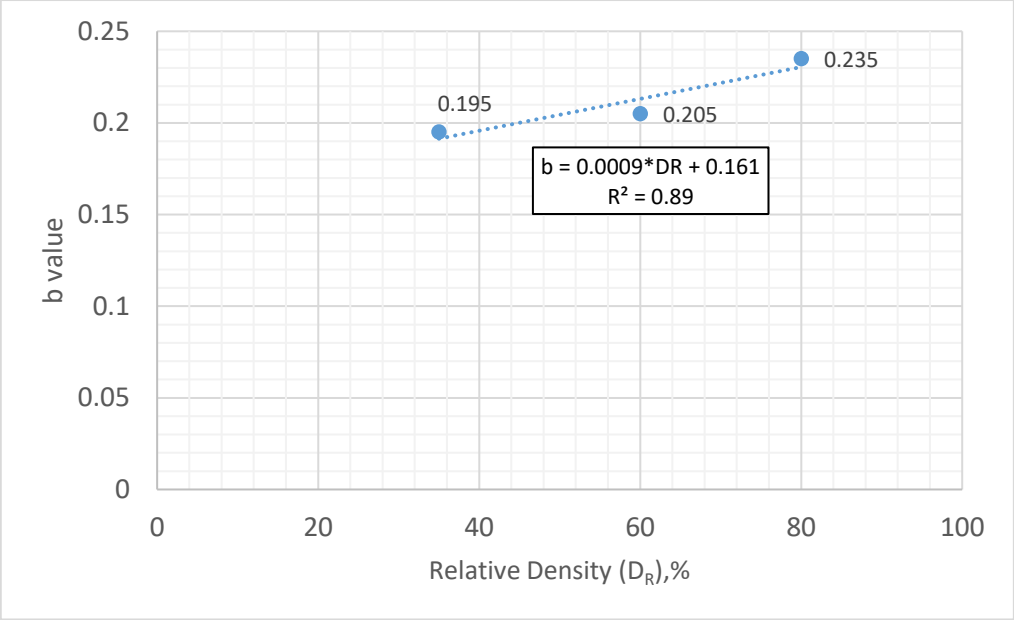

Figure 65. Dependency of b value on D_R

Figure 66 compares the b values of this study with the values reported in Ulmer et al. (2022). Their study used the data sets of Tatsuoka et al. (1986). As part of the Tatsuoka database, air-pluviated samples of Sengenyama sand were anisotropically consolidated and tested in a cyclic triaxial shear setup. A reasonable match is observed between the b values of this study compared to those reported by Ulmer et al. (2022) despite the different sandy soils used and different thresholds for liquefaction triggering. Note that 10% DA shear strain as liquefaction initiation was used in our study, whereas Ulmer et al. (2022) regarded that value as 15% DA.

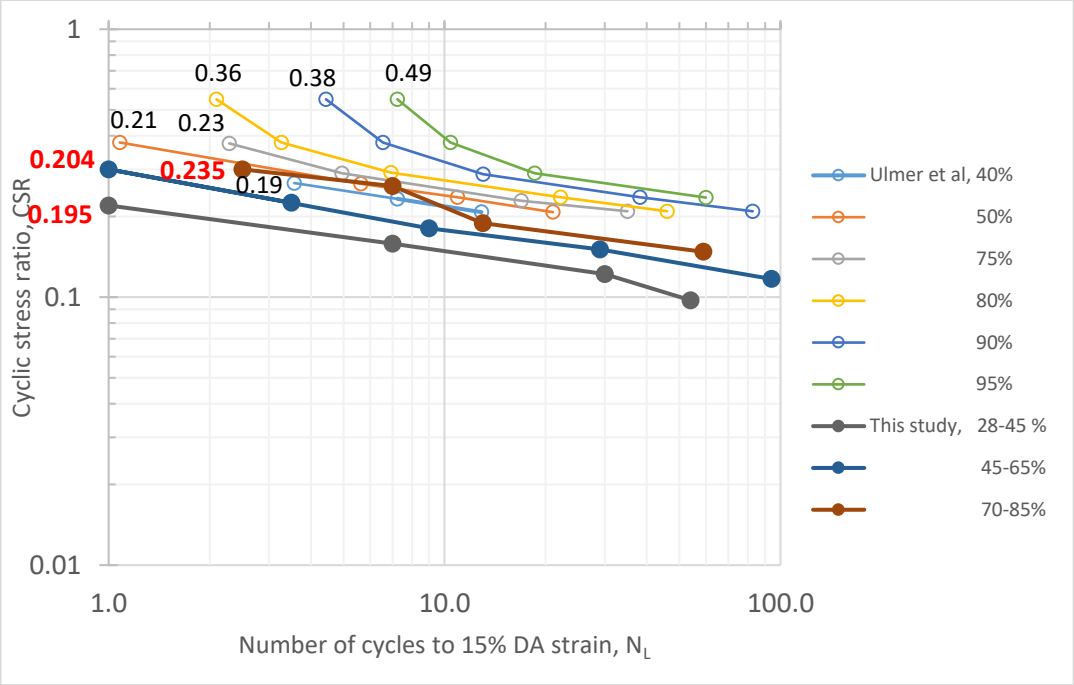

Figure 66. Comparison of b values with the values reported in Ulmer et.al (2022)

4.4.5 Comparison of CRR

In practice, CRR of the any soil specimen against liquefaction can be estimated by undrained cyclic laboratory tests (as it is done in this study) or by semi-empirical methods based on case history databases. Details about these two different approaches were discussed in Chapters 2 and 3.

In this section, it is aimed to compare the resulting CRR values with the predictions by Youd et. al. (2001), Idriss and Boulanger (2008) and Çetin et. al. (2014). In order to compare our laboratory-based findings with those from case-histories, relative density of the specimens should be converted to equivalent $(N_1)_{60}$ values. As shown in Table 10, Kulhawy and Mayne (1990) and Cubrinovski and Ishihara (1999) relationships were used to estimate the corresponding $(N_1)_{60}$ values.

Table 10. D_R to N_1 relationships

$\frac{(N_1)_{60}}{{D_R}^2} = 60 + 25 * \log(D_{50})$	Kulhawy and Mayne (1990)
$D_R = \sqrt{\frac{(N_1)_{78} * (e_{max} - e_{\min})^{1.7}}{9}}$	Cubrinovski &. Ishihara (1999)

The resulting CRR vs. N relationship is shown in Figure 67. The data used for the assessments are also tabulated in Table 11.

Table 11. A summary of CRR vs N database

D_R%	CRR	N, Number of cycles	Average D_R	$N_{1,60}$ Kulhawy and Mayne (1990)	$N_{1,60}$ Cubrinovski and Ishihara (1999)	$CRR_{N=22}$
87	0.15	59.0	0.83	34	35	0.182
85	0.19	13.0				
86	0.30	2.5				
73	0.26	7.0				
64	0.12	94.0	0.61	18	19	0.156
58	0.15	29.0				
56	0.18	9.0				
60	0.30	1.0				
65	0.23	3.5				
35.0	0.10	54.0	0.34	6	6	0.123
35.0	0.12	30.0				
35.0	0.16	7.0				
33.0	0.22	1.0				

If moment magnitude M_w=7.5 is assumed to produce 22 equivalent numbers of shear stress cycles, consistent with Cetin et al. (2021), then $CRR_{Mw=7.5}$ for loose, medium dense, and dense specimens as 0.123, 0.156, and 0.182, respectively.

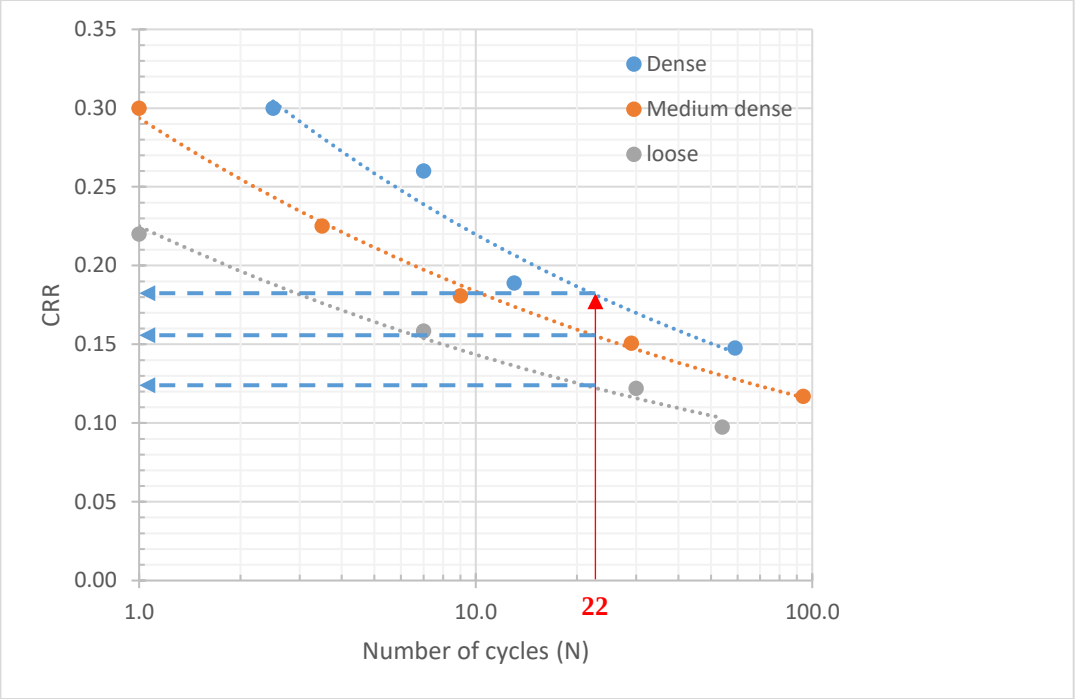

Figure 67. CRR vs. N relationship for loose, medium-dense, and dense samples

The estimated CRR values are comparatively shown in Figure 68 with the values suggested by semi-empirical methods. There is a reasonable match between CRR values especially for loose and medium dense soils. It should be noted that the semi-empirical model predictions provide CRR values under multi-directional loading conditions during an earthquake. However, laboratory test results provide CRR values under uni-directional loading. Hence, a perfect match was not expected. The difference is more pronounced for dense soil samples since semi-empirical models define liquefaction occurrences by surface manifestation, whereas laboratory-based methods use a threshold shear strain level (10 % double amplitude shear strain level in our study) to determine the onset of liquefaction. This difference is believed to be the reason behind the differences in the predictions at higher relative densities.

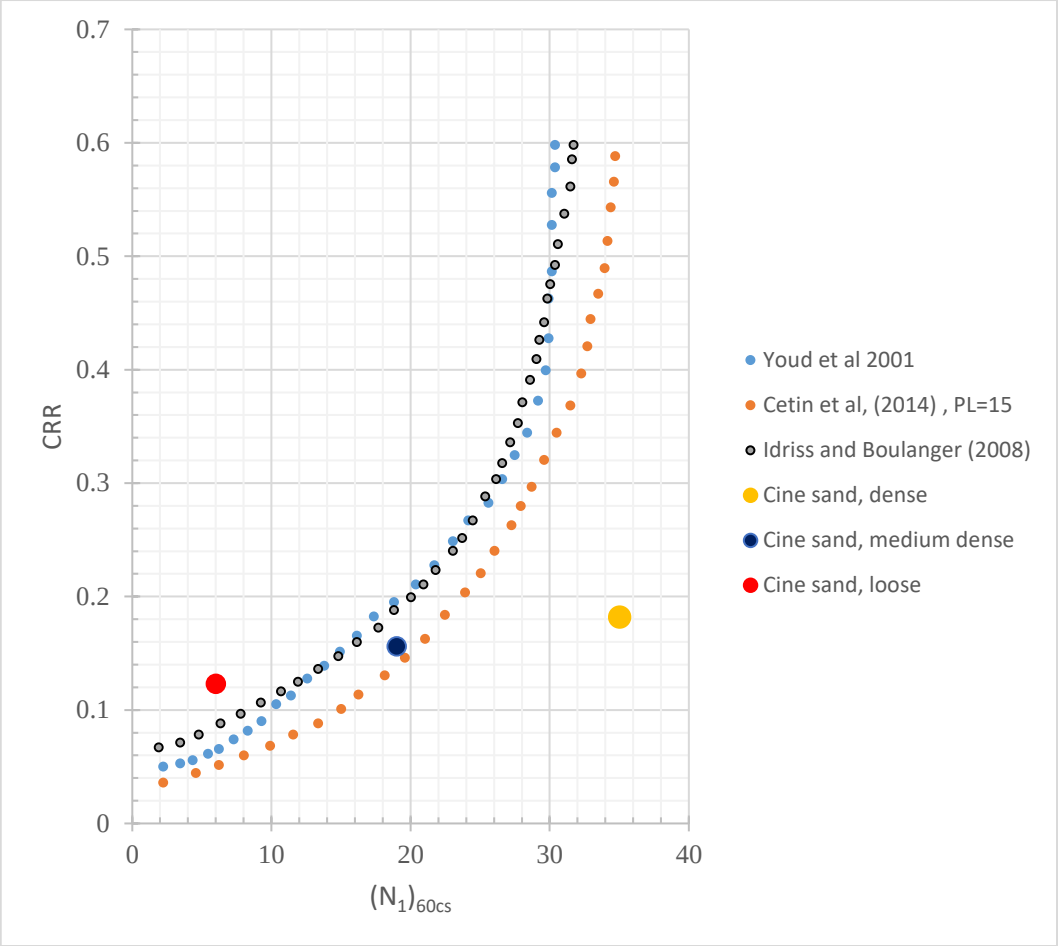

Figure 68. CRR vs. $N_{1,60}$ comparisons the values from semi-empirical model predictions

CHAPTER 5

SUMMARY, DISCUSSIONS AND CONCLUSIONS

5.1 Summary

This study aims to evaluate the effects of initial static shear stresses on liquefaction behavior of saturated Çine sand through hollow cylinder cyclic torsional tests. For this purpose, a new hollow cylinder torsional shear apparatus was designed and manufactured. As part of laboratory testing program, various parameters, including the relative density of the specimen, initial static shear stresses applied before cyclic loading, and the cyclic stress ratios were selected as variables to understand the liquefaction response of Çine sand. The pore water pressure and shear strain accumulations were monitored throughout the applied shear stress cycles. By using the test results, which were presented in the (CRR) vs. log(N) domain, the effects of initial static shear stresses, commonly known as slope correction factor, K_α, were estimated specific to Çine sand. The resulting K_α factors are to be compared with available literature, which is discussed next.

5.2 Comparisons with Available Literature

As part of the experimental program, 25 cyclic tests were performed to assess the effect of initial static shear stress on the liquefaction resistance of Çine sand. The results of this study are illustratively compared in Figure 69 with recent laboratory test-based K_α recommendations of Park et al. (2020) and Umar et al. (2022), along with those of NCEER (1997). In Figure 69, the shaded regions show the recommendations of NCEER (1997). Based on visual inspections of Figure 69, following conclusions were made:

- Consistent in all four studies (i.e.: NCEER (1997), Park et al., Umar et al., and this study) the liquefaction resistance of loose samples decreases upon applying initial static shear stresses,
- This decrease becomes more significant with increasing static shear stresses.

- For α < 0.05, no significant change in CRR was observed, and K_α was estimated as nearly 1.0.
- As α increases to 0.10 to 0.13, K_α values decrease to the values of 0.89 and 0.73, respectively.
- For the four tests performed on medium-dense specimens with α values in the range of 0.19 to 0.25, K_α values were estimated to vary in the range of 0.98 to 1.36. Hence, it is concluded that presence of initial static shear stresses positively affects liquefaction resistance.
- Similarly, for the four tests performed on dense specimens with α values in the range of 0.15 to 0.22, K_α values were estimated to vary in the range of 1.27 and 1.71. Hence, for denser specimens, initial static shear may increase the liquefaction resistance by as much as 70 %.
- Confirming this, Test #25, with D_R=80% and α=0.18, produced a K_α value as high as 1.71, which is even higher than the recommended K_α ranges by NCEER, (1997). Note that NCEER (1997) recommendations are suggested to be used for sandy soils with D_R values up to 70%.
- In general, the estimated K_α values by this study are observed to be in conformance with the recommendations of NCEER (1997) and Parker et al. (2020). They are higher and lower than the values suggested by Umar et al. (2021) for denser and looser soils respectively.
- Inconsistencies in laboratory-based recommendations and wide range of recommended K_α suggest that further research is needed on their more accurate and precise assessment. Moreover, it is also recommended that they should be estimated specific to the sand type and stress and density state under consideration.

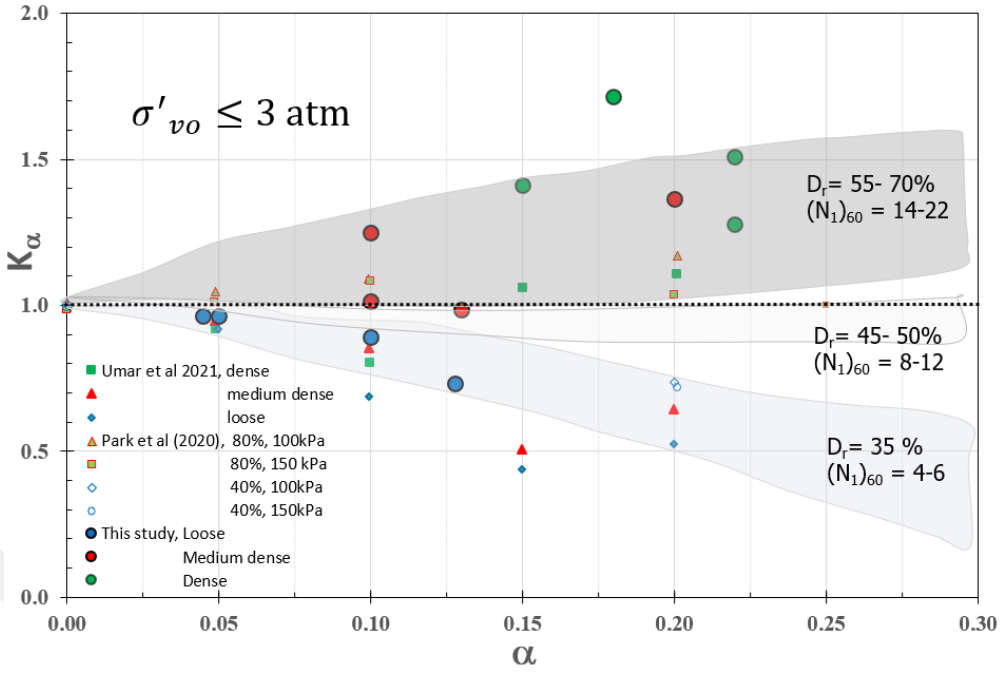

Figure 69. A comparison of the test results with available literature and NCEER recommendations (shaded regions).

5.3 Future Studies

The following future studies are believed to improve the current state of knowledge regarding the effects of initial static shear stresses on liquefaction resistance of sands:

- Initial effective confining stresses other than 100 kPa are recommended to be selected to study the cyclic response of Çine sand. In this study, a 100 kPa (nearly 1 atm) consolidation pressure was applied on all samples.
- A more densely selected and higher α values are recommended to be used as part of the testing program. In this study, the maximum α value was selected as 0.15, whereas in literature, there are some laboratory testing research studies where α values were selected as high as 0.3 or 0.4. Similarly, smaller α values should also be considered as low as α = 0.03 to 0.06

- The direction of the initial static shear stresses is recommended to be considered. In the literature, there are studies where direction of static shear loading was selected to be perpendicular to cyclic loading, especially by using the direct simple shear apparatus.
- Different kinds of sands with different grain size, distribution and shape characteristics are also recommended to be tested.

REFERENCES

Aksoy, A. S., 2024. The Effects of Grain Sphericity and Roundness on Critical State Parameters [MA thesis]. Middle East Technical University.

Andrus, R. D., and Stokoe, K. H., II. 1997. Liquefaction resistance based on shear wave velocity. Proc., NCEER Workshop on Evaluation of Liquefaction Resistance of Soils, Nat. Ctr. For Earthquake Engrg. Res., State Univ. of New York, Buffalo, 89-128.

Andrus, R. D., and Stokoe II, K. H. 2000. Liquefaction resistance of soils from shear wave velocity. Journal of geotechnical and geo environmental engineering, 12611, 1015-1025.

ASTM D 1140-17, Standard Test Methods for Determining the Amount of Material Finer than 75-µm (No. 200) Sieve in Soils by Washing

ASTM D 4253-00, Standard test methods for maximum index density and unit weight of soils using vibratory table. ASTM International, West Conshohocken, PA, 2014, www.astm.org

ASTM D 4254-00, Standard test methods for minimum index density and unit weight of soils and calculation of relative density. ASTM International, West Conshohocken, PA, 2014, www.astm.org

Boulanger, R. W., Seed, R. B., Chan, C. K., Seed, H. B., Sousa, J.. 1991. Liquefaction behavior of saturated sands under uni-directional and bidirectional monotonic and cyclic simple shear loading, Geotechnical Report No. UCB/GT/91-08, University of California, Berkeley, California

Boulanger, R. W., and Seed, R. B. 1995. Liquefaction of sand under bidirectional monotonic and cyclic loading. Journal of geotechnical engineering, 12112, 870-878.

Boulanger, R. W. 2003. High overburden stress effects in liquefaction analyses. Journal of Geotechnical and Geoenvironmental Engineering, ASCE, 12912, 1071-1082.

Boulanger, R.W., and Idriss, I. M.. 2004. State normalization of penetration resistances and the effect of overburden stress on liquefaction resistance, Proc., 11th International Conference on Soil Dynamics and Earthquake Engineering, and 3rd International Conference on Earthquake Geotechnical Engineering, D. Doolin et al., eds., Stallion Press, Vol. 2, 484-491.

Bhattacharya, S., Orense, R.P. and Lombardi, D. (2019) Seismic design of foundations: Concepts and applications. London: ICE Publishing.

Bardet JP and Tobita T (2001) NERA: A Computer Program for Nonlinear Earthquake Site Response Analyses of Layered Soil Deposits. Department of Civil Engineering, University of Southern California, Los Angeles, CA, USA.

Cetin, K. O., and Seed, R. B. 2004. Nonlinear shear mass participation factor rd for cyclic shear stress ratio evaluation, Soil Dynamics and Earthquake Engineering, 242, 103-113. https://doi.org/10.1016/j.soildyn.2003.10.008

Cetin, K. O., Seed, R. B., Der Kiureghian, A., Tokimatsu, K., Harder, Jr., L. F., Kayen, R. E., et al. 2004. SPT-Based probabilistic and deterministic assessment of seismic soil liquefaction potential. ASCE J. of Geotechnical and Geoenvironmental Engineering, 13012:1314-1340.

Cetin, K. O., and Bilge, H. T. 2012. Performance-based assessment of magnitude duration scaling factors, J.Geotec.Geoenviron. Eng., ASCE, 1383:324–34.

Cetin, K. O. and Bilge, H. T. 2013. Stress Scaling Factors for Seismic Soil Liquefaction Engineering Problems: A Perfomance-based Approach. International Conference on Earthquake Geotechnical Engineers, Istanbul, Turkey.

Cetin, K., & Bilge, H. (2015). Stress Scaling Factors for Seismic Soil liquefaction engineering problems: A performance-based approach. In A. Atilla, & M. Sakr, Perspectives on Earthquake Geotechnical Engineering (pp. 113-140). Springer International Publishing

Cetin, K. O., Seed, R. B., Kayen, R. E., Moss, R. E. S., Bilge, H. T., Ilgac, M., and Chowdhurry K. 2018a. SPT-Based Probabilistic and Deterministic Assessment of Seismic Soil Liquefaction Triggering Hazard. Soil Dynamics and Earthquake Engineering. https://doi.org/10.1016/j.soildyn.2018.09.012

Cetin, K. O., Altinci, E., Bilge. H. T., (2021). Probability-based assessment of number of equivalent uniform stress cycles, Soil Dynamics 10.1016/j.soildyn.2021.106583.

Chiaro G, Koseki J, Sato T. Effects of initial static shear on liquefaction and large deformation properties of loose saturated Toyoura sand in undrained cyclic torsional shear tests. Soils Found 2012;52(3):498–510. https://doi.org/10.1016/j.sandf.2012.05.008.

Cubrinovski, M., Ishihara, K., 1999. Empirical correlation between SPT N-value and relative density for sandy soils. Soils Found. 39 (5), 61–71.

Dobry, R., and T. Abdoun.. 2015. Cyclic shear strain needed for liquefaction triggering and assessment of overburden pressure factor Kσ. J. Geotech. Geoenviron. Eng. 141 11: 04015047. https://doi.org/10.1061/ASCEGT.1943-5606.0001342

Drnevich V.P., Richart F.E. Jr. (1970), "Dynamic pre-straining of dry sands," Journal of Soil Mechanics and Foundations Divisions, Proceedings of the American Society of Civil Engineers, vol. 96 pp. 451-469 No. SM2, March

Golesorkhi, R. 1989. Factors Influencing the Computational Determination of Earthquake-induced Shear Stresses in Sandy Soils, Dissertation Submitted in Partial Satisfaction of the Requirements for the Degree of Doctor of Philosophy, University of California at Berkeley.

Hardin, B. O. & Drnevich, V (1972). “Shear modulus and damping in soils: measurement and parameter effects”. J. Soil Mech. Found. Div. 98, 603–624

Harder, Jr., L. F. 1988. Use of penetration tests to determine the cyclic load resistance of gravelly soils, Ph. D. Thesis, University of California, Berkeley.

Harder LF Jr, Boulanger RW (1997) "Application of K_σ and K_α Correction Factors" Proc., NCEER Workshop on Evaluation of Liquefaction Resistance of Soils, State Univ. of New York at Buffalo, 195-218

Hashash YMA and Park D (2001) Non-linear one-dimensional seismic ground motion propagation in the Mississippi embayment. Engineering Geology 62(1–3): 185–206.

Hight, D.W., Gens, A. And Symes, M.J. (1983), “The development of investigating a new hollow cylinder the effects of principal rotation in soils”

Hynes, M. E., and Olsen, R. S. 1999. Influence of confining stress on liquefaction, Physics and Mechanics of Soil Liquefaction, Balkema, Rotterdam, 145-151

Idriss, I. M. 1999. An update to the Seed-Idriss simplified procedure for evaluating liquefaction potential. Publication No. FHWA-RD-99-165. Proceedings, TRB Workshop on New Approaches to Liquefaction, Federal Highway Administration.

Idriss, I.M. and Boulanger, R.W. (2003) Relating K_α and K_σ to SPT Blow Count and to CPT Tip Resistance for Use in Evaluating Liquefaction Potential. Proceedings of the 20th Annual Conference of Association of State Dam Safety Officials, ASDSO, Lexington, 8-10 September 2003, 7-10.

Idriss, I. M., and Boulanger, R. W. 2006. Semi-empirical procedures for evaluating liquefaction potential during earthquakes, J. Soil Dynamics and Earthquake Eng. 26, 115–30.

Idriss, I. M., and Boulanger, R. W. 2008. Soil liquefaction during earthquakes. Monograph MNO-12, Earthquake Engineering Research Institute, Oakland, CA, 261 pp.

Idriss, I. M., and Boulanger, R. W. 2010. SPT-based liquefaction triggering procedures. Report UCD/CGM-10/02 Davis, CA: Center for Geotechnical Modeling, Department of Civil and Environmental Engineering, University of California, 136p.

Imai, T., Tonouchi, K., and Kanemori, T. 1981. The simple evaluation method of shear stress generated by earthquakes in soil ground. Rep. No. 3, Bureau of Practical Geological Investigation, 39–58.

Ishibashi I., Sherif M.A., “Soil Liquefaction By Torsional Simple Shear Device”, Journal of Geotechnical Engineering.,ASCE, Vol.100, No.8, August, 1974, pp 871- 888

Ishihara K., Tatsuoka F., Yasuda S. 1975. Undrained Deformation and Liquefaction of Sand Under Cyclic Stresses. Soils and Foundations, 15 (1): 29-44.

Ishihara, K., Troncoso, J., Kawase, Y. and Takahashi, Y. (1980), "Cyclic Strength of Tailings Materials," Soils and Foundations, Vol. 20, No. 4, pp. 433-449.

Ishihara, K. 1993. Liquefaction and flow failure during earthquakes. Geotechnique, 433, 351-451.

Iwasaki, T., Tatsuoka, F., Tokida, K., and Yasuda, S. (1978). “A practical method for assessing soil liquefaction potential based on case studies at various sites in Japan.” Proc., 2nd Int. Conf. on Microzonation, San Francisco, 885−896.

Jefferies, M and Been, K., (2016) “Soil Liquefaction: A Critical State Approach”

Kottke AR and Rathje EM (2008) Technical Manual for Strata. University of California, Berkeley, CA, USA, PEER Report 2008/10.

Kulhawy, F.H. and Mayne, P.W. (1990) Manual on Estimating Soil Properties for Foundation Design. Electric Power Research Institute EL-6800, Project 1493-6, Electric Power Research Institute, Palo Alto, Calif.

Lade P.V., “Torsion Shear Apparatus for Soil Testing”, Laboratory Shear Strength of Soils, ASTM STP 740, R.N. Young and F.C. Townsend, Eds. American Society for Testing and Materials, 1981, pp 145-163

Lasley, S. J., Green, R. A., and Rodriguez-Marek, A. 2016. New stress reduction coefficient relationship for liquefaction triggering analyses. Journal of Geotechnical and Geoenvironmental Engineering, 142(11), 06016013. https://doi.org/10.1061/(ASCE)GT.1943-5606.0001530.

Macky, T. A. and Saada, A. S. (1984): "Dynamics of anisotropic clays under large strains, " Journal of Geotechnical Engineering, ASCE, Vol.110, No.4, pp. 487-504.

Mandokhail, Su.J., Park, D. & Yoo, JK. Development of normalized liquefaction resistance curve for clean sands. *Bull Earthquake Eng* **15**, 907–929 (2017). https://doi.org/10.1007/s10518-016-0020-7

Manmatharajan, V., and Sivathayalan, S. 2011. Effect of overconsolidation on cyclic resistance correction factors Kσ and Kα. In Proc., Fourteenth Pan-American Conference on Soil Mechanics and Geotechnical Engineering and the Sixty- Fourth Canadian Geotechnical Conference.

Montgomery, J., Boulanger, R. W. and Harder, Jr., L. F.. 2012. Examination of the Kσ overburden correction factor on liquefaction resistance. Rep. No. UCD /CGM-12-02. Davis, CA: Univ. of California.

Montgomery, J., Boulanger, R. W., and Harder, Jr., L. F. 2014. Examination of the Kσ overburden correction factor on liquefaction resistance. J. Geotech.Geoenviron. Eng, 10.1061/ASCEGT. https://doi.org/10.1061/(ASCE)GT.1943-5606.0001172

Moss RES, Seed RB, Kayen RE, Stewart JP, Der Kiureghian A and Cetin KO (2006) CPT-based probabilistic and deterministic assessment of in situ seismic soil liquefaction potential. Journal of Geotechnical and Geoenvironmental Engineering, ASCE 132(8): 1032–1051.

National Academies of Sciences, Engineering, and Medicine. 2021. State of the Art and Practice in the Assessment of Earthquake-Induced Soil Liquefaction and Its Consequences. Washington, DC: The National Academies Press. https://doi.org/10.17226/23474.

NCEER. In: Youd TL, Idriss IM, editors. Proceedings of the NCEER workshop on evaluation of liquefaction resistance of soils (Technical Report No. NCEER-970022). National Center for Earthquake Engineering Research, SUNY, Buffalo; 1997. x

Olsen, R. S. 1984. Liquefaction analysis using the cone penetrometer test CPT" Proc. 8th World Conference on Earthquake Engineering, San Francisco, California.

Park, S. S., Nong, Z. Z., and Lee, D. L.. 2020. Effect of vertical effective and initial static shear stresses on the liquefaction resistance of sands in cyclic direct simple shear tests. Soils and Foundations 60 2020 1588–1607. https://doi.org/10.1016/j.sandf.2020.09.007

Pillai, V. S., and Byrne, P. M. 1994. Effect of overburden pressure on liquefaction resistance of sand. Canadian geotechnical journal, 311, 53-60.

Robertson, P. K., and Wride, C. E.. 1998. Evaluating cyclic liquefaction potential using the cone penetration test. Canadian Geotechnical Journal, 353: 442– 459.

Saada, A.S., Bianchini, G.F., and Shook, L.P., (1978). "The Dynamic Response of Anisotropic Clay", Proceedings, Geotechnical Engineering Division Specialty Conference on Earthquake Engineering and Soil Dynamics, Vol. 11 ASCE, Pasadena, CA, June.

Saada, A.S., and Townsend, F.C. (1981). State- of-the-Art: Laboratory strength testing of soils. ASTM STP 740, 7-77

Saada, A.S. and Macky, T.A. "Dynamics of Anisotropic Clays Under Large Strains," Journal of Geotechnical Engineering., Proceedings of the American Society of Civil Engineers, Vol.110, No.4, April, 1984, pp 487- 504

Saada, A., & Macky, T. (1985). Integrated Testing and Properties of a Gulf of Mexico Clay.

Saada, A. S. (1988), "Hollow Cylinder Torsional Devices: Their Advantages and Limitations," Advanced Triaxial Testing of Soil and Rock

Sayao A. and Vaid Y. P. (1991) “A Critical Assessment of Stress Non – Uniformities in Hollow Cylinder Test Specimens”

Santamarina, J. C., & Cho, G. C. (2001). Determination of critical state parameters in sandy soils—simple procedure. Geotechnical testing journal, 24(2), 185-192.

Schnabel PB, Lysmer J and Seed HB (1972) SHAKE: A Computer Program for Earthquake Response Analysis of Horizontally Layered Sites. Earthquake Engineering Research Center, University of California, Berkeley, CA, USA, Report UCB/EERC-72/12.

Seed HB and Idriss IM (1971) Simplified procedure for evaluating soil liquefaction potential. Journal of Soil Mechanics and Foundation Division, ASCE 97(9): 1249–1273.

Seed, H. B., Idriss, I. M. 1982. Ground motions and soil liquefaction during earthquakes. EERI Monograph, Berkeley, California.

Seed, H. Bolton (1983) “Earthquake-Resistant Desing of Earth Dams,” Proceedings of a Symposium on Seismic Desing of Embankment and Caverns, ASCE, Philadelphia, Pennsylvania, May 6-10, 1983

Seed, H. B., Tokimatsu, K. Harder, L. F., and Chung, R. M.. 1984. The Influence of SPT Procedures in Soil Liquefaction Resistance Evaluations, Earthquake Engineering Research Center Report No. UCB/EERC-84/15, University of California at Berkeley, October 1984.

Seed, H. B., Tokimatsu, K., Harder, L. F., and Chung, R. M. 1985. The Influence of SPT Procedures in Soil Liquefaction Resistance Evaluations, Journal of Geotechnical Engineering, ASCE, Vol. 111, No. 12, p. 1425-1445.

Seed, R.B., and Harder, L.F., Jr. (1990) “SPT-based analysis of Cyclic Pore Pressure Generation and Undrained Residual Strength,” Proceedings of the H. Bolton Seed Memorial Symposium, May,1990

Sivathayalan, S., and Ha, D.. 2011. Effect of static shear stress on the cyclic resistance of sands in simple shear loading. Can. Geotech. J. 48, 1471–1484.

Suzuki, Y., Tokimatsu, K., Taya, Y., and Kubota, Y. 1995. Correlation between CPT data and dynamic properties of in situ frozen samples. in Proceedings, 3rd International Conference on Recent Advances in Geotechnical Earthquake Engineering and Soil Dynamics, Vol. I, St. Louis, MO.

Tastan, E. O., and H. A. J. Carraro. 2022. “Effect of principal stress rotation and intermediate principal stress changes on the liquefaction resistance and undrained cyclic response

of Ottawa sand." J. Geotech. Geoenviron. Eng. 148 (5): 04022015. https://doi.org/10.1061/(ASCE)GT.1943-5606.0002772

Tatsuoka, F., K. Ochi, S. Fujii, and M. Okamoto. 1986. "Cyclic undrained triaxial and torsional shear strength of sands for different sample preparation methods." Soils Found. 26 (3): 23–41. https://doi.org/10.3208/sandf1972.26.3_23.

Towhata, I. (2008) Geotechnical Earthquake Engineering. Springer Science & Business Media, Berlin.

Ulmer, K. J., R. A. Green, and A. Rodriguez-Marek. 2022. "Recommended b-value for Computing Number of Equivalent Cycles and Magnitude Scaling Factors for Simplified Liquefaction Triggering Evaluation Procedures." J. Geotech. Geoenviron. Eng. 148 (12): 04022113. https://doi.org/10.1061/(ASCE)GT.1943-5606.0002926

Umar M, Chiaro G, Kiyota T, Ullah N. Deformation and cyclic resistance of sand in large-strain undrained torsional shear tests with initial static shear stress. Soils Found 2021;61(3):765–81. https://doi.org/10.1016/j.sandf.2021.02.008.

Vaid, Y. P., and Finn, W. D. L.. 1979. Static shear and liquefaction potential" J. Geotech. Eng. Div.,10510, 1233-1246.

Vaid, Y. P., and Chern, J. C.. 1983. Effect of static shear on resistance to liquefaction" Soils and Foundations, 1231, 47-60. 242

Vaid, Y. P., Chern, J. C., and Tumi, H.. 1985. Confining pressure, grain angularity and liquefaction. J. Geotech. Eng., 11110, 1229-1235.

Vaid, Y.P., Sayao, A, Hou, E., and Negussey, D. 1990. Generalized stress-path-dependent soil behaviour with a new hollow cylinder torsional apparatus. Canadian Geotechnical Journal, 27: 601–616

Vaid, Y. P., and Thomas, J. 1995. Liquefaction and post-liquefaction behaviour of sand" Journal of Geotechnical Engineering, ASCE, 1212, 163-173. https://doi.org/10.1061/(ASCE)0733-9410(1995)121:2(163).

Vaid, Y. P., and Sivathayalan, S. 1996. Static and cyclic liquefaction potential of Fraser Delta sand in simple shear and triaxial tests. Canadian Geotechnical Journal, 332, 281-289.

Vaid, Y. P., Stedman, J. D. and Sivathayalan, S.. 2001. Confining stress and static shear effects in cyclic liquefaction. Can. Geotech. J., 580-591.

Wu, J., Seed, R. B., and Pestana, J. M.. 2003. Liquefaction triggering and post liquefaction deformations of Monterey 0/30 sand under uni-directional cyclic simple shear loading. Geotechnical Engineering Research Report No. UCB/GE-2003/01, University of California, Berkeley, California.

Youd, T. L., and Noble, S. K. (1997). ‘‘Magnitude scaling factors.’’ Proc., NCEER Workshop on Evaluation of Liquefaction Resistance of Soils, Nat. Ctr. for Earthquake Engrg. Res., State Univ. of New York at Buffalo, 149–165

Youd, T.L., Idriss, I.M. Andrus, R.D., Arango, I., Castro, G., Christian J.T., Dobry, R., Finn, W.D.L., Harder, L.F., Hynes, M.E., Ishihara, K., Koester, J.P., Liao, S.S.C., Marcuson, W.F., Martin, G.R., Mitchell, J.K., Moriwaki, Y., Power, MS., Robertson, P.K., Seed, R.B. and Stokoe, K.H. (2001). Liquefaction resistance of soils: summary report from the 1996 NCEER and 1998 NCEER/NSF Workshops on evaluation of liquefaction resistance of soils. J. Geotechnical and Geo-environmental Engineering, ASCE, Vol. 127, No. 10, 817–834.

Zheng, J., & Hryciw, R. D. (2016). Roundness and sphericity of soil particles in assemblies by computational geometry. Journal of Computing in Civil Engineering, 30(6), 04016021.

APPENDICES

A. 4-way plots of the test results

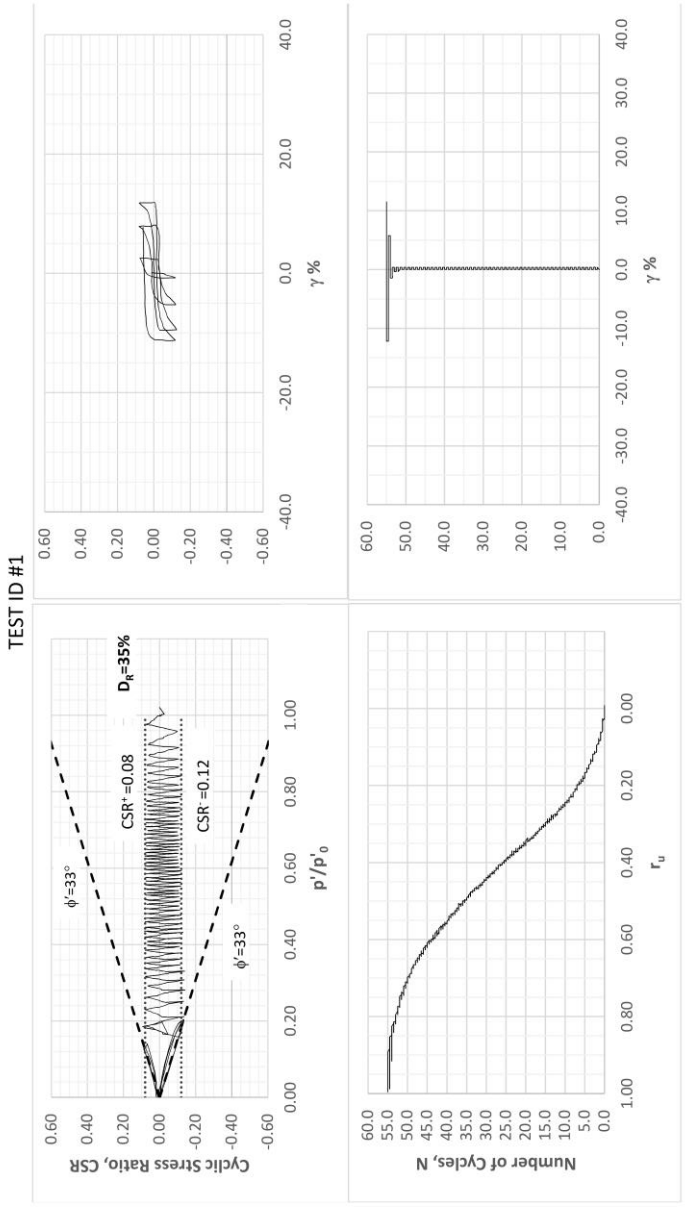

TEST ID #1 D_R=35%, α =0, CSR=0.10

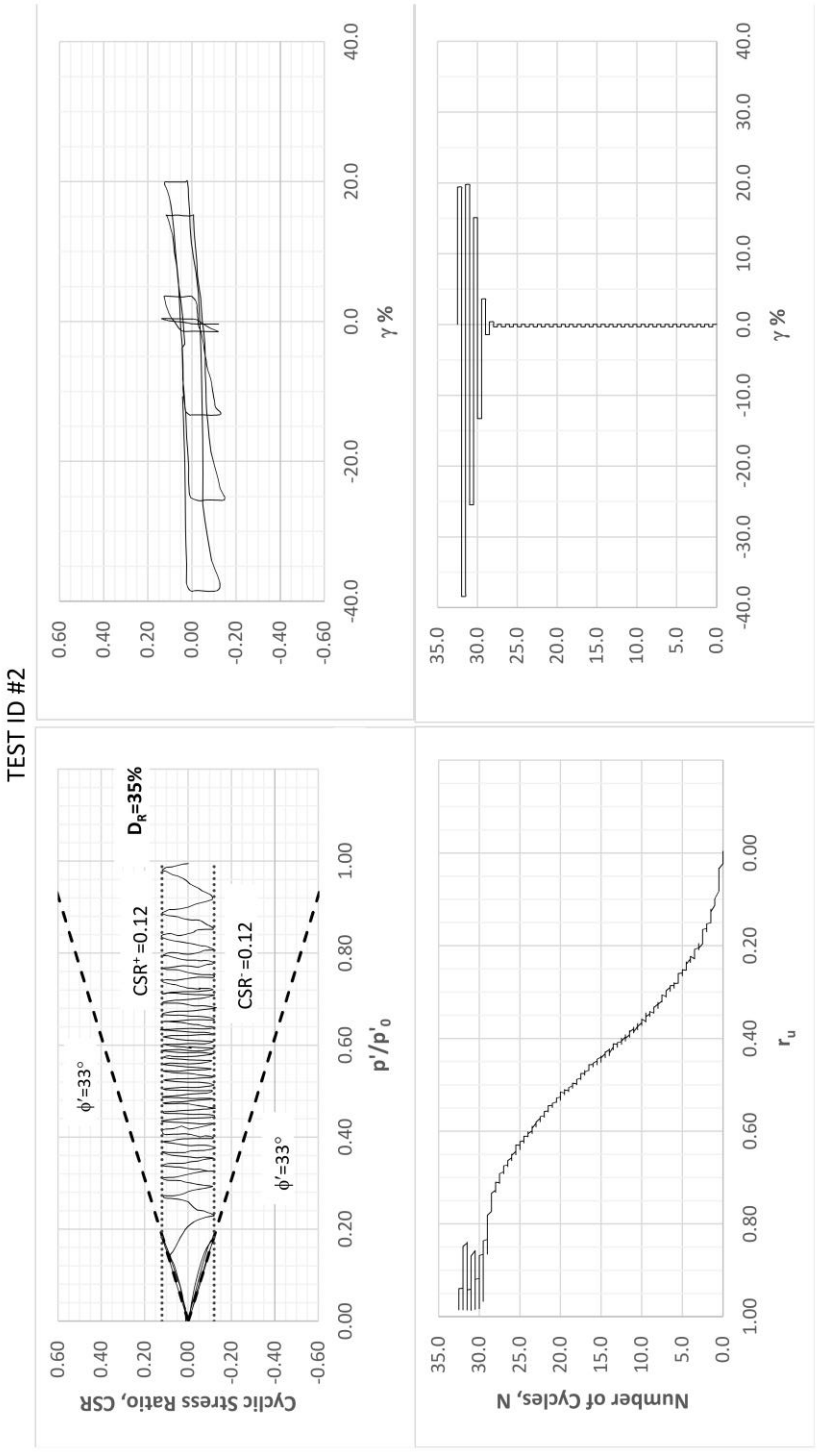

TEST ID #2 D_R=35%, α =0, CSR=0.12

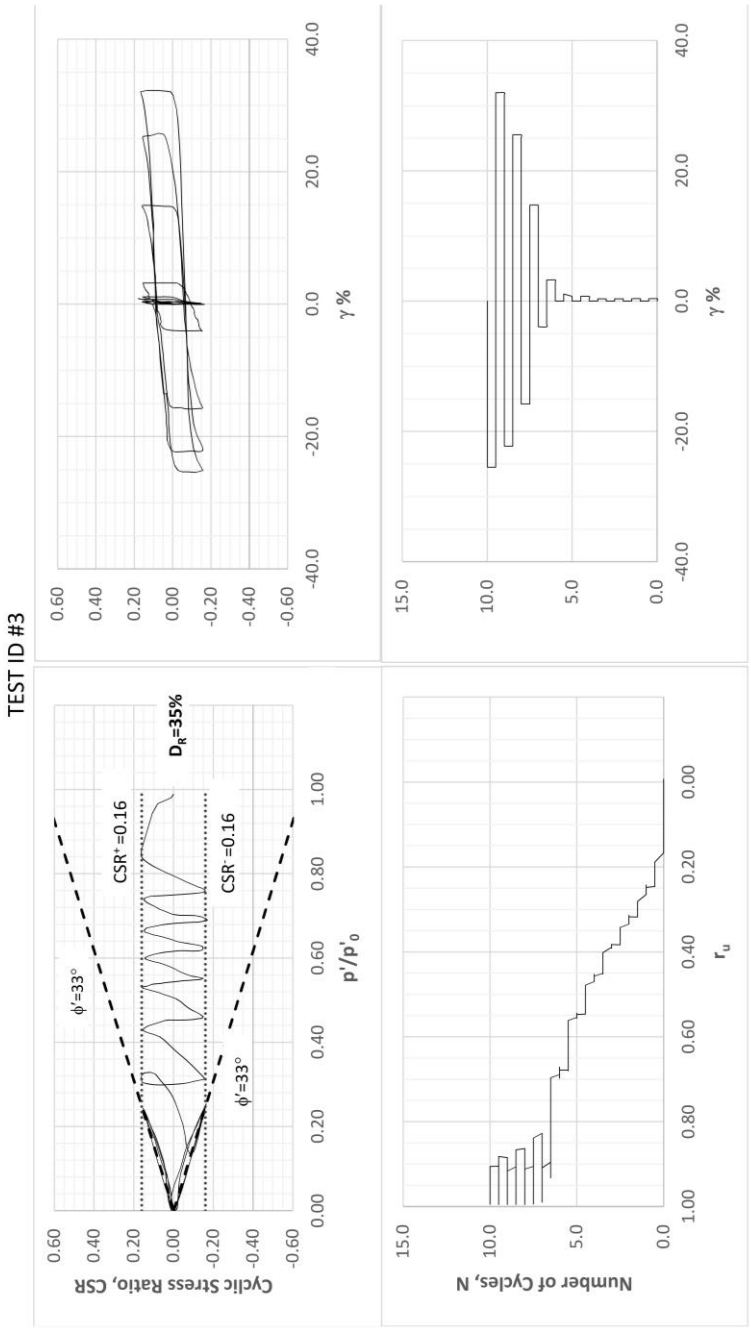

TEST ID #3 D_R=35%, α =0, CSR=0.16

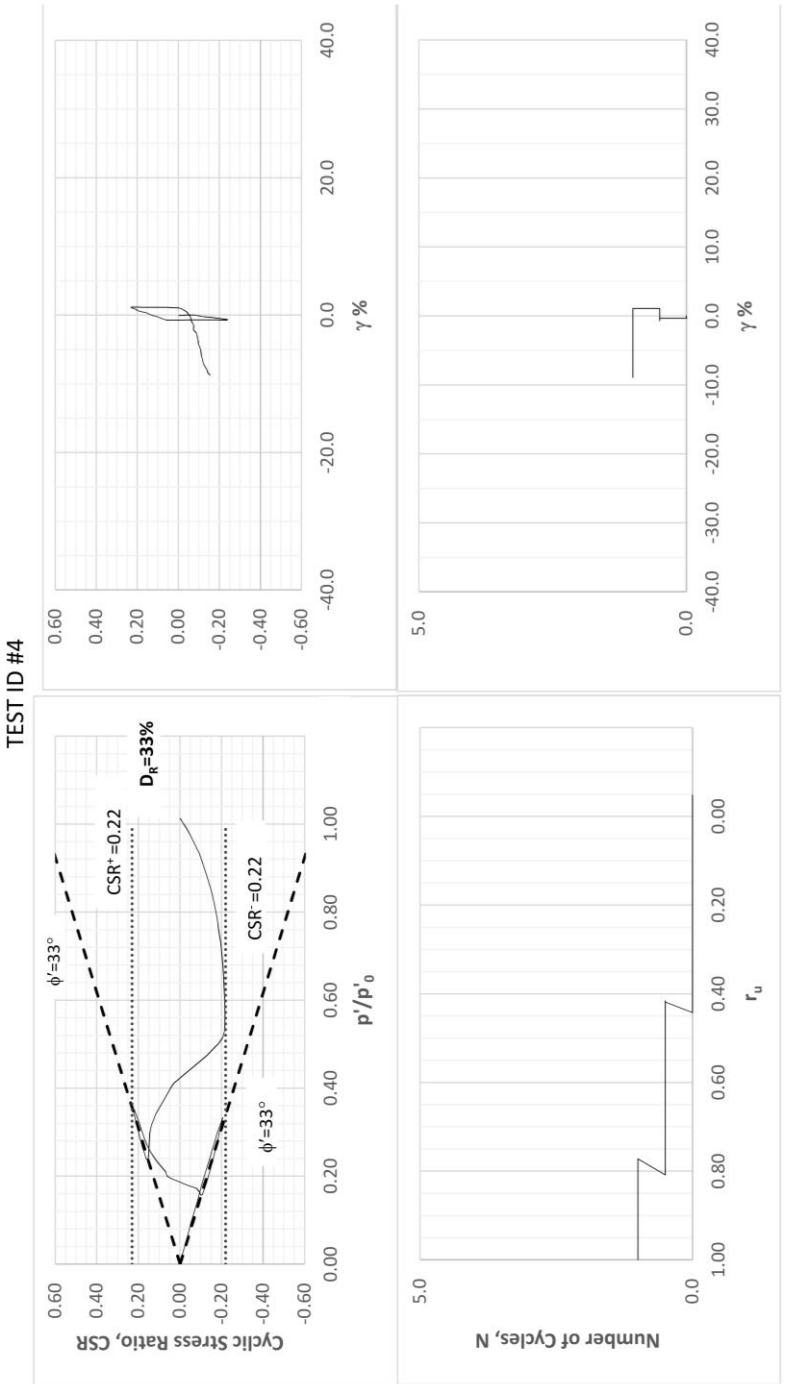

TEST ID #4 D_R=33%, α =0, CSR=0.22

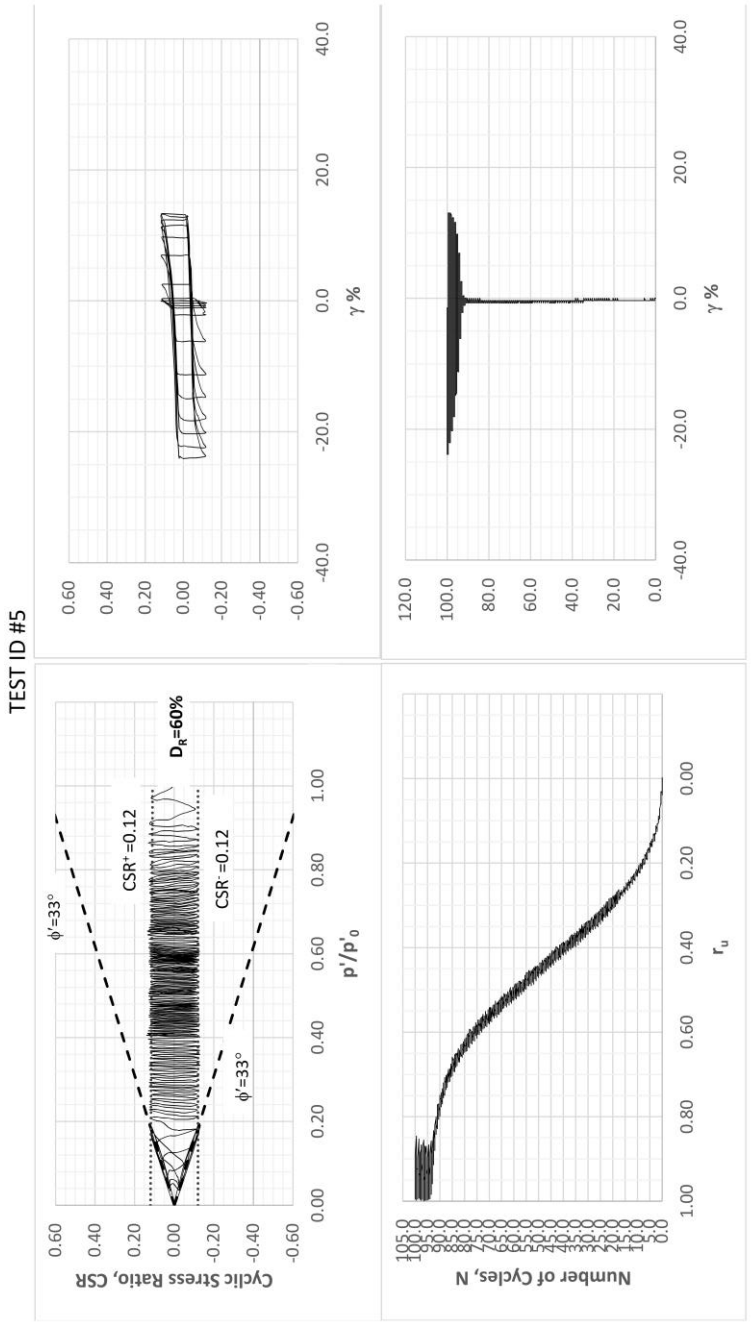

TEST ID #5 D_R=60%, α =0, CSR=0.12

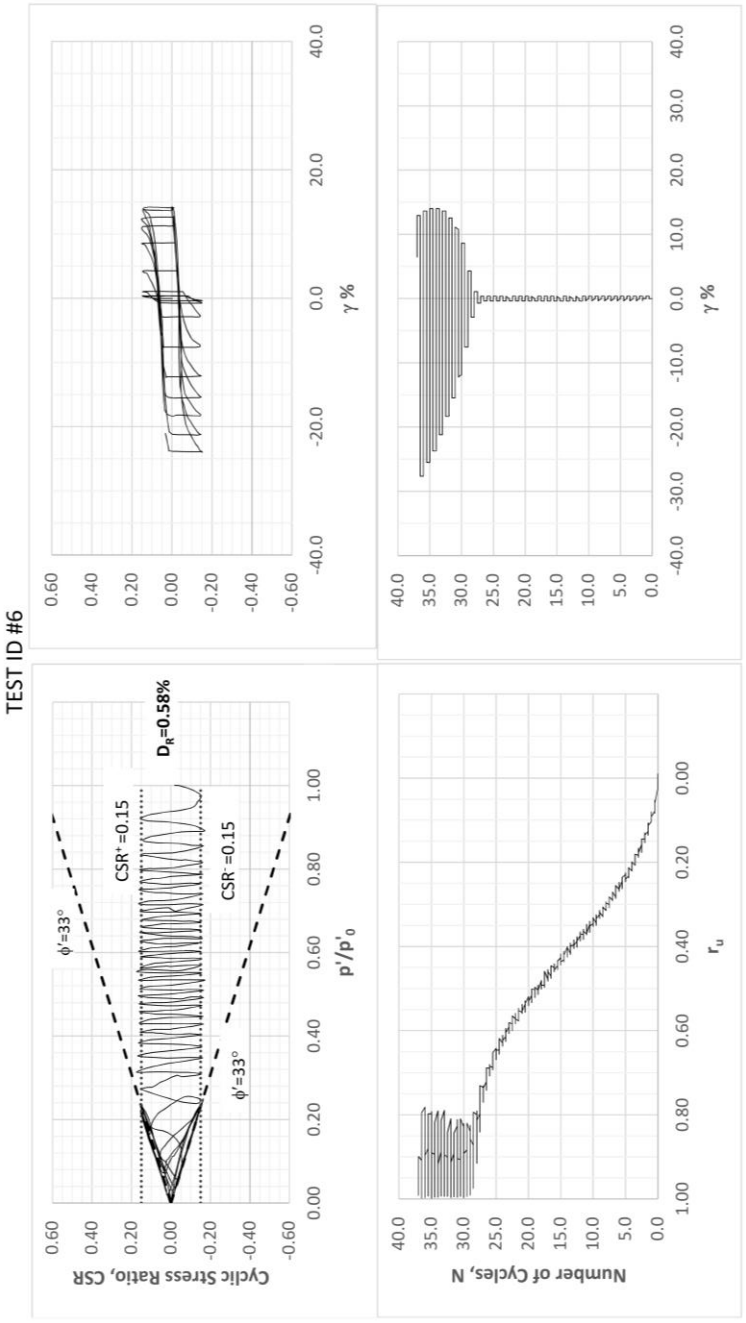

TEST ID #6 D_R=58%, α =0, CSR=0.15

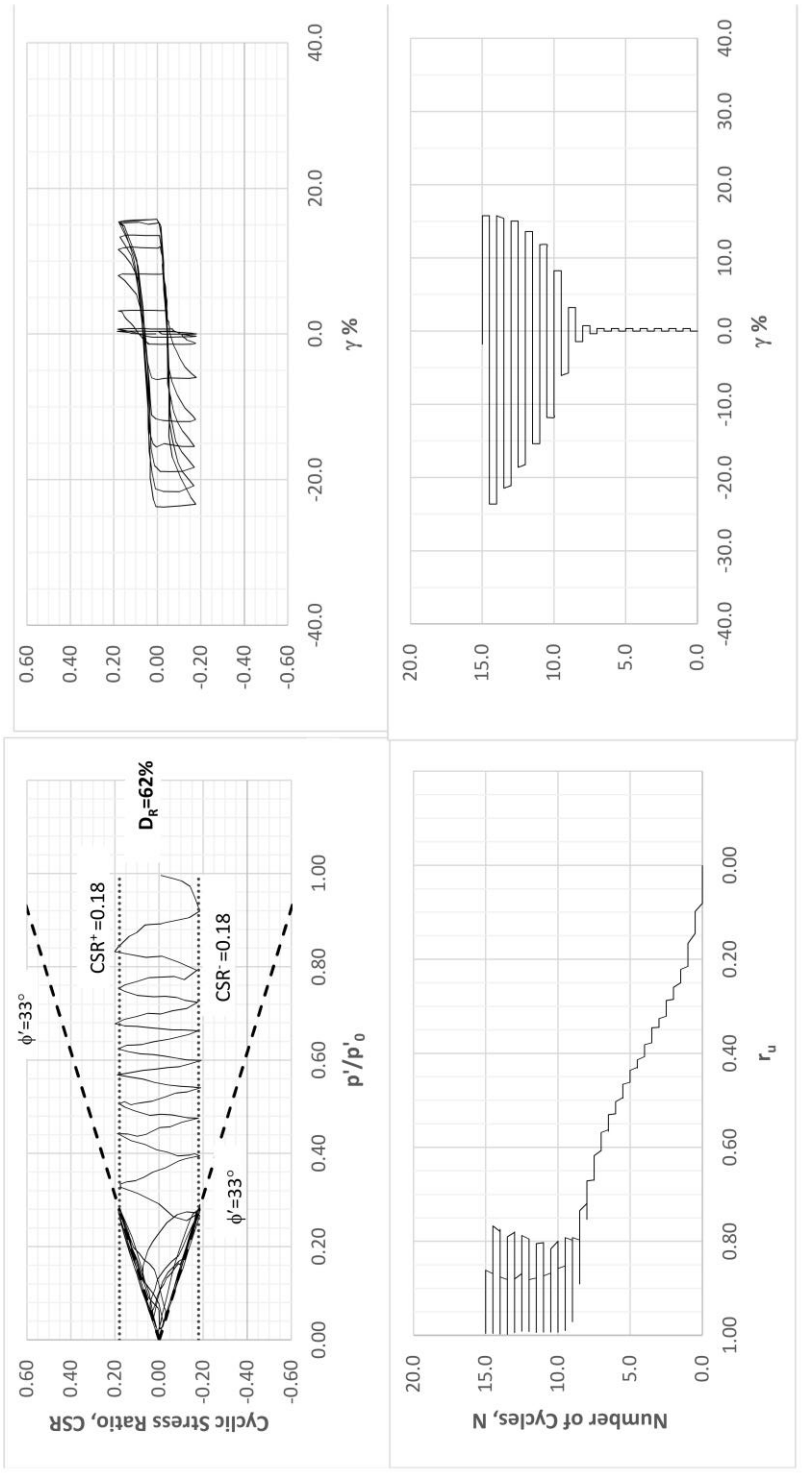

TEST ID #7 D_R=62%, α =0, CSR=0.18

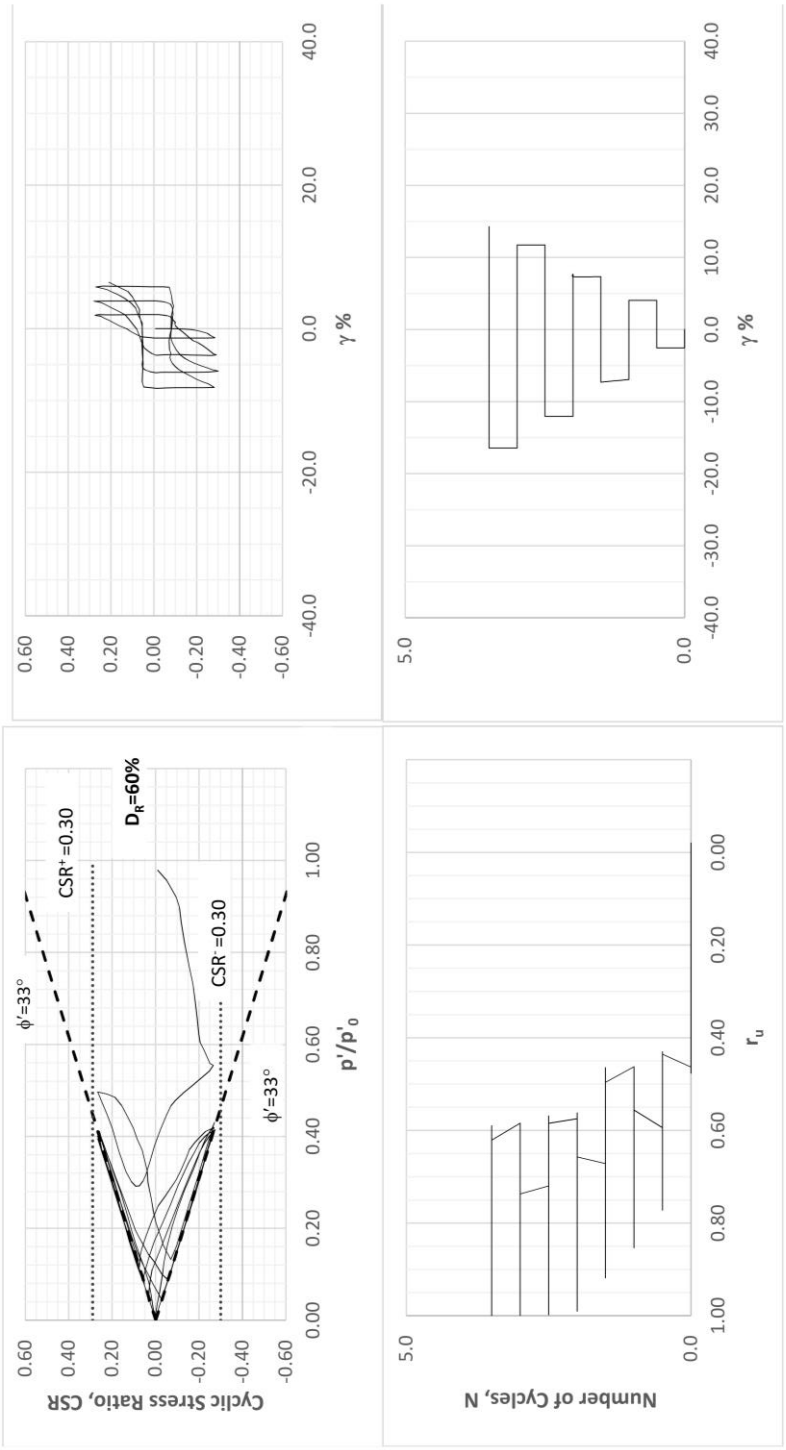

TEST ID #8 D_R=60%, α =0, CSR=0.30

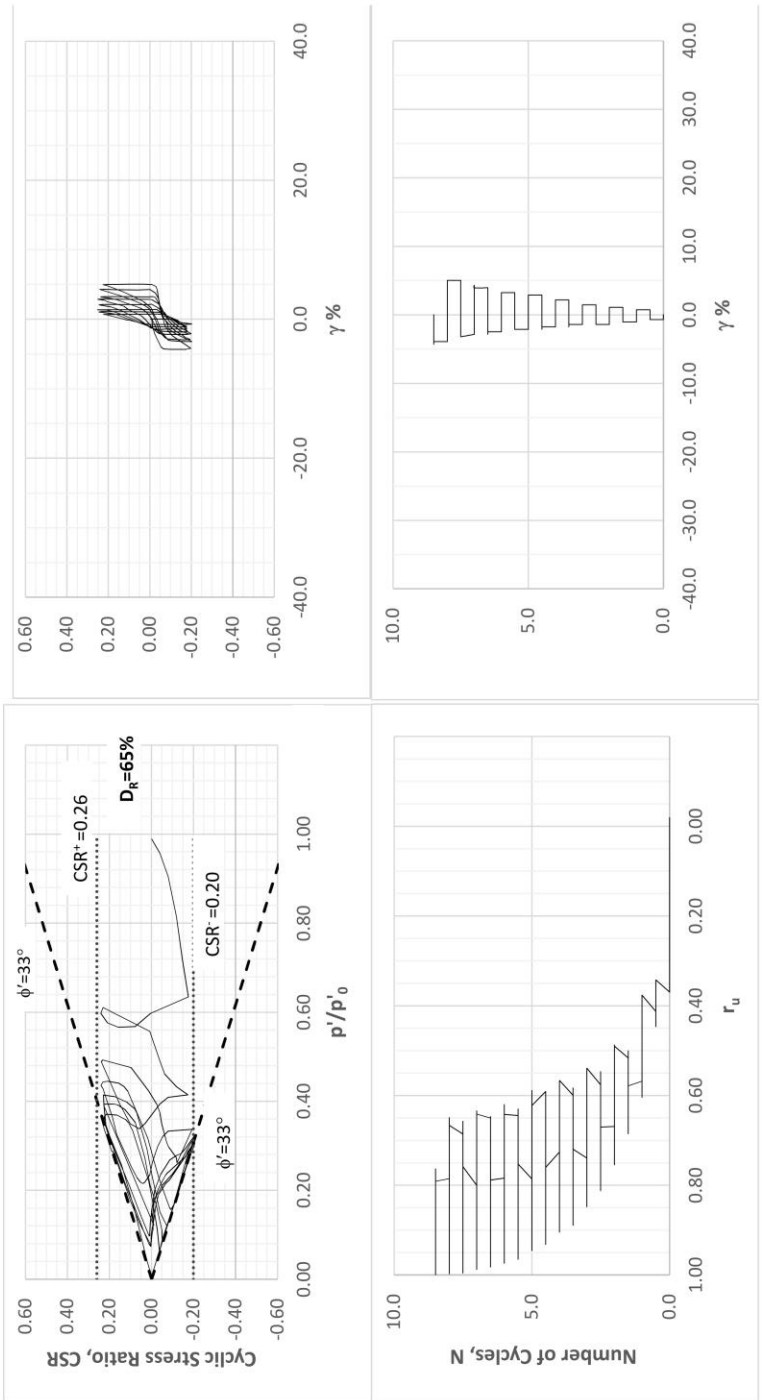

TEST ID #10 D_R=65%, α =0, CSR=0.23

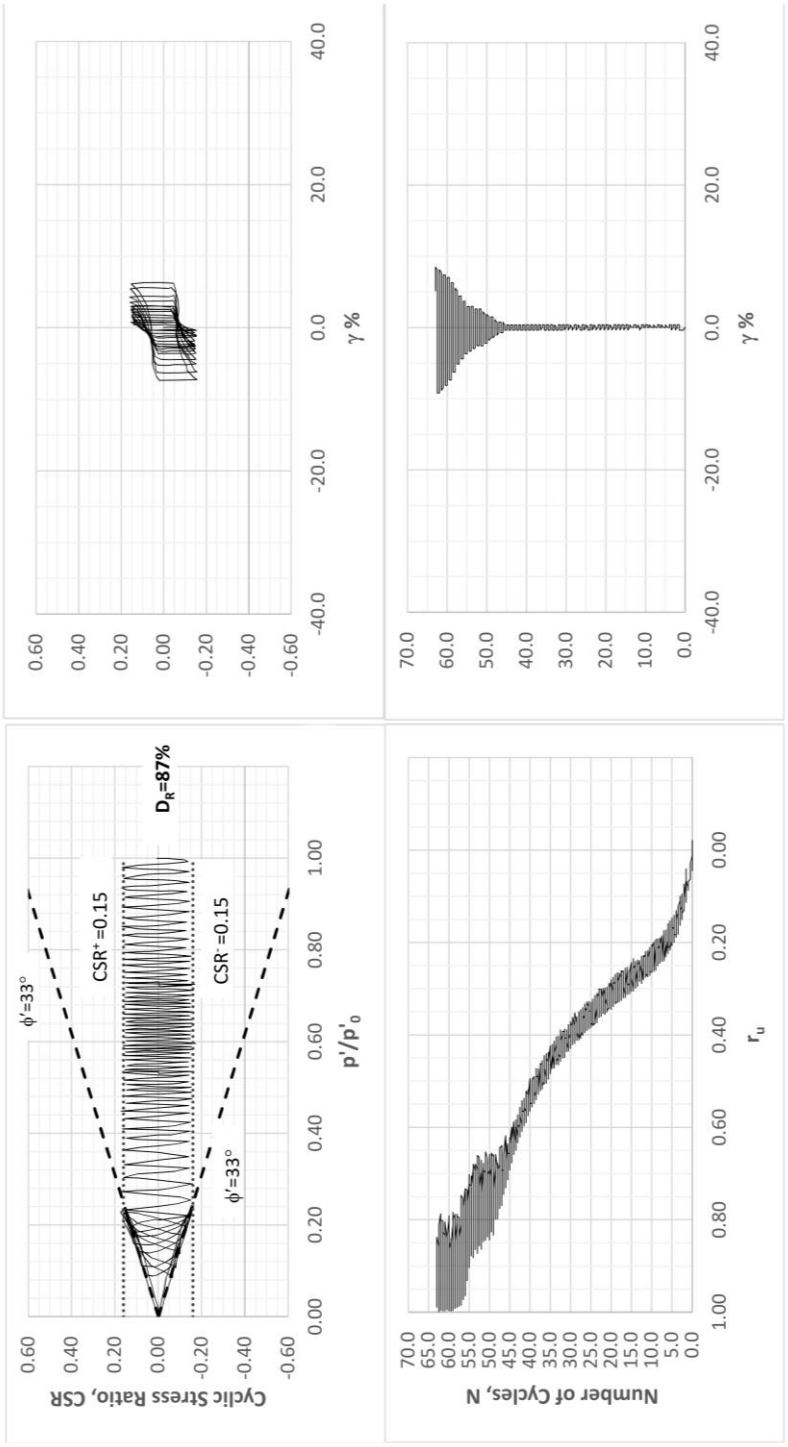

TEST ID #12 D_R=87%, α =0, CSR=0.15

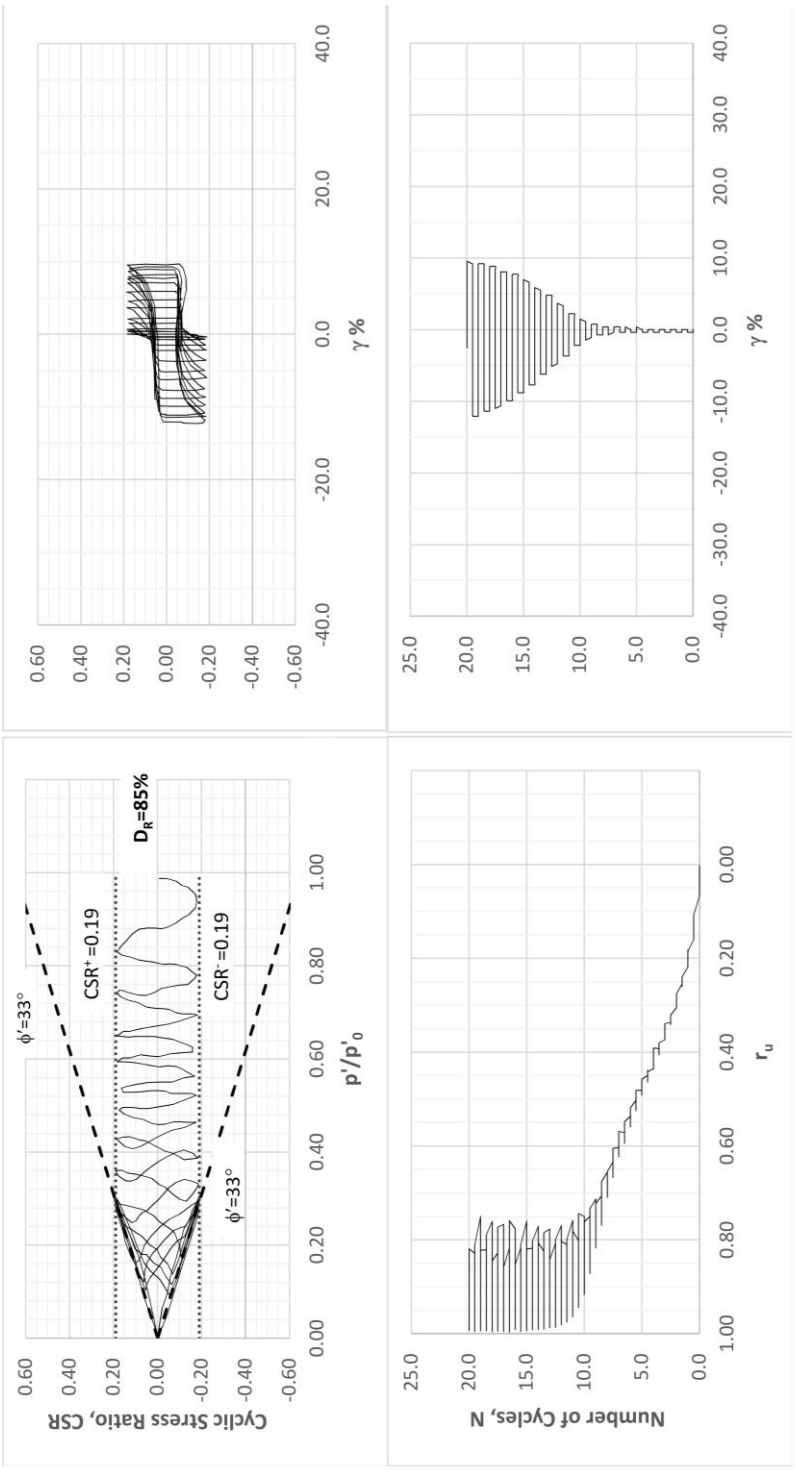

TEST ID #13 D_R=85%, α =0, CSR=0.19

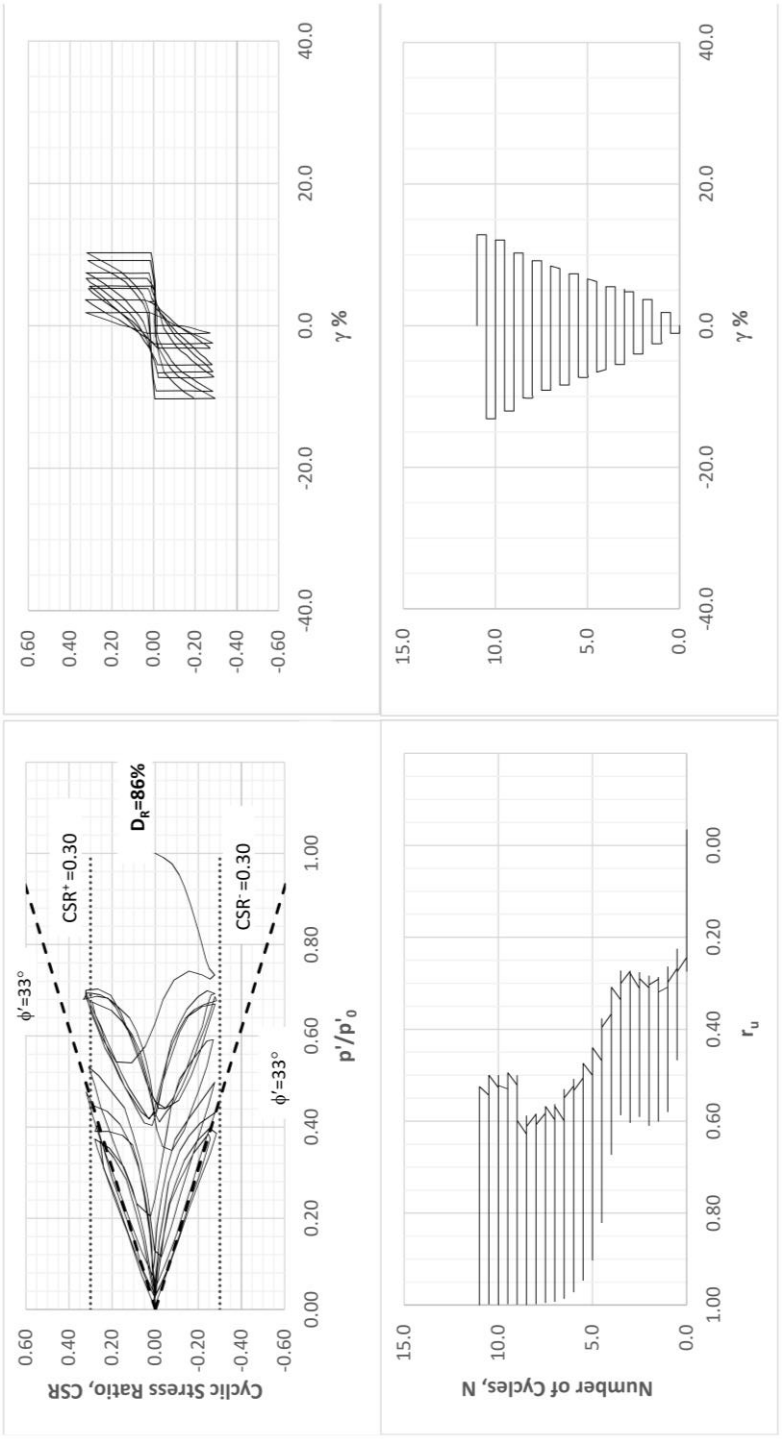

TEST ID #14 D_R=86%, α =0, CSR=0.30

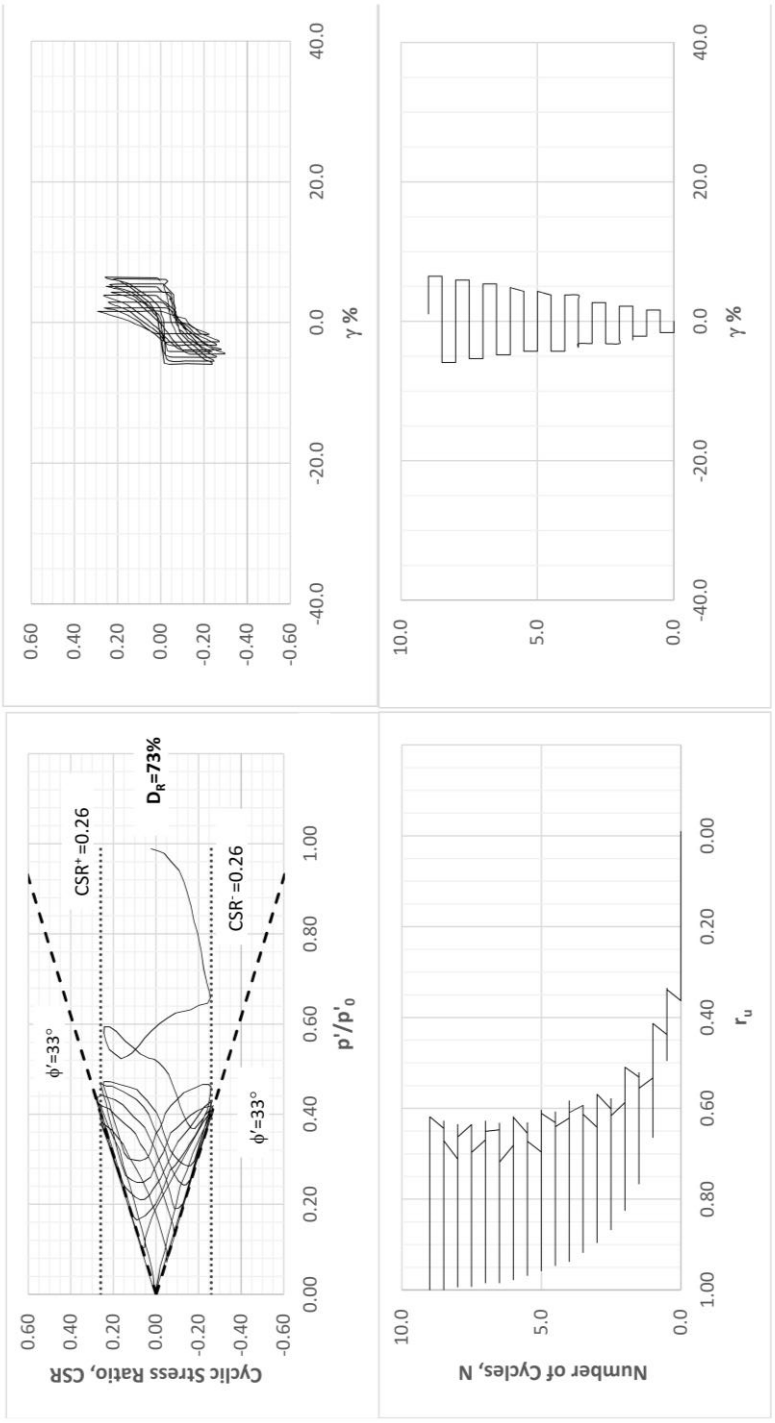

TEST ID #15 D_R=73%, α =0, CSR=0.26

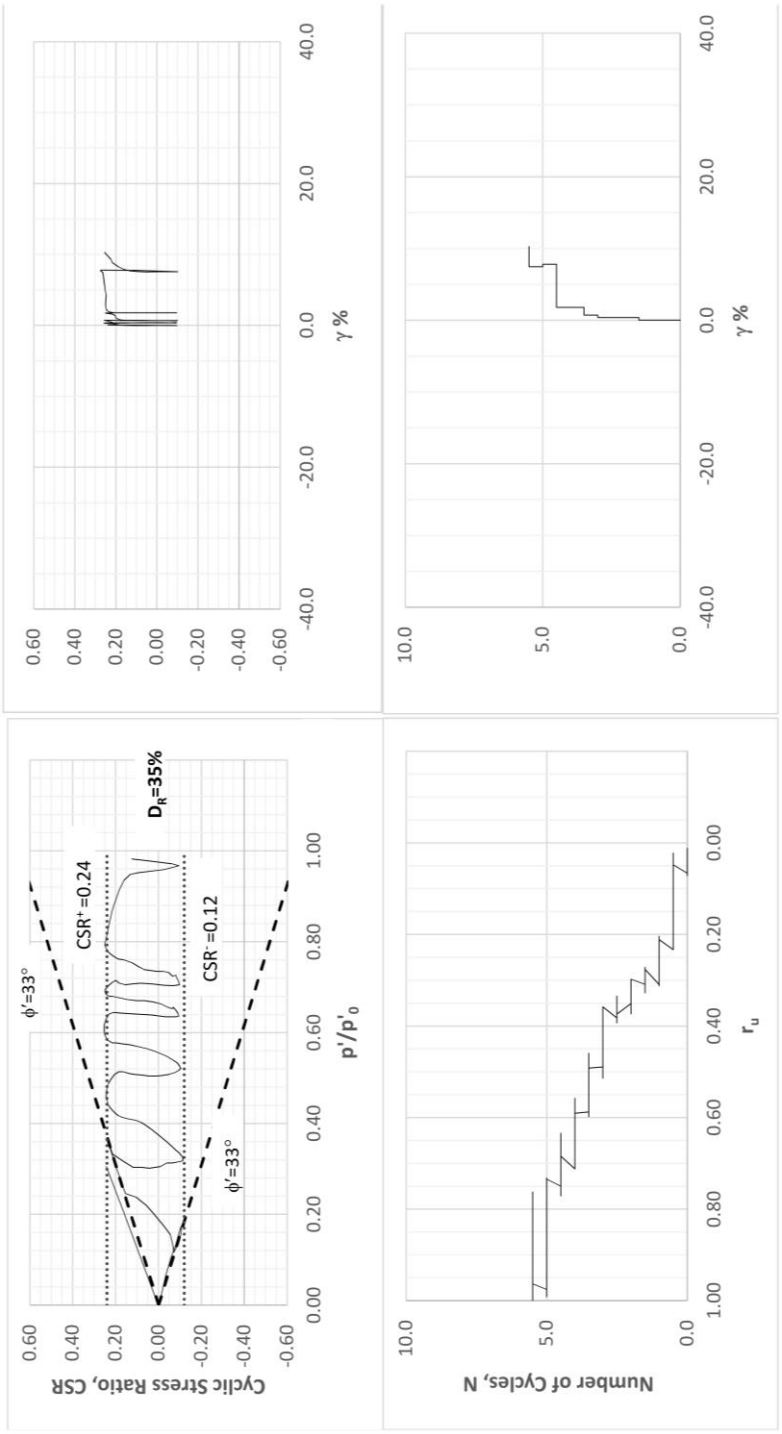

TEST ID #16 D_R=35%, α =0.13, CSR=0.16

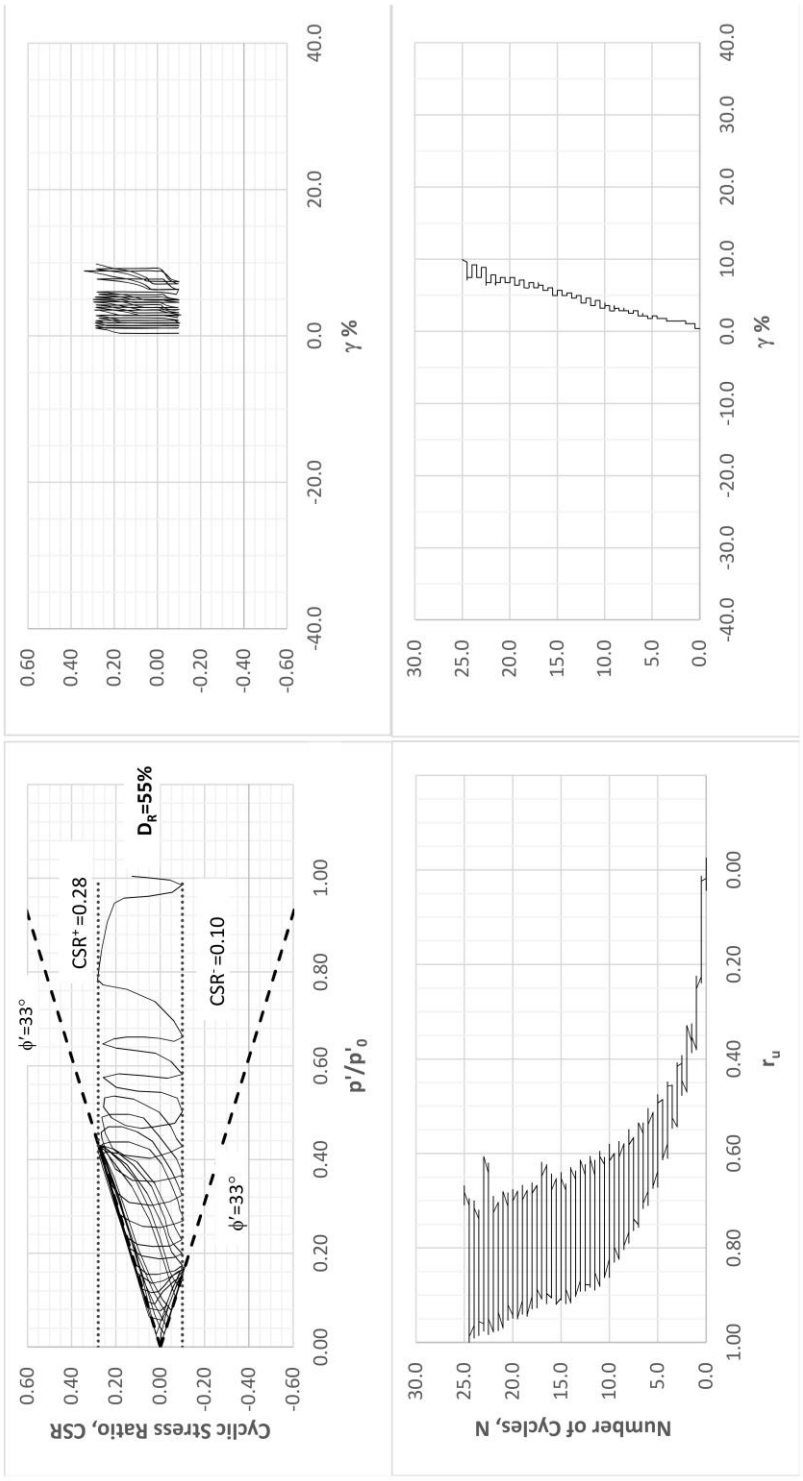

TEST ID #18 D_R=55%, α =0.10, CSR=0.19

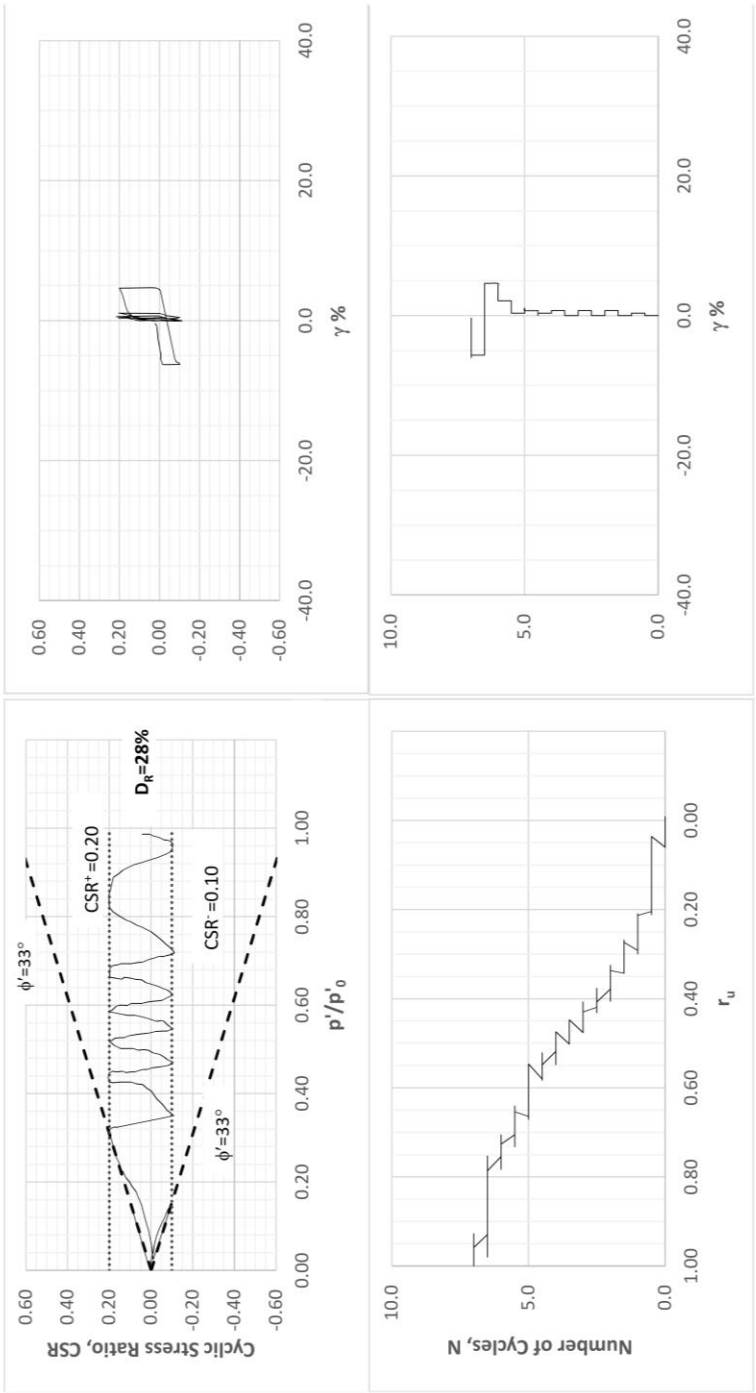

TEST ID #21 D_R=28%, α =0.5, CSR=0.15

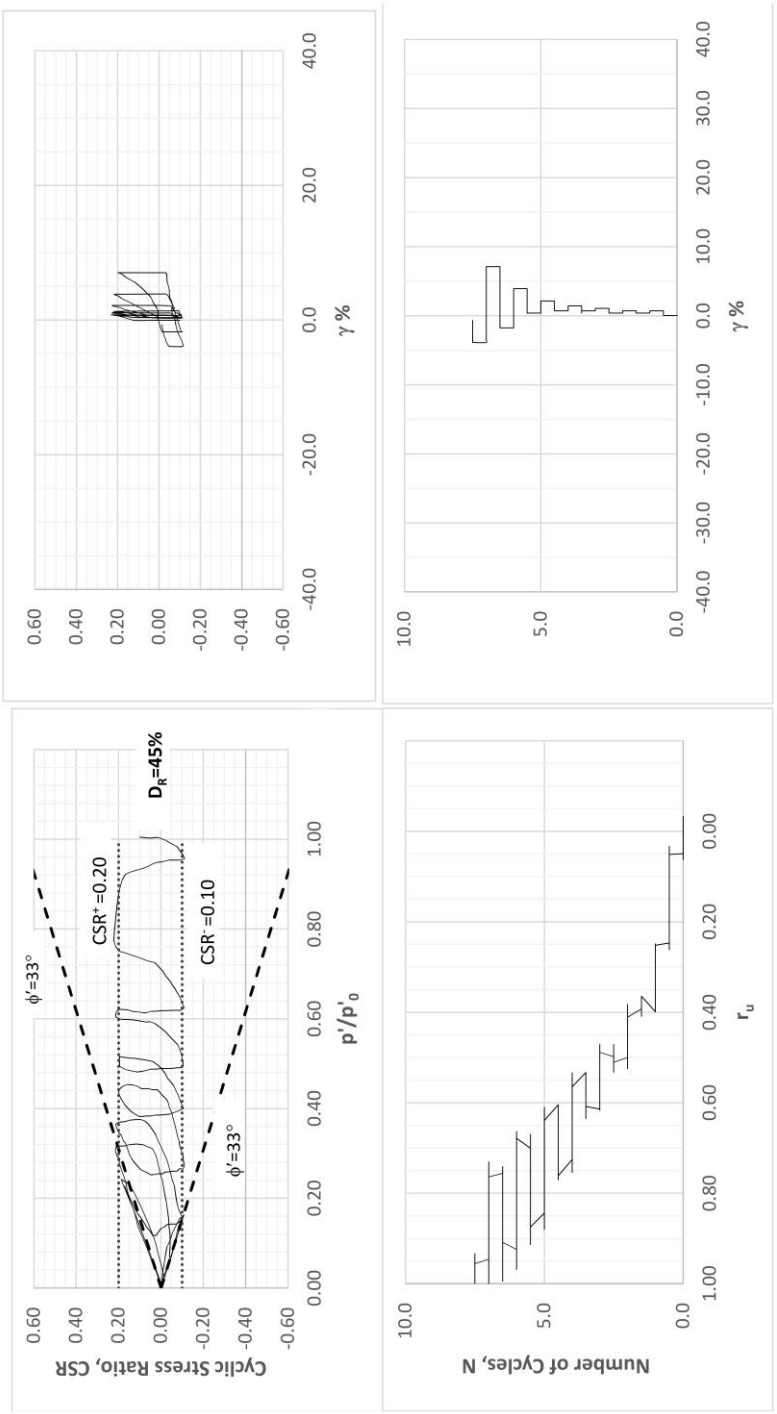

TEST ID #22 D_R=45%, α =0.05, CSR=0.15

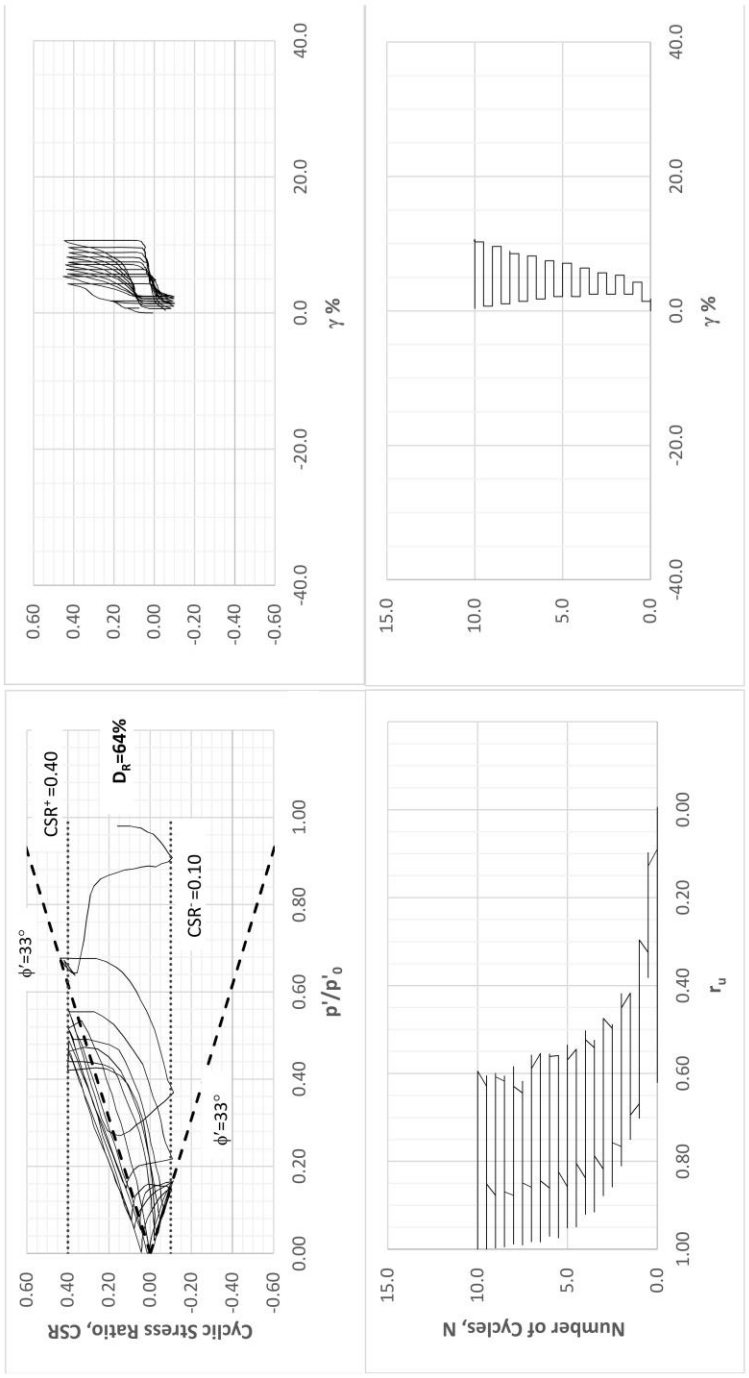

TEST ID #23 D_R=64%, α =0.20, CSR=0.25

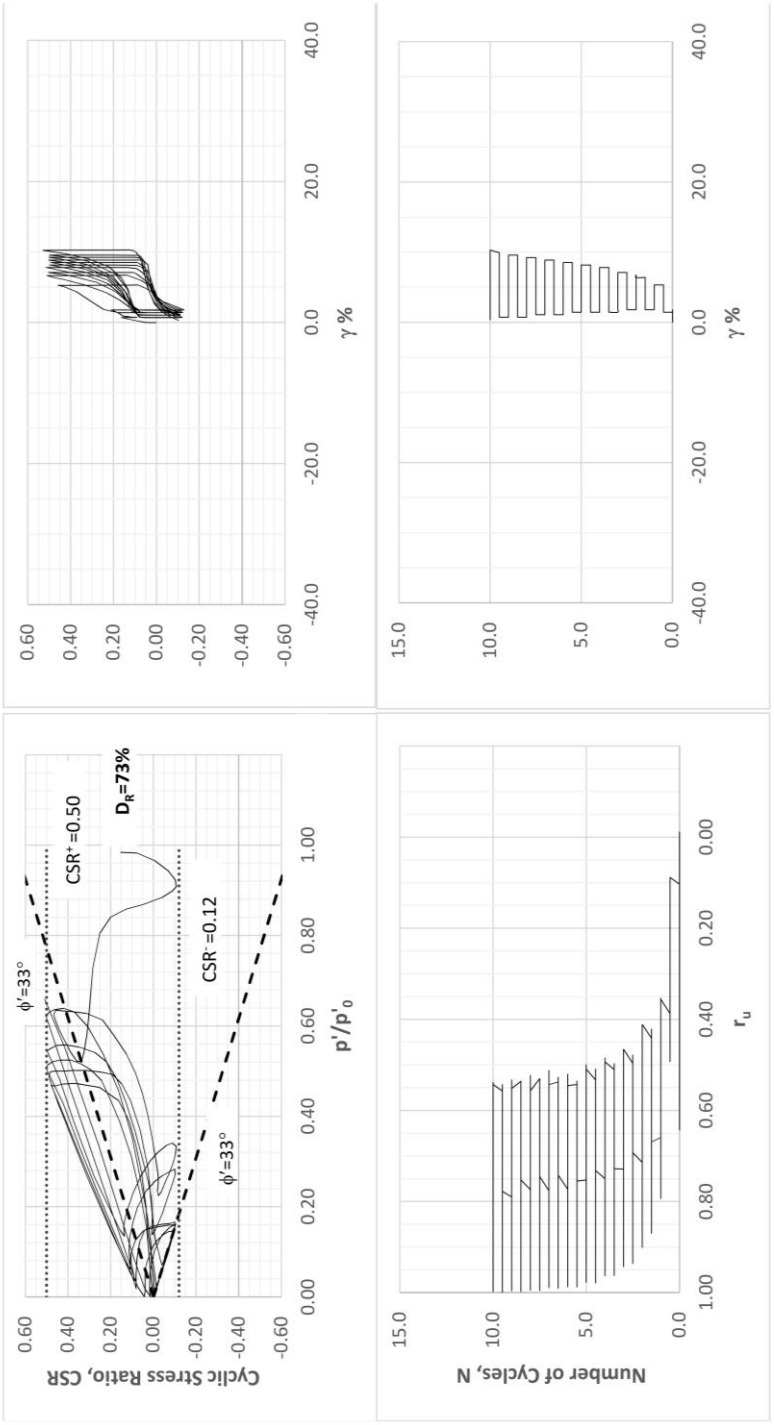

TEST ID #24 D_R=73%, α =0.15, CSR=0.31

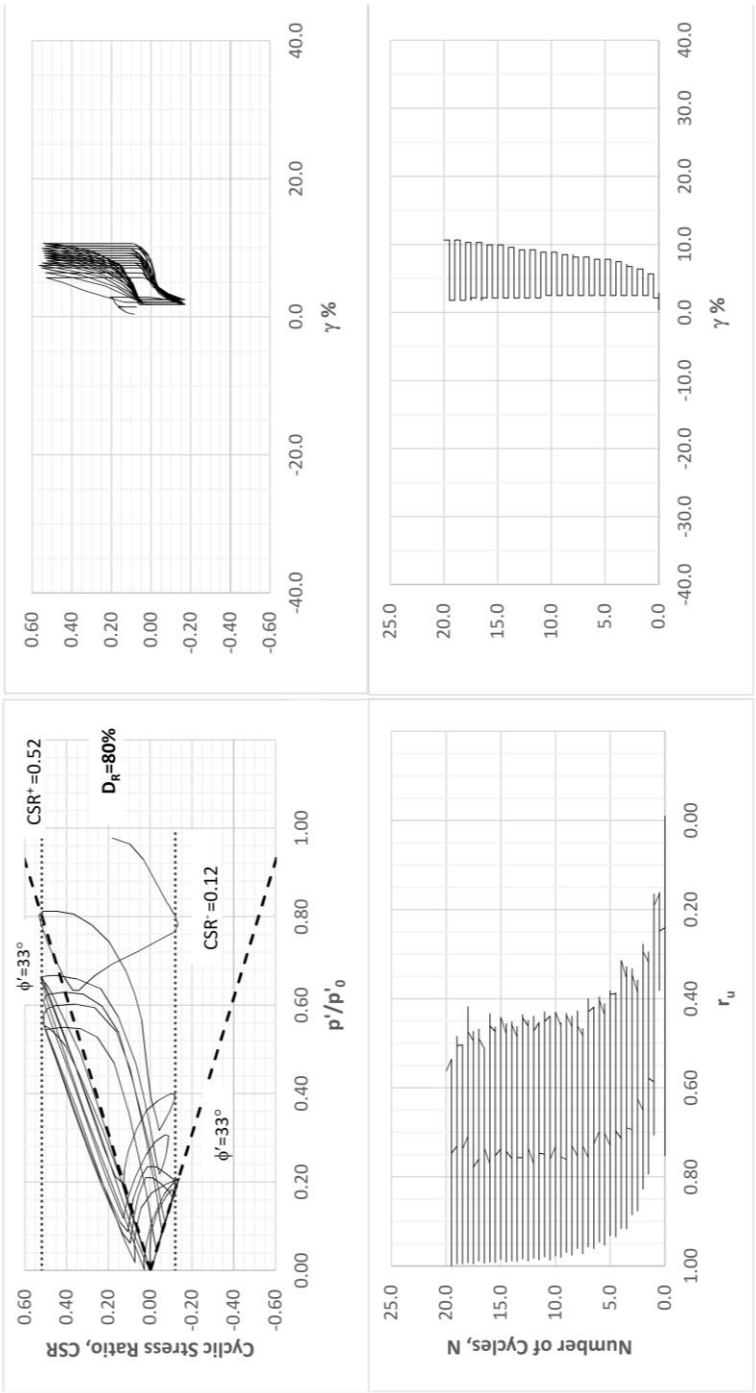

TEST ID #25 D_R=80%, α =0.18, CSR=0.32

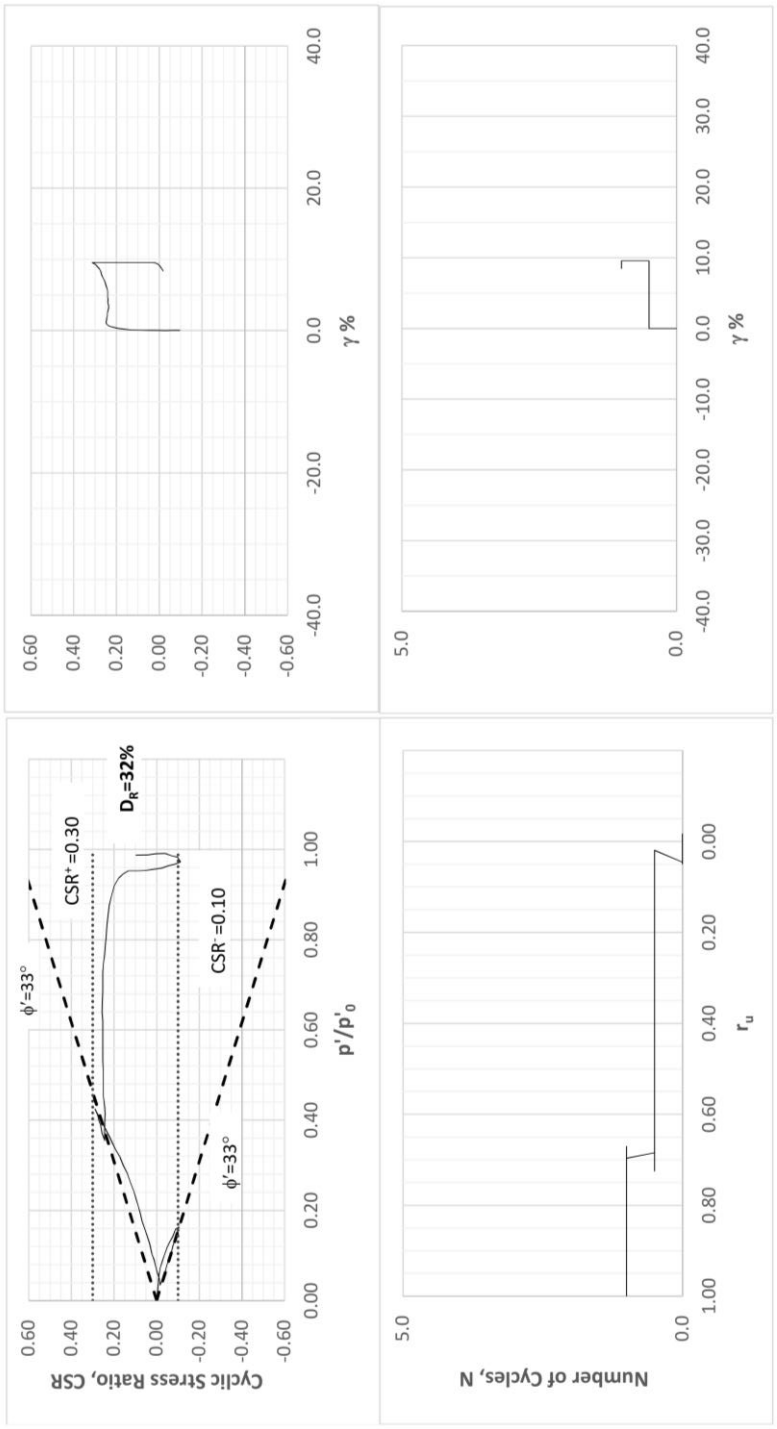

TEST ID #26 D_R=32%, α =0.10, CSR=0.20

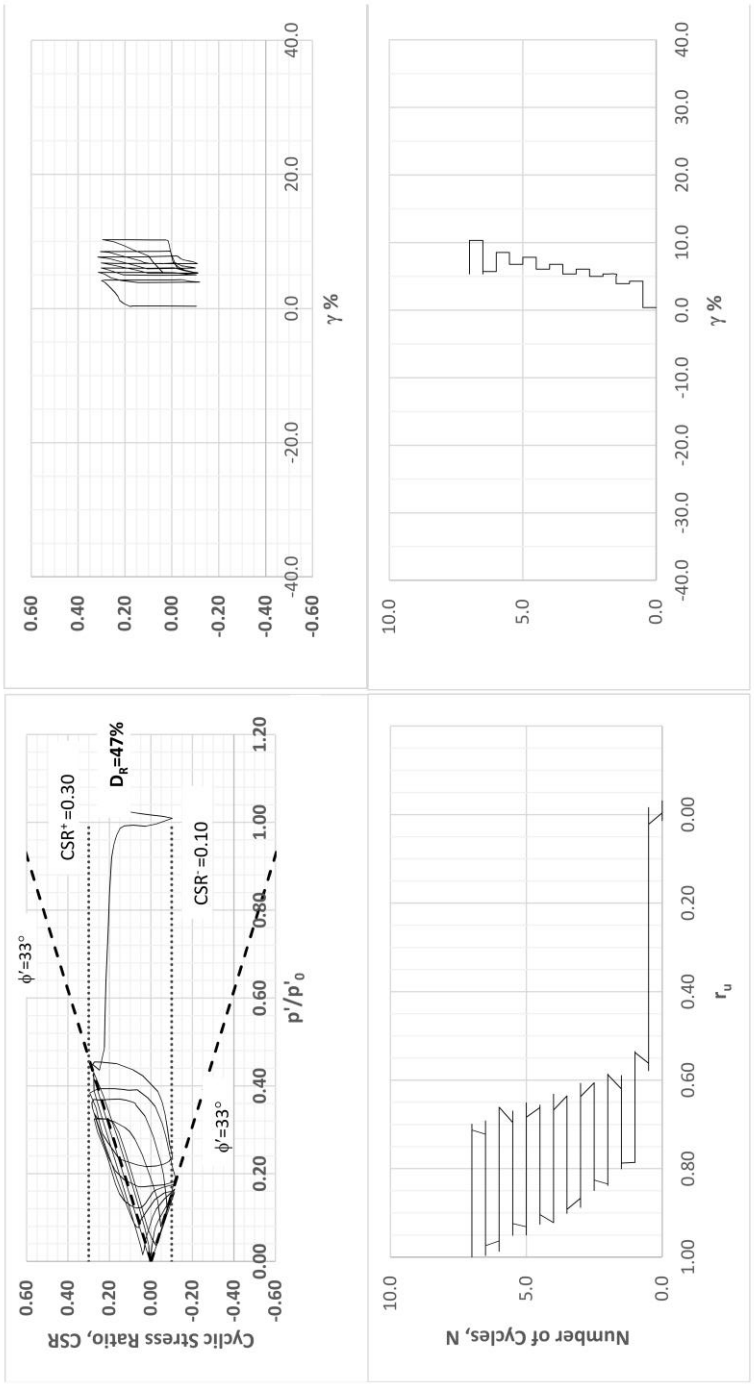

TEST ID #27 D_R=47%, α =0.10, CSR=0.20

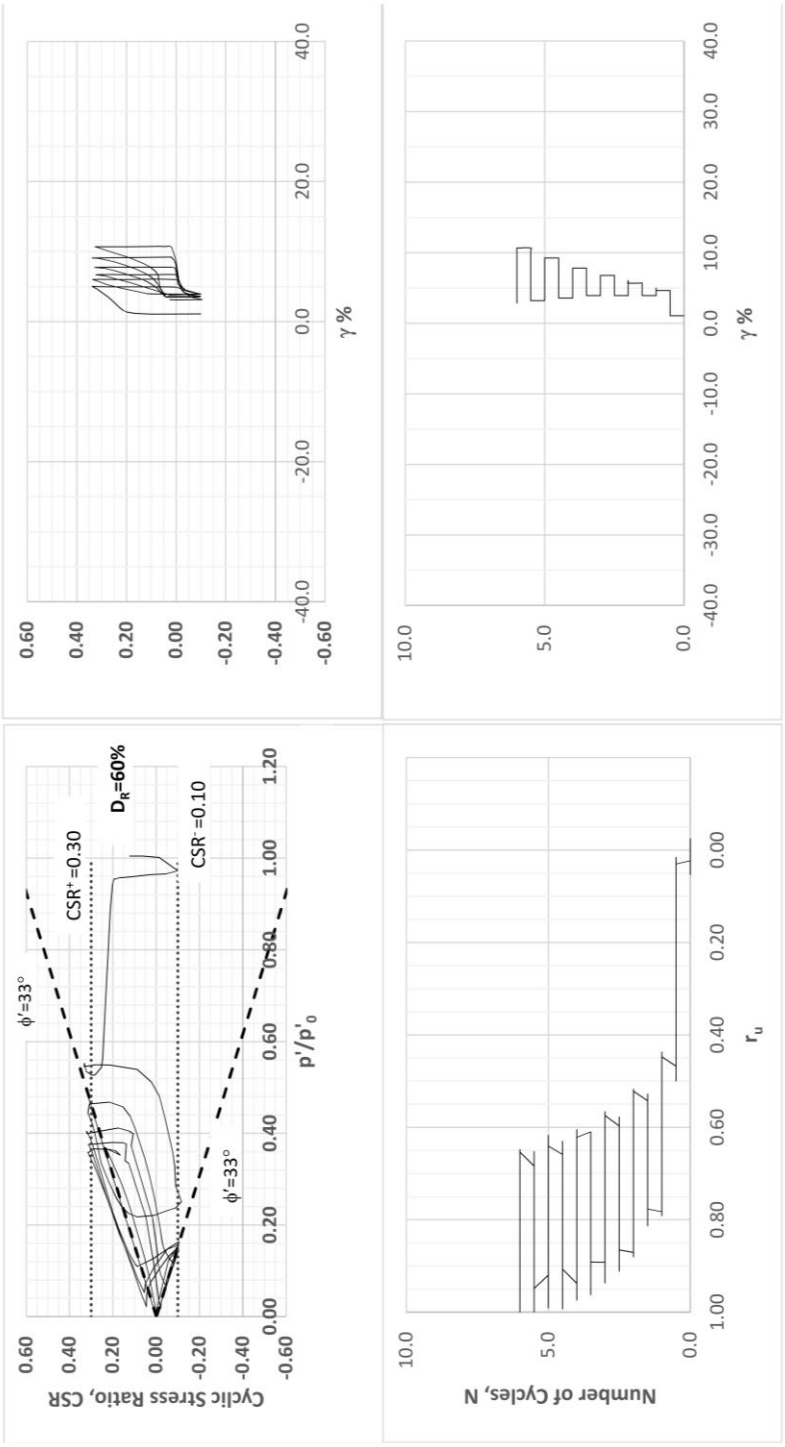

TEST ID #28 D_R=60%, α =0.13, CSR=0.20

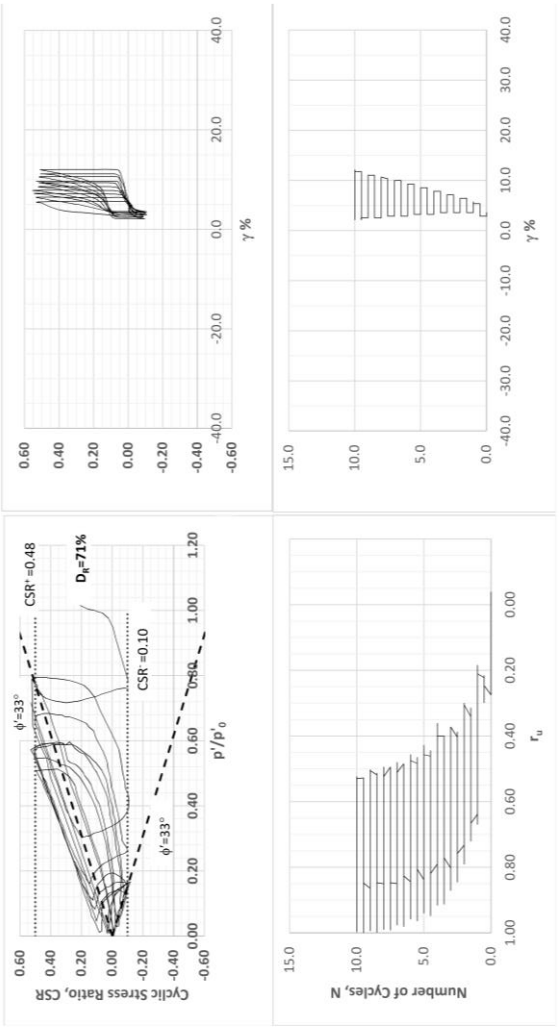

TEST ID #29 D_R=35%, α =0.22, CSR=0.28

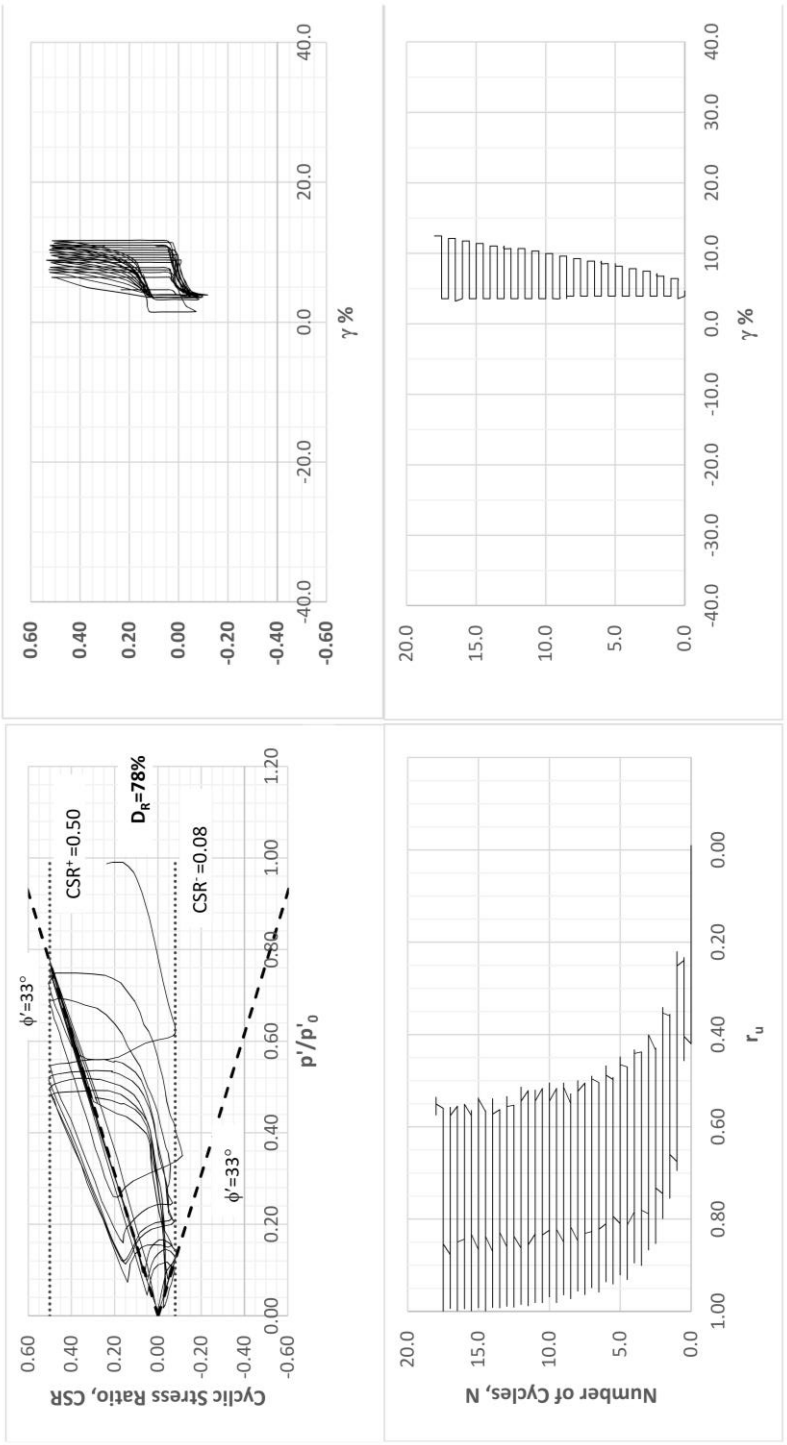

TEST ID #30 D_R=35%, α =0.22, CSR=0.29

CURRICULUM VITAE

Surname, Name: Söylemez, Berkan

EDUCATION

Degree	Institution	Year of Graduation
MS	METU Civil Engineering	2017
BS	METU Civil Engineering	2014
High School	Ankara Atatürk High School, Ankara	2007

FOREIGN LANGUAGES

Turkish (Native Speaker), English (Fluent), Spanish (Beginnerr)

ACADEMIC WORK EXPERIENCE

Year	Place	Position
2014 – 2024	Middle East Technical University Dept. of Civil Eng.	Research Assistant

PUBLICATIONS

- Cetin, K.O., **Soylemez, B.,** Guzel, H., Cakir, E., 2024. Soil liquefaction sites following the February 6, 2023, Kahramanmaras ¸-Türkiye earthquake sequence. Bull. Earthq. Eng. https://doi.org/10.1007/s10518-024-01875-3.

- Çetin, K. O., S. Altun, A. Askan, M. Akgün, A. Sezer, C. Kıncal, Ö. C. Özdağ, Y. İpek, B. Unutmaz, Z. Gülerce, **Soylemez, B.** et al. 2022.The site effects in Izmir Bay

of October 30 2020, M7. 0 Samos earthquake. Soil Dynamics and Earthquake Engineering152:107051. doi:10.1016/j.soildyn.2021.107051.756

- K.O. Cetin, …. , **Soylemez B.,** ….. et al., Geotechnical aspects of reconnaissance findings after 2020 January 24th, M6.8 Sivrice–Elazig–Turkey earthquake, Bull. Earthq. Eng. vol. 19 (9) (2021) 3415–3459, https://doi.org/10.1007/s10518-021-01112-1.

- **Soylemez, B. (2017).** Laboratory Experiments on Improvement of Buried Flexible Pipes by Using Geofoam, MSc. Thesis, Middle East Technical University, Ankara, Turkey.